Universidade de Brasília
IQ | Programa de Pós-Graduação em Química

DOCTORAL THESIS

SORPTION INTERACTIONS OF SULFAMETHOXAZOLE AND DICLOFENAC WITH FRESH, UV-AGED, AND HUMIC ACID-COATED MICROPLASTICS

Student: Imisi Michael Arowojolu

Supervisor: Prof. Dr. Fernando Fabriz Sodré

Brasília, 12th September, 2024

Universidade de Brasília
IQ | Programa de Pós-Graduação em Química

SORPTION INTERACTIONS OF SULFAMETHOXAZOLE AND DICLOFENAC WITH FRESH, UV-AGED, AND HUMIC ACID-COATED MICROPLASTICS

IMISI MICHAEL AROWOJOLU

Thesis submitted to the Graduate Program in Chemistry, University of Brasília, Brasília, in partial fulfillment of the requirements for the degree of Doctor of Philosophy in Chemistry.

Supervisor: Prof. Dr. Fernando Fabriz Sodré

Brasília, 12th September, 2024

APPROVAL/EVALUATION PAGE

The doctoral thesis of the student Imisi Michael Arowojolu, registration number 19/0079436, titled "Sorption Interactions of Sulfamethoxazole and Diclofenac with Fresh, UV-Aged, and Humic Acid-Coated Microplastics," will be presented via the Microsoft Teams platform on 12th September 2024 and evaluated by the following examining committee:

Prof. Dr. Fernando Fabriz Sodré

Chairman, Examination Committee (IQ/UnB)

Prof. Dr. Fabricio Machado Silva

Full Member, Examination Committee (IQ/UnB)

Prof. Dr. Walter Ruggeri Waldman

Full Member, Examination Committee (UFSCar/Campus Sorocaba)

Prof. Dra. Andreia Neves Fernandes

Full Member, Examination Committee (IQ/UFRGS)

Prof. Dr. Marcos Juliano Prauchner

Alternate Member, Examination Committee (IQ/UnB)

Prof. Dra. Cassiana Carolina Montagner

Alternate Member, Examination Committee (IQ/UNICAMP)

iii

DEDICATION

To Him, through Whom all is conceived and perfected.

ACKNOWLEDGEMENTS

You are forever in my heart.

ABSTRACT

This study investigated sorption between microplastics (MPs) and contaminants of emerging concern, notably sulfamethoxazole (SMX) and diclofenac (DCF) as models for hydrophilic and hydrophobic interactions. Polyethylene (PE), polypropylene (PP), and polystyrene (PS) were cryogenically milled to MP sizes (150 to 300 µm), while poly(vinyl chloride) (PVC) was obtained in micrometer size, and stored as fresh MPs. MP portions were treated to create UV-aged and humic acid-coated MPs, simulating potential environmental transformations. Characterization of the MPs indicates that UV exposure increased the crystallinity of PE and PS, but not for PP and PVC. Surface changes, including cracks, roughness and wrinkles, were noticed for all MPs after UV and humic acid modification, with a noticeable increase in oxygen-containing groups. The contaminants were individually exposed to the different MPs in simulated freshwater (SFW) and their remaining concentrations were measured after filtration (0.22 µm PVDF) using liquid chromatography tandem mass spectrometry (LC-MS/MS). Results showed that the sorption of both SMX and DCF onto fresh and modified MPs attained equilibrium within 24 h. The kinetic data were predominantly explained by the pseudo-second-order model, indicating a multi-step adsorption process of SMX and DCF onto the surface sites of MPs. The physicochemical properties of both the adsorbents and the adsorbates are primarily responsible for the adsorption behaviour and interactions. Five sorption isotherms models (Henry, Langmuir, Freundlich, Langmuir-Freundlich and Dubinin-Radushkevich) were fitted. In general, sorption rates increased with MP modification, ranging from 17.23 to 58.56% for SMX and from 12.03 to 60.82% for DCF, with the highest in UV-aged MPs. The sorption capacity of the MPs decreased in the following order: UV-aged PVC > PP > PS > PE > HA-coated PP > PE > PVC > PS > fresh PS > PVC > PE ≈ PP for SMX, and UV-aged PP > PVC > PS > PE > HA-coated PP > fresh PS > HA-coated PE > PS > PP > fresh PP > PE > PVC for DCF. All the isotherms exhibit a type-C shape, with some—especially those after treatment—approaching a type-L shape. Furthermore, all models demonstrated a good fit ($R^2 > 0.9$). The hydrophobic effect strongly influences the sorption capacity of fresh MPs, with possible contributions from van der Waals forces and π-π interactions. After modification, hydrogen bonding became more significant due to the presence of oxygen-containing groups on the microplastic surface. Desorption studies on fresh MPs were conducted in SFW, artificial gastric fluid (AGF), and artificial intestinal fluid (AIF). The results revealed that both contaminants desorbed across all media, with a gradual increase in desorption rate observed in SFW, while the rate remained constant in the gastrointestinal fluids. Desorption behaviour was likely influenced by analyte hydrophobicity, pH, and enzymatic activity of the biological fluids. All results indicate that MPs can interact with contaminants, adsorbing and transporting them in the environment, with the potential to release them into freshwater ecosystems and the fluids of exposed organisms, depending on environmental conditions and the organisms' biochemical nature.

Keywords: Microplastics; contaminants of emerging concern; sorption, photodegradation; humic substances; eco-corona.

INTERAÇÕES SORTIVAS DE SULFAMETOXAZOL E DICLOFENACO COM MICROPLÁSTICOS PRISTINOS, ENVELHECIDOS POR UV E RECOBERTOS COM ÁCIDO HÚMICO

Este estudo investigou a sorção entre microplásticos (MPs) e contaminantes emergentes, notadamente sulfametoxazol (SMX) e diclofenaco (DCF) como modelos para interações hidrofílicas e hidrofóbicas. Polietileno (PE), polipropileno (PP) e poliestireno (PS) foram moídos criogenicamente até tamanhos de MPs (150 a 300 µm), enquanto o policloreto de vinila (PVC) foi obtido em tamanho micrométrico e armazenado como MPs frescos. Porções de MPs foram tratadas para criar MPs envelhecidos por UV e recobertos por ácido húmico, simulando possíveis transformações ambientais. A caracterização dos MPs indica que a exposição aos raios UV aumentou a cristalinidade do PE e PS, mas não do PP e PVC. Mudanças de superfície, incluindo rachaduras, rugosidades e enrugamentos, foram observadas em todos os MPs após a modificação por UV e ácido húmico, com um aumento notável nos grupos contendo oxigênio. Os contaminantes foram individualmente expostos aos diferentes MPs em água doce simulada (SFW), e suas concentrações remanescentes foram medidas após filtração (PVDF de 0,22 µm) usando cromatografia líquida acoplada à espectrometria de massas em tandem (LC-MS/MS). Os resultados mostraram que a sorção de SMX e DCF nos MPs frescos e modificados atingiu o equilíbrio em 24 h. Os dados cinéticos foram predominantemente explicados pelo modelo de pseudo-segunda ordem, indicando um processo de adsorção em múltiplas etapas nos sítios de superfície dos MPs. As propriedades físico-químicas dos adsorventes e adsorbatos são as principais responsáveis pelo comportamento de adsorção e interações. Cinco modelos de isotermas de sorção (Henry, Langmuir, Freundlich, Langmuir-Freundlich e Dubinin-Radushkevich) foram ajustados. Em geral, as taxas de sorção aumentaram com a modificação dos MPs, variando de 17,23 a 58,56% para SMX e de 12,03 a 60,82% para DCF, sendo maior nos MPs envelhecidos por UV. A capacidade de sorção dos MPs diminuiu na seguinte ordem: PVC envelhecido por UV > PP > PS > PE > PP revestido por ácido húmico > PE > PVC > PS > PS fresco > PVC > PE ≈ PP para SMX, e PP envelhecido por UV > PVC > PS > PE > PP revestido por ácido húmico > PS fresco > PE revestido por ácido húmico > PS > PP > PP fresco > PE > PVC para DCF. Todas as isotermas exibiram uma forma tipo-C, com algumas—especialmente após tratamento—aproximando-se de uma forma tipo-L. Além disso, todos os modelos demonstraram um bom ajuste ($R^2 > 0{,}9$). O efeito hidrofóbico influencia fortemente a capacidade de sorção dos MPs frescos, com possíveis contribuições de forças de van der Waals e interações π-π. Após a modificação, a ligação de hidrogênio tornou-se mais significativa devido à presença de grupos contendo oxigênio na superfície dos MPs. Estudos de dessorção em MPs frescos foram conduzidos em SFW, fluido gástrico artificial (AGF) e fluido intestinal artificial (AIF). Os resultados revelaram que ambos os contaminantes dessorveram em todos os meios, com um aumento gradual na taxa de dessorção observado em SFW, enquanto a taxa permaneceu constante nos fluidos gastrointestinais. O comportamento de dessorção provavelmente foi influenciado pela hidrofobicidade do analito, pH e atividade enzimática dos fluidos biológicos. Todos os resultados indicam que os MPs podem interagir com contaminantes, adsorvê-los e transportá-los no ambiente, com o potencial de liberá-los em ecossistemas de água doce e nos fluidos de organismos expostos, dependendo das condições ambientais e da natureza bioquímica dos organismos.

Palavras-chave: Microplásticos; contaminantes emergentes, sorção; fotodegradação; substâncias húmicas; eco-corona.

LIST OF FIGURES

ix

LIST OF TABLES

LIST OF ABBREVIATIONS AND ACRONYMS

AGF	Artificial gastric fluid
AIF	Artificial intestinal fluid
CECs	Contaminants of emerging concern
DCF	Diclofenac
FTIR	Fourier-transform infrared spectroscopy
HA	Humic acid
LC-MS/MS	Liquid Chromatography Tandem Mass Spectrometry
MPs	microplastics
PE	Polyethylene
PP	Polypropylene
PS	Polystyrene
PVC	Poly(vinyl chloride)
PVDF	Poly(vinylidene fluoride)
PZC	Point of zero charge
SEM	Scanning electron microscope
SFW	Simulated freshwater
SMX	Sulfamethoxazole
UV	Ultraviolet

CONTENTS

1 INTRODUCTION

Plastics have revolutionized modern life over the years, offering unmatched versatility, durability, and affordability. These characteristics have made plastics indispensable in homes and industries ranging from packaging and construction to medical devices and consumer goods (Abuwatfa et al., 2021; Taheri et al., 2023). About 475 million tons of plastic materials have been produced from polymers (long chains of repetitive molecules) throughout the world between 1950 and 2021 (Rangel-Buitrago et al., 2022). The most widely used polymers are polyethylene (PE), polypropylene (PP), polystyrene (PS), polyvinyl chloride (PVC), polyethylene terephthalate, and polyurethane, with PE, PP, PS, and PVC alone accounting for 77% of the total market share (Ali et al., 2021). The very qualities that make plastics so useful also contribute to their prevalent presence as pollutants, and between 60 and 99 million metric tonnes of plastic waste were improperly managed annually as of 2021 (Williams & Rangel-Buitrago, 2019). According to Rangel-Buitrago et al. (2022), nearly 91% of all plastics discarded since 1950 have neither been reused, recycled nor recovered, and roughly 35% of used plastics end up directly in the environment. So far, an estimated 99 million tons of mismanaged plastic debris entering waterways worldwide (Jambeck et al., 2023). Environmental plastics pollution has emerged as a critical issue, with plastic debris infiltrating terrestrial, marine, and freshwater ecosystems (Wong et al., 2020). The resilience and stability of plastics, while beneficial in their intended applications, lead to long-term environmental persistence, particularly when they disintegrate into micro-sized particles known as microplastics (MPs), which may pose significant threats to wildlife and ecosystems (Desforges et al., 2014).

Microplastics, mostly referred to as plastic particles smaller than 5 mm (Arthur et al., 2009), have become a particular focus of environmental discussion due to their prevalence and potential hazards. So far, from the literature, these tiny particles originate from both primary sources, such as microbeads in personal care products and industrial plastic pellets, and secondary sources, where larger plastic items degrade through weathering and fragmentation (Khan et al., 2020; Peng et al., 2017; Saeedi, 2023). Both primary and secondary sourced MPs are difficult to differentiate in the environment, posing similar threats to nature. They have been repeatedly found in the environment at elevated concentrations in recent years (Ashrafy et al., 2023). The

widespread mismanagement of plastic waste worsens the problem, leading to the ubiquitous accumulation of MPs in diverse environments.

Microplastics undergo some kinds of transformations in environmental systems driven by physical, chemical, and biological processes. Physical weathering, such as abrasion and fragmentation, breaks down larger MPs into smaller particles, influencing their transport and persistence (Liu et al., 2020). Chemical ageing, such as oxidation, alters MPs' surface chemistry by introducing functional groups (e.g., carbonyl, carboxyl), thereby affecting their sorption affinity for both hydrophobic and hydrophilic organic contaminants in aquatic environments (Guo & Wang, 2019). Similarly, biological ageing, including natural organic matter, further modifies MPs by introducing organic coatings and facilitating degradation (Duan et al., 2021). These transformations collectively impact the fate and transport as well as their interactions across various environmental compartments, other pollutants and organisms.

Microplastics have been extensively studied for their interactions with environmental surroundings and co-existing pollutants (Du et al., 2022; Elizalde-Velazquez et al., 2020; Guo et al., 2019; Guo & Wang, 2019). These interactions with water constituents such as ions, natural organic matter, suspended organic matter, and other pollutants play a crucial role in influencing the bioavailability, toxicity, and transformation processes of MPs and associated contaminants. These processes significantly impact the ageing dynamics of MPs. For instance, humic acid (HA), a ubiquitous natural organic matter component, has been documented to either facilitate or hinder the photooxidation of water pollutants and MPs (van Zomeren, 2008; Wu et al., 2021).

Various intermolecular forces and van der Waals interactions between MPs and pollutants in freshwater ecosystems have been reported by Xiang et al. (2022). Li et al. (2022) investigated the interactions between Cr and MPs to be electrostatic, surface complexation and van der Waals force of attraction. Another study by Liu et al. (2022) has reported π-π conjugated, halogen bonding and electrostatic interaction for Pb, Cu, Cr and Cd with polypropylene (PP), polystyrene (PS) and polyvinyl chloride (PVC) in freshwater. Similar interactions exist between most MPs and organic pollutants. Guo et al. (2019) proposed electrostatics and hydrogen bonding interactions between sulfamethoxazole (SMX) and six different microplastics while Tseng et al. (2022) found van der Waals and π-π interactions between polyethylene (PE), PS and PVC, and six contaminants of emerging concern (CECs). Interaction studies involving aged MPs involving artificial ageing

using ultraviolet (UV-A) and HA-coating have also been reported. Also, the desorption of progesterone from MPs in simulated biological has been reported by Siri et al. (2021).

1.1 Objective of the study

As far as we know, only a small number of studies have exposed MPs to UV-C light (Lin et al., 2020; Liu et al., 2023), particularly PE, PP, PS, and PVC, which dominate global production and are frequently reported in the environment (Ali et al., 2021; Dimitris & Achilias, 2014). MPs interact with both hydrophobic and hydrophilic organic pollutants, as well as natural organic matter such as biofilm, humic acid, and fulvic acid in environmental systems (Du et al., 2022; Elizalde-Velazquez et al., 2020; Guo et al., 2019; Guo & Wang, 2019; Leiser et al., 2020; Xu et al., 2018a), but information on their interactions with diclofenac (DCF) and sulfamethoxazole (SMX) is limited. Moreover, no studies have investigated the coating of MPs with humic acid prior to conducting adsorption with organic contaminants experiments. Existing research has either focused on the interaction of humic acids as adsorbates with MPs or the simultaneous interaction of organic contaminants with humic or fulvic acids. Lastly, there are limited studies on the release of organic pollutants commonly found in the environment into environmental systems, as well as into biological fluids prepared using comprehensive formulations (Siri et al., 2021). Therefore, this study aims to investigate sorption interactions between common MPs (PE, PP, PS, and PVC) and hydrophilic (SMX) and hydrophobic (DCF) environmental contaminants under varying environmental conditions.

1.1.1 Specific objectives

Specifically, this study seeks to:

i. prepare fresh microplastics from purchased plastic pellets and modify them by UV-C and humic acid exposure;

ii. physicochemically characterize fresh and modified MPs;

iii. investigate the sorption mechanisms and interactions between fresh and modified MPs and the analytes in simulated freshwater; and

iv. investigate the desorption rate of the environmental contaminants from the fresh MPs in artificial gastric fluid and artificial intestinal fluid.

2 LITERATURE

This chapter explores current knowledge related to the sorption interactions between microplastics and environmental contaminants. It delves into the properties of various plastic polymers and their ability to sorb hydrophilic and hydrophobic substances from aquatic environments. Understanding these interactions is essential for evaluating the potential environmental impacts of microplastic pollution.

2.1 Plastics

Plastic, one of the world's most extensively produced and used materials, is composed of synthetic organic polymers, which are often generated by polymerizing monomers sourced from petroleum, coal, or biologically-based substances (Bellasi et al., 2020). The term "plastic" was derived from the word "pliable," which means "easily shaped." Plastics were discovered in the nineteenth century with the invention of vulcanized rubber and polystyrene, and they continue to play an important role in both technical innovation and everyday life up till today. Plastic mass production began in the 1950s with an annual growth of about 8.4% due to its durability, corrosion and chemical resistance, lightweight, flexibility, strength, easy processability and cheaper cost. The global plastic output of 373 megatons (Mt) in 2020 and 7.1 Mt in Brazil in 2021, with disposable items accounting for about half of that total (ABIPLAST, 2022; Barnes et al., 2009; Sarkar & Aparna, 2020; C. Zhang et al., 2020).

Plastics are classified based on some factors, including polymer source, usage, and life cycle. The useful lifespan of plastic materials could be short, average or long with $0 - 1$, $1 - 5$, and more than 5 years, respectively (ABIPLAST, 2022). Polymers can be sourced from both petroleum-based and biologically-based materials. Petroleum-based polymers are derived from crude oil and non-renewable fossil fuels. Conversely, biologically-based polymers, also known as biopolymers, are produced using renewable biomass, including plants, algae, bacteria, and other similar sources. Some plastics exhibit unique characteristics, such as rapid biodegradation in the environment, while many others do not and take years to degrade. This distinction has led to a growing interest in biodegradable plastics across various sectors, including packaging, agriculture, medical devices, and single-use products (ABIPLAST, 2022; Singla, 2020).

Among the hundreds of plastics' polymer sources, PE, PP, PS, polyethylene terephthalate, PVC, and polyurethane which are all thermostatic account for about 77% of global plastic demand, and they are, unfortunately, most found plastic debris in the environment due to a wide and, sometimes, uncontrollable usage; resistant to biodegradation, inadequate waste management system, and unsafe disposal practices (C. Zhang et al., 2020). Plastic debris has become a global concern due to its extensive dispersion and environmental consequences, and it (of all sizes) has accumulated in the environment over time and has been documented in every environmental compartment and matrix.

2.2 Physicochemical properties of MPs considered in this study

Polymers generally exhibit several physicochemical characteristics that determine their mode of production, strength, applications and weathering of plastic materials in the environment, among others. These properties are somewhat peculiar to each polymer type. Some of these properties are considered below.

2.2.1 Crystallinity

Polymer crystallinity is the extent to which the polymer chains are aligned with each other. It influences the degree of regularity of the monomolecular chains, which could be crystalline, amorphous, or semi-crystalline. Crystalline polymers exhibit well-organized molecular chains, tightly packed to form crystalline domains with repetitive chain alignment. Unfortunately, there is no polymer with a completely crystalline domain. Amorphous polymers have a random, disordered arrangement with no defined crystalline regions in their molecular chains, while semi-crystalline polymers contain both amorphous and crystalline regions, giving them a combination of properties from both types (see Figure 1). The ability of a polymer to be crystalline at any condition depends on the chemical makeup, and the orientation of a chain into a regular array of crystalline domain depends on the stereoregularity of the monomers (Nicholson, 1991; O'Driscoll, 1964).
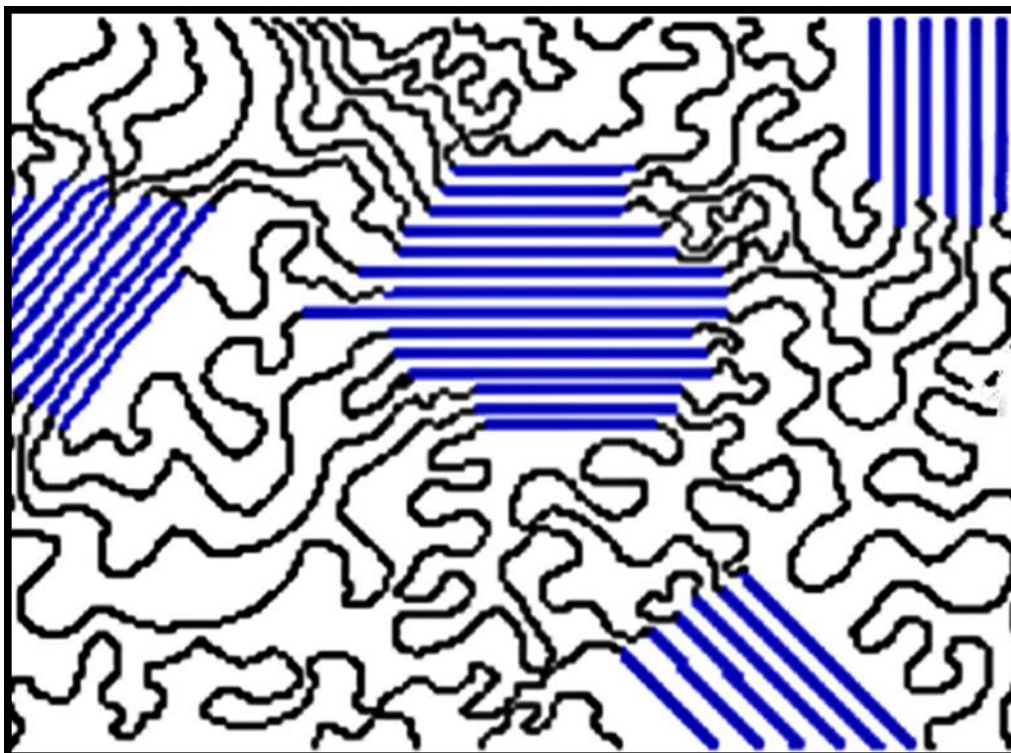
Figure 1. Schematic of a semi-crystalline polymer, with the crystalline regions represented by the blue line and the amorphous regions by the black line.

2.2.2 Particle Size distribution

The particle-size distribution represents a collection of values that characterizes the proportionate mass of particles in a material based on their respective sizes. In material characterization, particle size represents a fundamental attribute of materials, playing a significant role in comprehending their properties, such as reactivity, surface area, and flowability (Bittelli et al., 1999). Gaining insight into the particle-size distribution of MPs aids in a more accurate characterization and comprehension of their behaviour within the environment.

2.2.3 Surface morphology

The surface morphology of polymeric materials plays a crucial role in determining their wettability, adhesiveness, and suitability for various processes such as printing, dyeing, lamination, water repellency, and biocompatible activities. Different polymers exhibit diverse characteristics and structural arrangements, which ultimately influence their resulting morphologies. Key factors like molecular weight, crystallinity, branching, and crosslinking might impact the overall polymeric structure and, consequently, the final surface morphology. It is

essential for understanding the surface characteristics, ageing level and the environmental trajectory of MPs (Borghi et al., 2018; Popelka et al., 2020).

2.2.4 Zeta potential

Zeta potential is the electrostatic potential within the electrical double layer encompassing a nanoparticle in a solution. In simple terms, zeta potential refers to the surface charge exhibited by nanoparticles when they are in a solution. It is deduced from the electrical double layer (EDL) on the surface of the suspended particles (Figure 2), and it determines the attractive and repulsive forces between the particles. This particular characteristic plays a crucial role in assessing the stability of colloidal dispersions. (Clogston & Patri, 2011a).
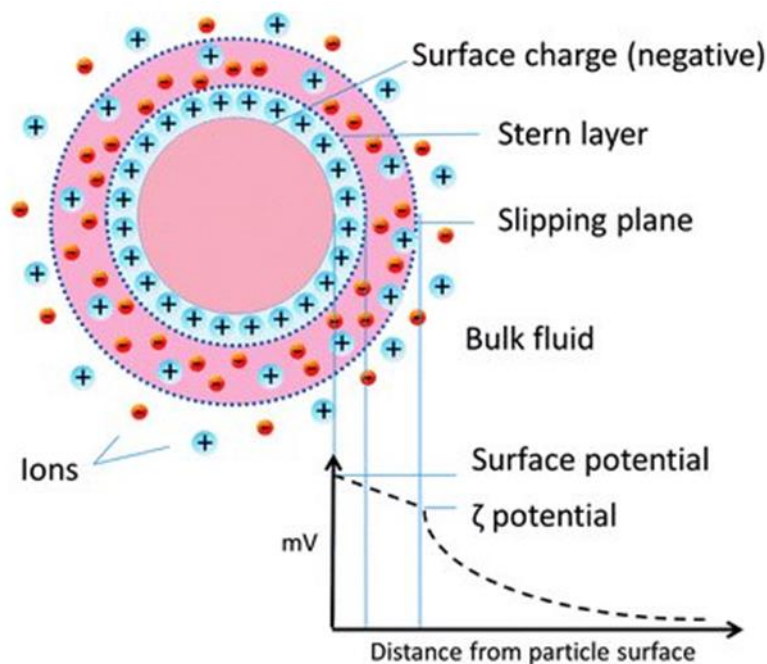
Figure 2. Zeta potential deduced from double-layer configuration
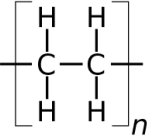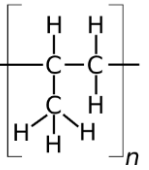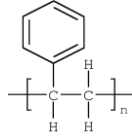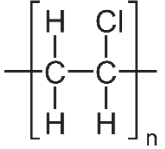
2.3 Properties of studied MPs

2.3.1 Polyethylene

Polyethylene is a versatile and widely used thermoplastic polymer in packaging materials, bottles, and household items. PE can be classified into five types based on its density: low-density polyethylene (LDPE), linear low-density polyethylene (LLDPE), metallocene linear low-density polyethylene (mLLDPE), very low-density polyethylene (VLDPE), and high-density polyethylene

(HDPE). LDPE is known for its flexibility and resistance to impact and chemicals, while HDPE is tough, chemically resistant, and UV radiation resistant. LLDPE is a blend of LDPE and HDPE, which has improved tensile strength and puncture resistance. LDPE and HDPE are the most commonly used forms of polyolefin in food packaging. PE has unique physicochemical properties that make it a popular choice for a wide range of applications in various industries, and in turn, it is ubiquitous in the environment. PE has a high degree of crystallinity and a low glass transition temperature. PE is highly resistant to chemicals due to its non-polar nature, which makes it an ideal material for several industrial applications. It has a low surface energy and lacks a permanent electric charge, leading to a low potential of zero charge (PZC) and making bonding much more difficult. The density of PE can vary depending on the specific type, ranging from 0.89 to 0.98 g/L, with a typical tensile strength of 45-90 MPa (Sarkar & Aparna, 2020). Table 1 presents selected physicochemical properties of the MPs examined in this study, adapted from Miloloža et al. (2020) and Duis and Coors (2016).

Table 1. Some physicochemical properties of studied MPs

Polymer	PE	PP	PS	PVC
Structure				
Crystallinity (%)[a]	45 – 95	50 – 80	0	5 – 15
Density (g/L)[a, b]	0.91 – 0.97	0.83 – 0.97	0.90 – 1.05	1.16 – 1.58
T_m (°C)[a]	90 – 130	168 – 175	240 – 270	200 – 310
T_g (°C)[a]	(-120) – (-52)	(-20) – (-10)	74 – 105	75 – 105
Tensile strength (MPa)[a]	8 – 32	31 – 41	36 – 52	41 – 52
Estimated lifespan (year)[a]	10 –600	10 – 600	50 – 80	50 – 150

T_g = glass transition temperature; T_m = melting temperature; [a] = (Miloloža et al., 2020); [b] = (Duis & Coors, 2016)

2.3.2 Polypropylene

Polypropylene is one of the two common thermoplastic polyolefins. It is more transparent, harder and less dense than PE and finds application in numerous products, including food packaging, textiles, and automotive parts. PP is characterized by a high melting point, and

excellent resistance to heat, chemicals, and fatigue. PP possesses impressive stiffness, toughness, and dimensional stability, making it an ideal material for manufacturing caps and closures, disposable cups, and medical devices. Its excellent chemical resistance and other properties have resulted in its widespread usage in the automotive and medical industries. The density of PP ranges from 0.83-0.92 g/L, which is lower than that of PE. PP can exhibit high crystallinity, resulting in superior mechanical properties, with typical tensile strengths of around 36-52 MPa, rendering it a robust and durable material.

2.3.3 Polystyrene

Polystyrene (PS) is an exceptionally useful thermoplastic polymer that finds extensive application in the production of packaging materials, insulation, and disposable cups. This material possesses a low density, high stiffness, and outstanding electrical insulation properties, including dielectric. The two most common categories of PS are general-purpose polystyrene (GPPS) and high-impact polystyrene (HIPS). While GPPS is transparent and brittle, HIPS is opaque and displays superior impact resistance. It has a relatively high glass transition temperature of between 74-105 °C and a high melting temperature of 240-270 °C. PS is a reliable and adaptable polymer with a density of 1.04-1.1 g/L. PS has a low PZC, making it a material of choice for electrophoresis applications. In terms of strength, PS has a typical tensile strength of 36-52 MPa, making it a resilient and durable material (Guazzotti et al., 2022; Peters, 2002).

2.3.4 Polyvinyl chloride

Poly(vinyl chloride) is a thermoplastic polymer that finds wide application in construction materials, medical devices, and packaging materials. Its high chlorine content provides excellent resistance to heat and chemicals. PVC comes in two forms: rigid PVC and flexible PVC. Rigid PVC is a hard, inflexible material employed in pipes, windows, and doors, while flexible PVC is more pliable and used in medical tubing, inflatable products, and electrical cable insulation. However, recycling can be challenging due to the presence of additives and contaminants in PVC. With a relatively high density of 1.16-1.58 g/L, PVC is a dense material with low PZC. Its low crystallinity enhances flexibility and elasticity, making it a versatile material for diverse applications. PVC's tensile strength ranges from 41-52 MPa, making it a robust and durable material (Amobonye et al., 2023).

2.3.5 Hydrophobicity of the microplastics

Polymer hydrophobicity refers to the degree to which a polymer repels or resists interaction with water molecules. This property is critical in various applications, as it influences the material's behaviour in aqueous environments and its suitability for specific uses. Among the four microplastics studied, PVC exhibits the least hydrophobicity due to the presence of chlorine atoms, which draw electron density towards themselves (Meng et al., 2024). This creates a partial negative charge on the chlorine atoms, leaving the hydrogen atoms bonded to the same carbon with electropositive properties. Both PE and PP, as well as PS, lack polar groups in their backbones, rendering them more hydrophobic. The non-polar methyl group in PP and the even more non-polar benzene group in PS contribute to their increased hydrophobicity compared to PE (Hossain et al., 2019). PS emerges as the most hydrophobic among the studied microplastics, and the ascending order of hydrophobicity among the microplastics is PVC < PE < PP < PS (Lee et al., 2014; Lin et al., 2020).

2.4 Demand and production

Plastic is widely utilized in a variety of industries and goods, including construction, agriculture, manufacturing, medicine, electronics, furniture, packaging, and household appliances among others (Vadera & Khan, 2021). They submitted that plastics are used in the production of about 85% of the world's medical equipment and more than 2 million plastic bags and bottles are daily consumed in the packaging industry. Construction, foods, and wholesale and retail products account for 23.9, 21.6, and 8.1% of total plastics demand in Brazil (Figure 3), and they use synthetic polymers with long, short, and average useable life cycles, respectively (ABIPLAST, 2022).
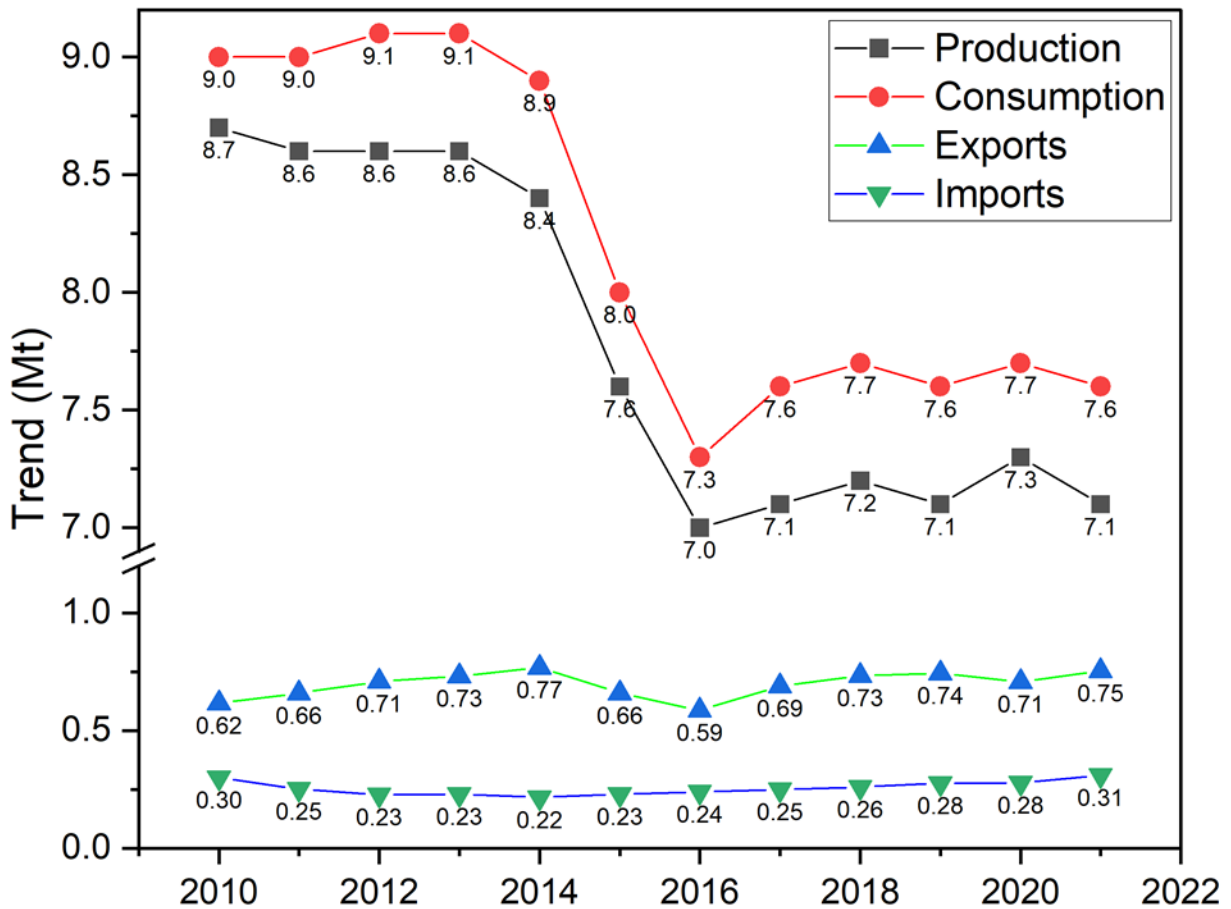
Figure 3. Brazilian plastic data. Data adapted from ABIPLAST (2022).

2.5 Environmental plastic waste

Plastic garbage is becoming an ever-increasing environmental hazard due to its unique properties, massive consumption and ubiquitous presence in all environmental compartments throughout continents, including Antarctica. Unfortunately, owing to the world's economic development and population increase, plastic waste is rapidly generated and exposed, and only around 9% of the world's plastic garbage was recycled, and 11% in Brazil, in 2021, which was a mere portion of global plastic output annually. They have been found across coastal ecosystems, accounting for about 85% of aquatic debris, and have substantial repercussions for ecosystems and organisms in a range of forms (Evode et al., 2021; Lee et al., 2019). Despite the fast growth in plastic use, little attention has been given to the influences of plastic debris on solid waste

management systems, which have been required to adjust to an inflow of new and unpredictable materials entering the solid waste stream.

Plastics enter aquatic environments either directly or indirectly by wind (Zhang, 2017), birds (Kang et al., 2023; Provencher et al., 2018), and runoff (Windsor et al., 2019), among other means, and they can be classified as sea-based and land-based sources. Considering anthropogenic sources, oil and gas platforms, maritime activities, and tourism are examples of sea-based sources where plastics are dumped into or mistakenly lost in aquatic bodies. While littering in public, improper trash disposal, waste dump run-offs, tourism, industrial operations, and combined sewer systems are all land-based sources, and they are estimated to account for 80% of aquatic litters (Donohue, 2005; Jambeck et al., 2015). According to Ryberg et al. (2019), microplastics may be lost into the environment during production, transportation and end-of-life stages, and they calculated about 9.2 Mt of plastics were released into the environment until 2015, consisting of 6.2 Mt macroplastics and 3.0 Mt microplastics, throughout the world.

Packaging and single-use plastics which, are consumed by almost every individual, are dumped in the trash stream shortly after use, contributing to the global problem inexplicably (Brooks et al., 2018). Before the 1950s, most fishing equipment and disposable packaging materials in the United States and Africa were made of biodegradable materials such as hemp rope or paper bags, which degraded fast, especially in the marine environment (Gregory, 2009; NOAA, 2014). The first research on aquatic plastic trash was published in the 1970s, and thereafter, several species, including marine mammals, seabirds, sea turtles, fish, crabs, corals, and others are reported at risk of entanglement due to lost or abandoned fishing gear and non-disposable plastics that are introduced to the aquatic environment as a result of the growing popularity of plastics in fishing and land-based activities.

2.6 Transformation and degradation of plastics in the freshwater ecosystem

Plastics' exceptional resistance to environmental conditions has differentiated them since their discovery, and it is one of the main reasons for their continuous global demand and mass production. Despite their resilience, plastics in the environment degrade at some points, and they disintegrate slowly. Because plastic debris is sourced from many commercially available synthetic polymers, they form *heteropolymers* in the environment. Polymer type usually influences

physicochemical properties, especially in the environment, bioavailability and degradation pattern. The degradation processes of plastics in the aquatic environment determine the fate, distribution, and aggregation of microplastics in the ecosystem (Klein et al., 2018).

2.6.1 Degradation

Polymer degradation refers to changes in properties caused by chemical, physical, or biological reactions, leading to bond scissions and chemical transformations. Degradation, whether occurring naturally in the environment or mimicked in the laboratory, is a complex process. Monitoring it can be laborious due to the heterogeneous components of plastics, which include monomers and chemical additives (Sun et al., 2020). Polymer degradation indicates that they have been subjected to a variety of circumstances for an extended period, causing their shape and other properties to change to some extent. The rates of plastic degradation are significantly influenced by the types and quantity of additives it contains. For example, the use of anti-oxidants and stabilizers as additives hinders the degradation of the polymer, whereas pro-oxidant additives render it more degradable. Also, the addition of starch can enhance biodegradability of some plastic materials, but this effect relies on the presence of a pro-oxidant (Gewert et al., 2015). The chemistry of the degradation process is influenced by several factors such as the type of plastic, its chemical composition, and the conditions of exposure to UV radiation. Different plastics have different chemical structures and properties, which can affect their susceptibility to weathering due to UV radiation.

Many studies have been reported on this, but experts are still curious about the degradation mechanisms, duration, and endpoint. The study of plastic ageing has been carried out by field observation and laboratory simulations. Through outdoor exposure, samples placed on testing racks are subjected to typical environmental conditions, allowing material ageing to be observed over time while the laboratory ageing replicates outdoor conditions using environmental chambers and artificial light sources. The correlation to real field behaviour diminishes with faster tests (Singh & Sharma, 2008). Although field monitoring has limitations due to environmental, geographical, and other complex factors, laboratory simulation is a preferable technique to understand the core process and mechanism of plastic weathering. Furthermore, under environmental stress, the adsorption of persistent organic pollutants, metals, microbes, and the production of bio-films, among other physicochemical factors, add to the process' complexity

([Kühn et al., 2018](#); [Sun et al., 2020](#)). Literature has it that polymer degradation can proceed through several mechanisms such as ([Cai et al., 2021](#); [Doğan, 2021](#); [Mena et al., 2020](#); [Wang et al., 2021b](#)):

a) Photodegradation (primarily initiated by light radiation)

b) Chemical degradation (oxidation or hydrolysis)

c) Biodegradation (initiated by organisms)

d) Oxidative (oxygen depended)

e) Thermo-oxidative degradation (initiated by heat in the presence of oxygen)

f) Thermomechanical degradation (initiated by heat under shear)

g) Thermal degradation (initiated by heat in an inert atmosphere), among others

Considering the environmental conditions that can influence the ageing of plastics, many of the mechanisms listed above are extremely limited, plastic ageing in the environment is usually a slow process. For example, the biodegradability of plastics in aquatic ecosystems depends on their (plastics) wettability for microorganisms to successfully colonise their surfaces, and most fresh plastics in the environment are not wettable. Similarly, the process of ageing, driven by oxidation, is significantly accelerated by stress and electron excitation agents such as sunlight. Moreover, chemical changes in synthetic polymers due to thermal effects may not occur because the ambient temperature are often insufficient to thermally initiate plastic ageing. Also, the mechanical forces in aquatic ecosystems, such as waves, currents, and tides, have also been identified as initiators of plastics ageing, but their contribution to the rate of degradation remains uncertain ([Min et al., 2020](#)). Meanwhile the collective effects of all these forces may accelerate plastics degradation in the environment.

Photodegradation

The weathering of plastics due to UV radiation occurs when the particles are exposed to sunlight and other UV light sources like mercury vapour lighting, tanning beds, etc. UV light is highly energetic and has a wavelength of 100 to 399 nm which is shorter than the wavelength of visible light. UV radiation causes some chemical reactions in exposed substances, and in plastics, it initiates the degradation process as described by the autoxidation circle in Figure 4, autoxidation applies to all forms of plastics degradation, and more details about it are presented in the next section. The chemistry of the fragmentation of microplastics due to UV radiation involves a

complex set of chemical reactions in exposed substances. When UV radiation penetrates the plastic surface, it can interact with the chemical bonds present in the plastic molecules and cause them to break apart. Photodegradation is influenced by the intensity of the light radiation, the duration of exposure, and the properties of the plastic, e.g. chemical composition, size and shape. The smaller the particle, the greater the surface area of photo exposure and the more susceptible it is to degradation (Grigg, 2006).
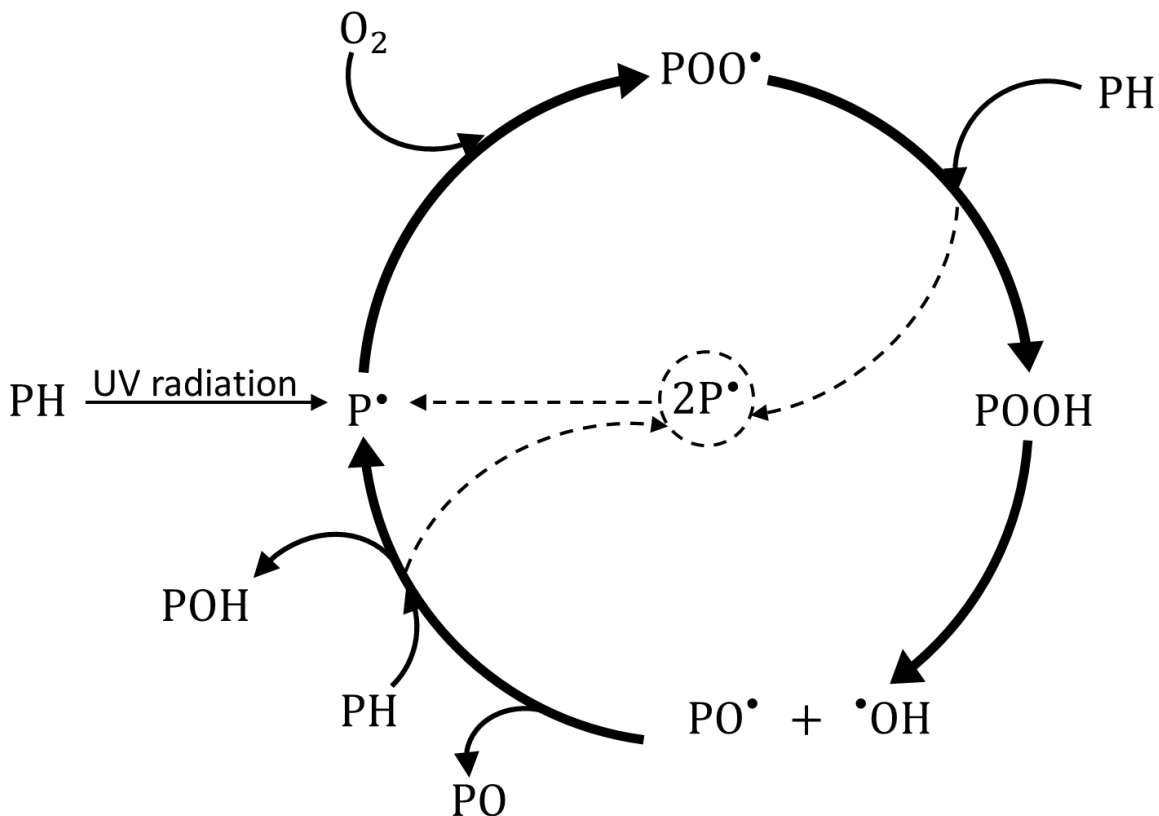
Figure 4. The autoxidation cycle. Adapted from Grigg (2006), Mena et al. (2020) and Sodré et al. (2023) with slight modification.

Autoxidation refers to the spontaneous oxidation of compounds or substances by molecular oxygen in various systems, following thermal, mechanical, or photochemical exposure. These external forces are prerequisites as thermodynamic and kinetic factors make the direct reaction of the polymer with molecular oxygen unfavourable. During the photochemical exposure, the polymer absorbs light, leading to excited states of the polymer's compound. The excitation susceptibility of a polymer depends on its structure and the presence of possible impurities. In polymers, some of the high degrees of branching, functional groups and unsaturation in the

backbones are chromophore in nature. However, polyolefins, such as PE, are saturated and lack essential functional groups that can absorb UV radiation, making them theoretically resistant to photodegradation (Hawkins, 1984). However, the presence of impurities and defects, which were introduced during polymer processing under conditions of high temperature and mechanical shear, as carbonyl groups, peroxy radicals, and unsaturations leads to the absorption of UV radiation and accelerates photodegradation reactions. Also, the catalysts (transition metals, radical initiators), monomer impurities and traces of oxygen react, creating peroxy radicals ($POO^{\bullet}$) that remove hydrogen from the polymer, resulting in the formation of an alkyl radical and a hydroperoxide which are potential photo radiation absorbers during the exposure (Grigg, 2006). The processes of polymer photodegradation occur in four stages according to the autoxidation circle, as shown in the equations presented in Figure 5, which are initiation, propagation, chain branching and termination.

Initiation:

$$PH \longrightarrow P^{\bullet} + P^{\bullet} \qquad \text{Equation 1}$$

Propagation:

$$P^{\bullet} + O_2 \longrightarrow POO^{\bullet} \qquad \text{Equation 2}$$

$$POO^{\bullet} + PH \longrightarrow POOH + P^{\bullet} \qquad \text{Equation 3}$$

Chain branching:

$$POOH \longrightarrow PO^{\bullet} + {}^{\bullet}OH \qquad \text{Equation 4}$$

$$POOH + POOH \longrightarrow PO^{\bullet} + POO^{\bullet} + H_2O \qquad \text{Equation 5}$$

Termination:

$$P^{\bullet} + P^{\bullet} \longrightarrow Non\ radical\ products \qquad \text{Equation 6}$$

$$P^{\bullet} + POO^{\bullet} \longrightarrow Non\ radical\ products \qquad \text{Equation 7}$$

$$POO^{\bullet} + POO^{\bullet} \longrightarrow Non\ radical\ products \qquad \text{Equation 8}$$

where PH is a macromolecular material, $P^{\bullet}$ is a radical, $POO^{\bullet}$ is a peroxy radical, $POO^{\bullet}$ is a hydroperoxide, $PO^{\bullet}$ is an alkoxy radical and ${}^{\bullet}OH$ is a hydroxyl radical.

Figure 5. Basic autoxidation reactions

Initiation is the first stage of the circle where the chromophore groups in the polymer backbone absorb sufficient light energy that leads to the formation of an alkyl radical (Equation 1). Alternatively, the peroxy radicals that were produced during the polymerization process may decompose upon absorbing photo radiation, resulting in the release of free radicals. This process precedes the spontaneous oxidation stage (Grigg, 2006; Mena et al., 2020).

In the **propagation** stage, the radicals then impulsively react with the ambient molecular oxygen to produce peroxy radicals according to Equation 2, which abstract hydrogen atoms from the polymer to form hydroperoxide groups and a new peroxy radical Equation 3. Due to the macromolecular nature of polymers, the peroxy radical can be primary, secondary or tertiary radical, which the stability of the radicals depends on. This reaction has low or no activation energy and is mostly unaffected by temperature but relies on the amount of oxygen, radical structure and light intensity. An increase in the radiation energy increases the rate of the reactions and subsequently increases the kinetic chain length, which is the number of propagation circles before the termination stage. These propagating reactions involve all carbon backbone polymers, generating hydroperoxide species which is crucial for the backbone cleavage. The abstraction process can occur intramolecularly, involving the removal of a hydrogen atom from the same polymer chain, or intermolecularly, removing from an adjacent molecule (Grigg, 2006).

Continuous exposure of polymers to light radiation leads to the breakdown of hydroperoxides via homolytic cleavage of the hydroperoxide groups at the O-O bond (Equation 4). This is primarily due to the low bond energy of this group (<200 kJ/mol) compared to the O-H and C-H bonds in the hydroperoxides which are approximately 500 and 417 kJ/mol, respectively. Consequently, this cleavage results in the formation of alkoxy and hydroxyl radicals. The cleavage of C-C or C-O bonds within the polymer chain is also possible. For example, in the case of PE, which is a commonly plastic used in packaging materials, fragments through the cleavage of C-C bonds. These radicals then abstract hydrogen from the polymer, leading to **chain branching** formation. At low light intensity, the hemolytic decomposition of the hydroperoxide is not favoured; instead, it promotes bimolecular decomposition, resulting from the interaction of two hydroperoxide radicals to produce alkoxy and peroxy radicals and water (Iyer et al., 2019) as represented in Equation 5. Conversely, at high incident light energy, homolytic decomposition

occurs before the accumulation of two hydroperoxide groups becomes possible. This autocatalytic effect of chain branching explains the self-acceleration of polymer oxidation.

Polymer autoxidation comes to a halt when the two radicals recombine, yielding an inert product at the **termination** stage through chain scission or crosslinking (Equation 6-8). This process can take place spontaneously, artificially in the presence of plastic stabilizers, or under conditions of high propagation oxygen pressure. Occasionally, an intermediate tetraoxide forms as a result of radical recombination, which eventually leads to the formation of the terminating products (Equation 9).

$$POO^{\bullet} + POO^{\bullet} \rightarrow POOOOP \rightarrow Inert\ products \qquad\qquad \text{Equation 9}$$
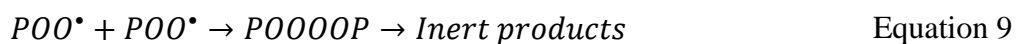
These termination products depend largely on the type of peroxy radical that is propagated. If the primary or secondary radical, the intermediate tetroxide will decompose into a carbonyl, an alcohol and oxygen molecules following the Russell mechanism (Figure 6). However, if it is a tertiary radical, two alkoxy radicals and an oxygen molecule will be produced. Possibly, with tertiary peroxy radical, an oxygen molecule and peroxide can be produced, where the peroxide linkage photolytically decomposes to an alkoxy radical that proceeds to the propagation stage of another autoxidation cycle.
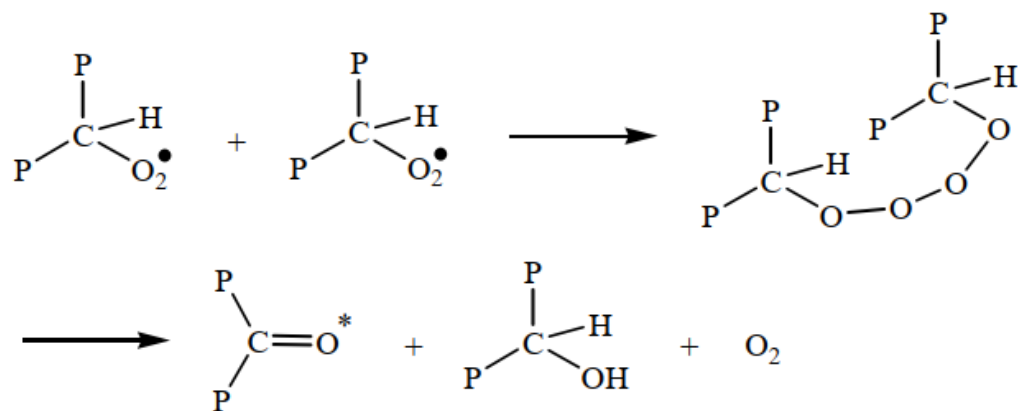
Figure 6. The Russell mechanism for peroxy radicals termination

The surface chemistry of UV-degraded microplastics can be significantly altered due to the breakdown of chemical bonds and the formation of reactive chemical groups on the surface of the particles. Plastic degradation can result in the exposure of previously buried or hidden functional groups on the surface of the plastic. One of the most common groups formed on the surface of

UV-degraded microplastics is carbonyl groups, which are highly reactive and can undergo further chemical reactions, such as condensation with other carbonyl groups or with nucleophiles in the environment. Other functional groups that can be formed on the surface of UV-degraded microplastics include carboxyl, hydroxyl, and amino groups. These groups are formed due to the oxidation of different types of chemical bonds present in the plastic molecules and can also undergo further chemical reactions in the environment.

As suggested by the autoxidation model, a degradation circle is continuous after a photochemical, mechanical or thermally initiation. The presence of reactive functional groups (carbonyl, carboxyl and hydroxyl) on the surface of UV-aged MPs can significantly impact their (MPs) interactions with the environment and living organisms. For example, they (the groups) can increase the wettability of UV-aged, making them accessible to microorganisms and other polar molecules in the environment. Additionally, the reactive groups can also facilitate the adsorption of organic and inorganic molecules onto the surface of the particles, potentially leading to the accumulation of harmful chemicals.

2.6.2 Ecological corona (eco-corona)

It is widely acknowledged that the majority of particles, including MPs, found in organic-rich aquatic systems are covered by a thin layer of natural organic material (NOM), specifically humic substances which are complex, heterogeneous and naturally occurring organic compounds in most of the environmental compartments (Grassi et al., 2000). The interaction of MPs with their surrounding environment, particularly the aquatic environment, is due to their complex physicochemical surfaces to form "eco-corona". When MPs are released into the environment, they can become coated with organic and inorganic colloids, including biomolecules (such as proteins and lipids), microorganisms, chemicals, environmental pollutants, and metals, through interactions like van der Waals forces, hydrogen bonding, electrostatic interactions, and hydrophobic forces, among others (Athulya & Chandrasekaran, 2023). This coating can potentially alter their behaviour, toxicity, and fate in the environment (Abbas et al., 2020).

"Eco-corona" refers to a collection of biomolecules and natural colloids that adhere to the surface of microplastics. The composition of colloids is not exactly the same in aquatic ecosystems based on their different physicochemical properties such as temperature and pH, as well as the

biotic and abiotic composition of the aquatic environment. Colloids have been reported to range in size from 1 nm to 10 µm (Bowen & Jenner, 1995), and due to their significantly smaller particle size, they can remain suspended in water systems over time. The formation of the eco-corona can either enhance or reduce the toxicity of microplastics, depending on the nature of the materials that form the aggregate. Bio-organic aggregates, for example, have been shown to decrease the toxic effects of certain microplastics (Athulya & Chandrasekaran, 2023).

The impacts of eco-corona on MP surfaces have been studied extensively (McColley, 2023; Shi et al., 2023; Witzmann et al., 2022). Ali et al. (2024) and McColley (2023) reported that eco-corona formation alters the physicochemical characteristics, fate, distribution, uptake, transport, biotransformation, and toxicological effects of MPs in aquatic environments. These changes influence the behaviour of MPs and play a crucial role in shaping their environmental impact and associated risks as Ali et al. (2024) suggested that eco-coronated MPs are more hazardous than pristine MPs. In his study, McColley (2023) found that HA coating on MPs enhanced the adsorption of Cu onto PS but hindered the adsorption of Zn and Cu onto PVC compared to uncoated plastics. HA, as a crucial element of humic substances, play a significant role in the behaviour of aquatic microplastics and requires in ongoing research concerning MPs.

Humic substances coating of MPs

Humic substances are brown or black diverse mixtures of polydispersed solid materials resulting from decomposition or decay of organic matter (primarily plant and microbial) followed by biosynthesis or humification (Ghabbour & Davies, 1998; Sharma & Anthal, 2016). They are richer in carbon than other living things and exist in organisms, soils, sediments and water; important for many life-sustaining processes; redox-active, and surface-active (i.e. bind to the surface of other substances) in the environment. humic substances exist in three classes based on their molecular weight, aggregation and mineral contents (Ghabbour & Davies, 1998).

Humic acids acid the largest class of humic substances, very rich in carbon and stabilize soil organic matter. Their solubility in water depends on pH; particularly insoluble at pH<2. Table 2 compares some of the elemental and functional group components of HA and fulvic acids. Fulvic acids are the smallest members of humic substances and can dissolve in water at all pH. They adsorb UV radiation and control the natural UV activities in aquatic environments. Humins are the

last class of humic substances, and they are coal-like. Humins are insoluble at all pH and exhibit weaker water retention, sorption, and metal binding capabilities compared to other humic substances, but have a higher aromatic nature (Ghabbour & Davies, 1998).

Table 2. Comparison of some elemental functional group components of HA and FAs (Sharma & Anthal, 2016)

Component	HA	FA
MW	>3,500 Da	<3,500 Da
C	+	−
H	−	+
O	−	+
Total acidic group	−	+
Carboxylic acid	−	+
Phenolic OH	≈	≈
Alcoholic OH	−	+
Keto C=O	+	−
Methoxy OCH3	−	+

HA = humic acids, FA = fulvic acids, MW = molecular weight, C = carbon, H = hydrogen, O = oxygen, Da = Dalton, + = more, − = less, ≈ = equivalent to

Humic substances are widely distributed in natural waters, and environmental MPs have been reported to interact with them. Due to the surface chemistry of both MPs and humic substances, various functional groups in particular, humic substances will inevitably interact with MPs and occupy most, if not all, of their active sites, leading to humic substances -MPs coating. Hydrophobic, and n-π and π-π electron donor-acceptor interactions have been reported between these substances. The ageing level of MPs and the type of humic substances would determine the level of the coronated MPs. This would impact the physicochemical properties, adsorption characteristics and surface functional groups of the MPs (Luo et al., 2022; Song et al., 2022).

2.7 Contaminants of emerging concern (CECs)
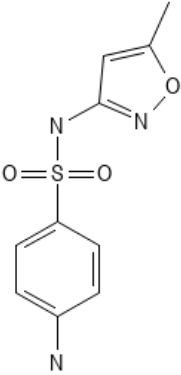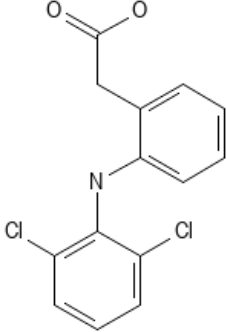
In water quality monitoring, certain chemicals and particles, such as nutrients, heavy metals, microorganisms, and priority pollutants are considered, excluding CECs. Contaminants of emerging concern (CECs) are a broad group of synthetic and naturally occurring chemical or biological substances that are already confirmed or suspected to negatively impact ecological or

public health but are not generally monitored in the environment. They include substances that have been well researched over decades as well, as many that are recently introduced into society, that have gained attention and concern in the public domain and exert a substantial influence on water quality and pose significant challenges to the efficiency of existing water treatment systems in terms of their removal but are not historically considered as 'contaminants' yet (Ahmed et al., 2021). They comprise pesticides, surfactants, pharmaceuticals, industrial chemicals, and personal care products that are regularly found in groundwater, surface water, municipal wastewater, drinking water, and foodstuffs (Rosenfeld & Feng, 2011). CECs can enter the environment through a variety of pathways, such as agricultural runoff, wastewater discharges, and atmospheric deposition, among others. The potential health and environmental impacts of CECs are still being studied. Presently, both short- and long-term reported effects include gene mutation, protein damage, endocrine disruption, nausea, irritation and itching among numerous others that have raised concerns about aquatic ecosystems, drinking water supplies, and human health (Ahmed et al., 2021; Khan et al., 2022). As such, CECs are at the centre of scientific discourse, sourcing evidence for their (CECs) regulation. In this study, sulfamethoxazole (SMX) and diclofenac (DCF) are studied as adsorbates due to their ubiquitous and hydrophobicity nature.

2.7.1 Sulfamethoxazole

Sulfamethoxazole is a synthetic antibiotic used to treat bacterial infections in humans and animals and is a member of the sulfonamides class. SMX is an amphoteric substance, sparingly soluble in water and belongs to a class of antibiotics called sulfonamides, which can interfere with the growth and metabolism of bacteria by inhibiting the synthesis of folic acid – a serious environmental concern. More physicochemical properties of SMX are presented in Table 3. SMX can infiltrate the ecosystem via sewage treatment plants, agricultural runoff, and livestock waste, persisting and accumulating in soil and water, thereby adversely affecting aquatic and terrestrial organisms. This disruption extends to non-target organisms like algae, fish, and aquatic invertebrates, disrupting their physiological processes, such as photosynthesis, growth, and reproduction. Moreover, its presence in the environment fosters the emergence of antibiotic-resistant bacteria, complicating the treatment of infections in both humans and animals. Therefore, vigilant monitoring and strategies to curtail its release are crucial.

Table 3. Physicochemical properties of the adsorbates

Property	SMX	DCF
Formula	$C_{10}H_{11}N_3O_3S$	$C_{14}H_{11}Cl_2NO_2$
Molecular weight (g/mol)	542.820	296.1
Structure		
LogK$_{ow}$	0.89	4.51
pK$_a$	1.6, 5.6	4.15
S$_w$ (mg/L at 25 °C)	459	2.37

LogK$_{ow}$ = octanol-water partition coefficient, pK$_a$ = acid dissociation constant, S$_w$ = aqueous solubility, SMX = Sulfamethoxazole

2.7.2 Diclofenac

Diclofenac is a non-steroidal anti-inflammatory drug (NSAID) commonly used to reduce pain and inflammation in the body. It is available in various forms, including tablets, capsules, gels, and topical solutions. Diclofenac works by inhibiting the production of prostaglandins, which are substances in the body responsible for causing pain and inflammation. DCF is often prescribed for conditions such as arthritis, muscle pain, joint pain, and various other inflammatory conditions. They can be purchased by prescription or, in some regions, over-the-counter.

These CECs can interact with MPs in the environment. MPs have a significant characteristic of a high surface area to volume ratio and are hydrophobic, making them highly prone to adsorbing both organic and inorganic pollutants. MPs have surfaces that are complex and can attract oppositely charged pollutants. Functional groups on the MPs' surface, like carboxylic acid or hydroxyl groups, foster hydrogen bonding interactions with pollutants. Additionally, in freshwater ecosystems, π-π conjugation is observed as an interaction mechanism between MPs and organic pollutants. Understanding these interactions is vital to grasping the potential impacts of

MPs on ecosystems and human health as MPs can serve as carriers and vectors for contaminants (Kuang et al., 2023; Strungaru et al., 2019).

2.8 Sorption

Sorption is a term that refers to the collective processes of adsorption and desorption. In absorption, the absorbate is taken up or assimilated by another substance, often referred to as absorbent, exemplified by the absorption of carbon dioxide gas by water when air is bubbled through water. On the other hand, adsorption involves the accumulation of adsorbate on an adsorbent's surface, like activated carbon removing dissolved impurities from water. Desorption is a reverse process involving the breaking of interactions and removal of adsorbed particles due to applied energy.

The adsorption process involves a mass transport and interaction phenomenon to examine the ability of certain solutes (adsorbate) to concentrate on the surface of other materials (adsorbent). Depending on the intensity of the interactions governing adsorption, adsorption can be physical (physisorption) or chemical (chemisorption). Physisorption is characterized by weak interactions between adsorbate and adsorbent, typically related to electrostatic, hydrogen bonding and Van der Waals interactions at a lower energy, and it is usually a reversible process. Conversely, chemisorption is associated with a stronger bonding between adsorbate and adsorbents like a covalent bond, usually favoured at higher energy than physisorption. In general, chemisorption is highly specific, occurring only at active sites, while physisorption occurs across the entire adsorbent surface. From a thermodynamic perspective, physisorption and chemisorption involve heats of adsorption less than 25 kJ/mol and greater than 40 kJ/mol, respectively.

Adsorption isotherms are graphical representations of the amount of adsorbate adsorbed per unit mass of adsorbent and the equilibrium concentration of the adsorbate in the medium at constant temperature. From the empirical data of the adsorption (amount of adsorbed solute calculated from equilibrium concentration, volume of the solute, and mass of adsorbate), it is possible to obtain information such as adsorptive capacity and the trend of adsorption by fitting isotherm curves using one or more of the isotherm equations which usually produce one of the 4 main types of isotherm curvature profile (see Figure 7).
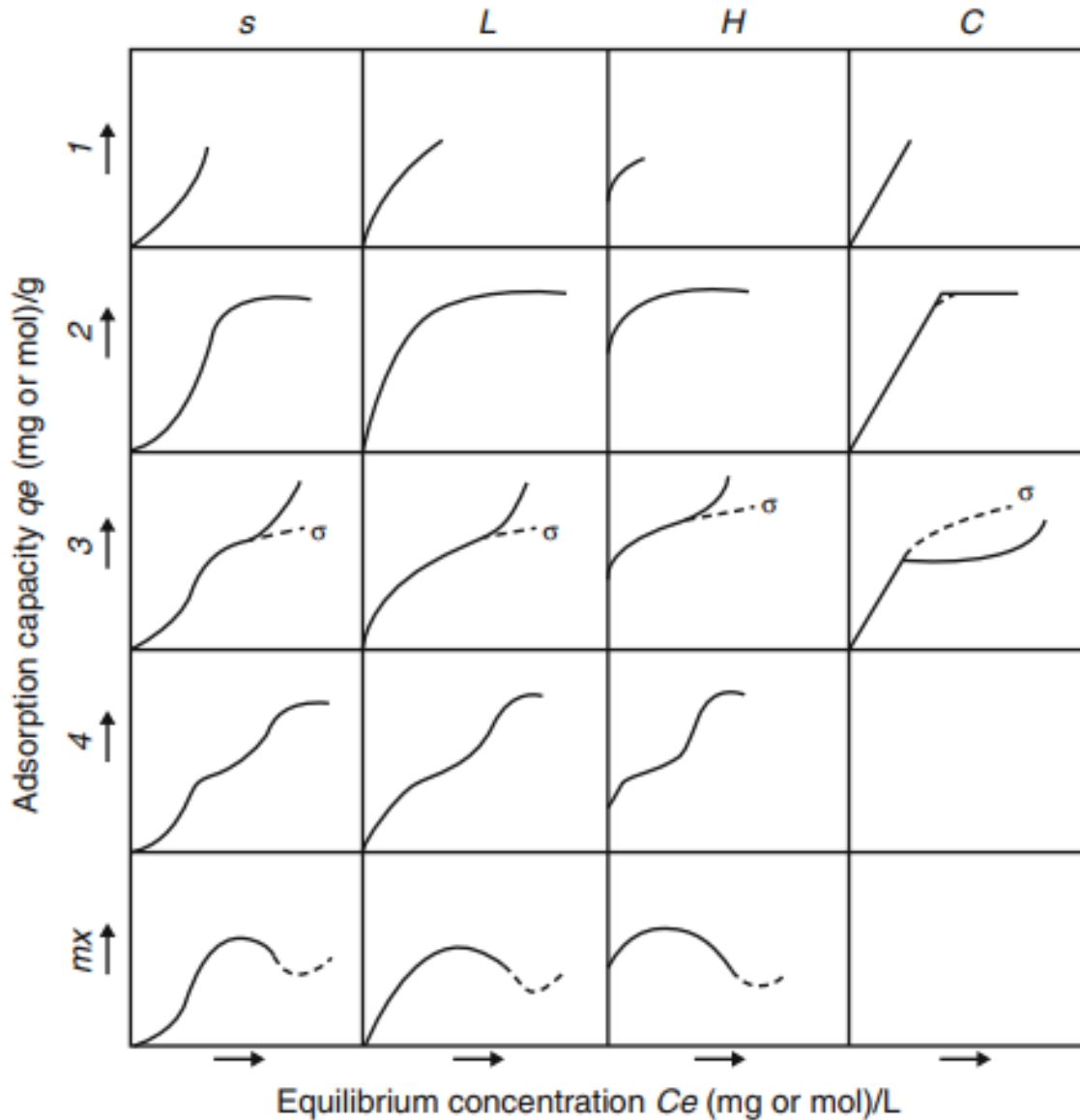
Figure 7. Classification of adsorption isotherm by curve types for organic adsorbates (adapted from (Giles et al., 1960))

There are several isotherm models, with Langmuir and Freundlich isotherms being commonly reported in the literature. The initial slope of an adsorption curve reveals crucial insights into the interaction between an adsorbent and a specific adsorbate within a given medium, determined by the rate at which active sites on the adsorbent alter with increasing solute adsorption. Typically, as the amount of adsorbed adsorbate increases, the availability of active sites decreases until saturation. This phenomenon is best illustrated by the type-L isotherm, as well as the advanced segments of type-S and type-H curves. This process is commonly referred to as

competitive adsorption. The L-curve suggests minimal competition between the adsorbent and solvent for the adsorbate, the S-curve indicates moderate adsorbate-adsorbent interaction with improved adsorption at higher solute concentrations, while H-curve isotherms underscore strong adsorbate-adsorbent interaction in dilute solutions. In the initial phase of the type-S curve, the more solute that is adsorbed, the easier it becomes for additional solute molecules to attach, i.e. the presence of adsorbed molecules facilitates adhesion of more solutes, a phenomenon known as cooperative adsorption. Finally, C-type isotherms, which have a linear start, indicate a constant number of sites, suggesting a relatively strong and specific adsorbate-adsorbent partitioning with solutes penetrating regions inaccessible to the solvent (Giles et al., 1960; Piccin et al., 2017).

2.8.1 Sorption interaction

Microplastics interact with environmental pollutants such as ions, organic substances, natural organic matter, and suspended organic matter, influencing their bioavailability, toxicity, and transformation processes (Du et al., 2022; Elizalde-Velazquez et al., 2020; Guo et al., 2019; Guo & Wang, 2019). These interactions; including hydrophobic, electrostatic, hydrogen bonding, π-π conjugation, van der Waals forces and surface complexation; drive the sorption of organic pollutants onto MPs in freshwater ecosystems (Li et al., 2022; Liu et al., 2022; Xiang et al., 2022). The composition of the MPs, the extent of ageing caused by environmental conditions, and the characteristics of the contaminants all influence the sorption interactions between MPs and environmental pollutants (Siri et al., 2021; van Zomeren, 2008; Wu et al., 2021).

The sorption of chemical contaminants by microplastics generally occurs through van der Waals interactions, facilitated by temporary dipoles from electron movement, particularly when other interactions are not evident (Agboola & Benson, 2021). These interactions involve relatively weak electric forces between the plastic polymers and organic compounds, facilitating their adhesion. van der Waals forces, described as intermolecular attractions, play a crucial role when sorption processes cannot be solely attributed to electrostatic or hydrophobic interactions (Wang et al., 2020). This mechanism underpins the sorption behaviour of aliphatic polymeric sorbents like polyethylene microplastics and poly(vinyl chloride), as highlighted in studies (Hüffer & Hofmann, 2016).

Hydrophobic interaction plays a significant role in the sorption of organic pollutants onto microplastics (MPs). Both microplastics and hydrophobic organic contaminants exhibit hydrophobic properties, leading to a strong affinity between them in aqueous environments (Vieira et al., 2021). This affinity is driven by nonpolar interactions, where the hydrophobic nature of microplastics facilitates the aggregation of nonpolar molecules from the aqueous phase (Hüffer & Hofmann, 2016). The sorption capacity of these pollutants on MPs correlates with their organic pollutant-water partition coefficients, indicating a preference for substances with higher hydrophobicity (Agboola & Benson, 2021). Additionally, the structure and surface characteristics of both polar and nonpolar microplastics influence their sorption behaviour towards organic pollutants. Hence, microplastics serve as effective sorbents for hydrophobic contaminants due to their hydrophobic surfaces and large surface area, enhancing their environmental impact.

Electrostatic interaction, defined by the electric charges between plastic polymers and organic compounds, is a common mechanism governing the sorption of micropollutants onto microplastics. This interaction facilitates adsorption when opposite charges attract, as observed in numerous studies (Wang et al., 2015; Guo et al., 2018). Conversely, electrostatic repulsion occurs when both plastic polymers and organic compounds possess the same electric charge, limiting sorption efficiency (Xu et al., 2018b). The pH conditions, including the medium pH and the pH of the point of zero charge, play significant roles in these interactions. MPs exhibit a negative surface charge at pH levels above their pH point of zero charge, enhancing attraction to positively charged pollutants (Agboola & Benson, 2021).

Hydrogen bonding interactions are reported to have a significant influence on the sorption behaviour of microplastics, particularly with organic compounds (Mei et al., 2020). These interactions occur when proton donor and acceptor groups on microplastics interact with organic compounds, thereby shaping sorption mechanisms. The oxygen-containing functional groups, predominantly introduced during the ageing of plastics, enhance hydrogen bonding interactions (Huang et al., 2024). These bonds exhibit intermediate strength between ionic or covalent bonds and van der Waals forces, and have been reported to have played significant roles in the sorption of organic pollutants on microplastics (P. Zhang et al., 2020; Zhao et al., 2020).

The π–π interaction, a noncovalent attraction between electron-donor and acceptor aromatic systems, significantly enhances the sorption capacity of plastic polymers containing

benzene rings. This interaction involves the aromatic moiety of microplastics and aromatic structures of organic pollutants, facilitating strong adsorption. Moreover, studies highlight its role in binding aromatic contaminants such as diclofenac, phenanthrene, sulfamethoxazole and pyrene to microplastics. The strength of π–π interactions is influenced by functional groups in contaminants, influencing adsorption efficiency. These findings underscore the importance of π–π interactions in understanding and mitigating microplastic pollution impacts (Agboola & Benson, 2021; Elizalde-Velázquez et al., 2020).

3 MATERIALS AND METHODS

This chapter outlines the materials, reagents, and methodologies employed in this study to investigate the adsorption and desorption behaviours of DCF and SMX on various the four different types of microplastics. The materials and reagents section details the specific types and sources of microplastics used, including fresh, UV-aged, and humic acid-coated microplastics. It also enumerates the chemicals and solutions utilized throughout the experiments. Following this, the methods section provides a comprehensive description of the experimental procedures, including the preparation of materials, execution of adsorption and desorption experiments, and the analytical techniques employed to quantify the results.

3.1 Materials and reagents

The reagents used are of analytical grade. PP (Pellets), PS (pellets), PVC (micro-size) and the standards of DCF and SMX were purchased from Sigma Aldrich. Table 4 presents some of the characteristics of the standards and the polymers. PE (HDPE, pellet) was purchased from Mercado Livre, methanol (>99.9%) from Honeywell, acetonitrile (HPLC grade) from Merck, formic acid and ammonium formate. Magnesium chloride hexahydrate ($MgCl_2$), sodium sulfate (Na_2SO_4) and sodium bicarbonate ($NaHCO_3$) purchased from Synth; calcium nitrate tetrahydrate ($Ca(NO_3)_2.6H_2O$) and potassium bicarbonate ($KHCO_3$) from Dinâmica; and calcium carbonate ($CaCO_3$) and calcium chloride dihydrate ($CaCl_2.2H_2O$) from Vetec. Ultrapure water (type I) was produced in an Arium Mini System (Sartorius)

Table 4. Properties of the standards and the plastics used in this study

MP/Analyte	Acronym	CAS	Classification	Density (g/mL)	T_g (°C)*	T_m (°C)*
Sulfamethoxazole	SMX	723-46-6	Antibiotic	na	nm	nm
Diclofenac	DCF	15307-86-5	Antimicrobial	na	nm	nm
Polyethylene	PE	9002-88-4	Semi-crystalline*	0.92*	-	130
Polypropylene	PP	9003-07-0	Semi-crystalline*	0.9	-10	153
Polystyrene	PS	9003-53-6	Amorphous*	1.05	105	nd
Polyvinyl chloride	PVC	9002-86-2	Amorphous*	1.4	95	nd

* = data from the current study; na = not applicable; nm = not measured; - = out of range; nd = not detected

3.2 Preparation of microplastics

Three out of the four commercial polymers (PE, PP, and PS) were pellet, and they were milled using a cryogenic miller (IKA A11 basic) until less than 300 µm particle size in liquid nitrogen. An image of the miller is presented in Figure 8a. Plastic pellets were loaded into the stainless cup of the cryogenic miller up to the mark Figure 8b, and then liquid nitrogen was added. The mixture was left for about 3 min for all the liquid nitrogen to evaporate and then milled for approximately 2 min. The process of adding nitrogen and milling was repeated until the desired size of MPs was achieved. Milled MPs were sieved using a mesh of size 50 (Figure 8c). The shifted MPs were then sieved using a finer mesh of size 100, and the unshifted (150 – 300 µm) MPs were stored and treated hereafter as fresh microplastics (fresh MPs, Figure 8d) for the sorption and degradation experiments.

Figure 8. MPs milling materials and stages(a) Cryogenic miller, (b) loading of polymer resin into the milling cup up to the mark, (c) sieving of milled MPs and (d) MPs samples used in this work

3.2.1 UV ageing of microplastics

The fresh microplastics were aged using a microwave-assisted photochemical reactor (Pittarello et al., 2019; Sodré et al., 2004). The principle of the reactor is based on the action of ultraviolet radiation generated in a microwave-activated reactor. The UV LAB EL 10 reactor, marketed by Umex (Dresden, Germany), can process up to 10 mL of sample. It consists of two concentric cylindrical glasses, with the inner made of quartz, which has high permeability to UV radiation, and the outer body is made of borosilicate glass, which has low permeability to UV. The space separating them contains low-pressure mercury vapour, whose atoms become excited due to the energy generated by a household microwave oven. As a result, this process emits extremely intense UV radiation at a precise wavelength of 254 nm. A representative schematic of the photochemical reactor is shown in Figure 9.
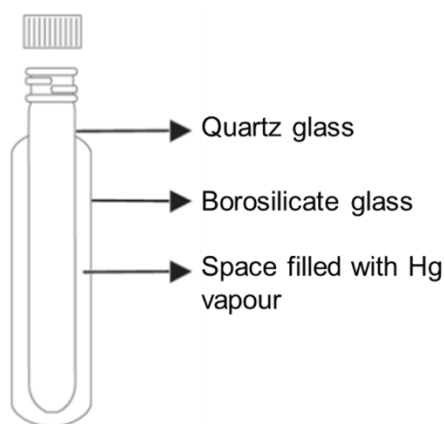
Figure 9. Scheme of microwave-activated photoreactor

A portion of 1 g of each fresh microplastics was weighed into the inner compartment of the reactor, which was filled with 10 mL ultrapure water, capped (Figure 10a) and exposed to UV-C irradiation activated by Panasonic (Style NN_ST654W) microwave for 2 to 3 min (Figure 10c), maintaining an average of 60 °C temperature. The exposure step was repeated until an accumulated 20 min was reached. The temperature was measured using mercury-in-glass thermometer immediately each exposure step and the average was calculated. Also, beakers filled with about 750 mL of cold water were placed inside the microwave to control the temperature. The window of the microwave was covered with an opaque plastic material to prevent exposure of people to UV-C radiation (Figure 10b). The microplastics obtained after this treatment are hereafter referred to as UV-aged MPs.
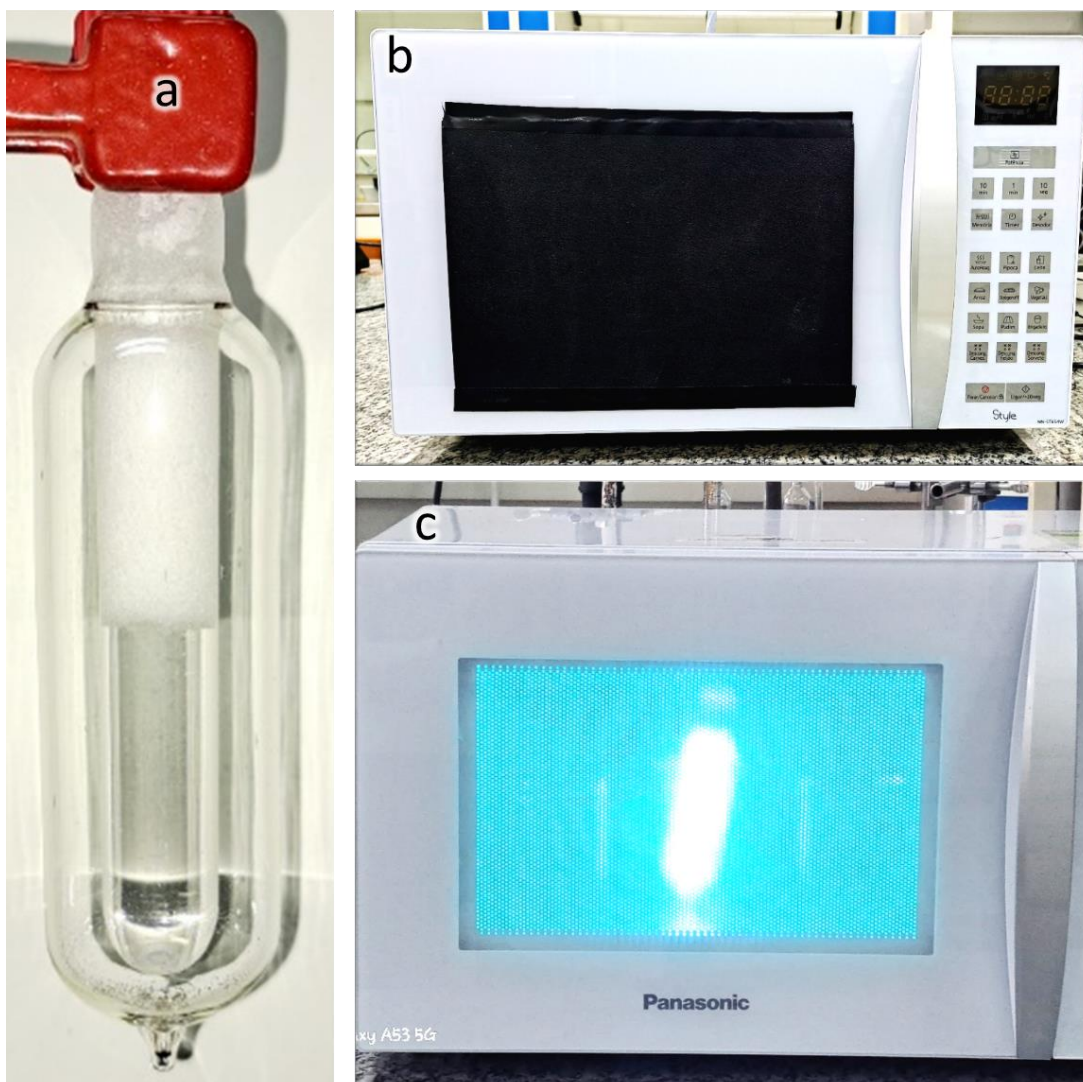
Figure 10. MP-loaded reactor (a), Panasonic (Style) microwave covered with opaque material (b) and UVC-irradiated reactor in the microwave during ageing

3.2.2 Coating of microplastics with humic acid

A humic acid (HA) stock solution was prepared by dissolving 1 g of HA in 50 mL of 0.1 mol/L NaOH, to aid a complete dissolution of HA, transferred to a 1 L volumetric flask, made the volume up to the mark with ultrapure water, stirred for 48 h and passed through a 0.22 μm cellulose acetate membrane filter. The stock solution was adjusted to pH 7.0 with concentrated HCl before use (Bazrafshan et al., 2012). Then, 1000 mg of each microplastic was weighed into a 15 mL glass test tube, filled with 10 mL of 1000 mg/L HA solution and then shaken for 48 h. The microplastics were filtered through a 0.22 μm cellulose acetate membrane filter, dried at room temperature overnight and transferred to a desiccator before FTIR measurement and use for the adsorption

experiment. The microplastics obtained after this treatment are hereafter referred to as HA-coated MPs.

3.3 Characterization of fresh and modified microplastics

3.3.1 Thermal stability and decomposition behaviour analysis

Shimadzu thermogravimetric analysis (TGA, DTG-60H) was employed to investigate the stability and decomposition behaviour of the fresh MPs under varying temperatures. The analysis was conducted in a platinum crucible under a N_2 atmosphere. The experimental measurements commenced at 20 °C and continued for 78 minutes with a temperature ramp of 10 °C/min until reaching 800 °C while maintaining a gas flow rate of 50 mL/min. The obtained TGA data were subsequently collected and plotted using OriginLab software.

3.3.2 Surface morphology and oxygen content analysis

The surface morphology and possible oxygen content on the surface of the fresh, UV-aged, and HA-coated microplastics were analyzed using a Hitachi Tabletop Scanning Electron Microscope (TM4000 Series), Hitachi High-Technologies Corporation, Tokyo, Japan. Double-sided carbon tape was placed on a standard sample plate, and a portion of about 2 mg of each microplastic was spread on it for analysis. Images with 500x magnification were recorded.

For oxygen concentration analysis, an image at 100x magnification was taken and transferred to the Energy Dispersive X-ray Spectroscopy (EDS) system by Bruker (Quantax 75), which is coupled to the Hitachi TM4000 Series, for qualitative and quantitative oxygen characterization. For the qualitative analysis, a portion of the acquired image was selected and quantified, and the mapped images were saved. The mapped oxygen points, averaging five per image, were then selected and quantified, and the mean oxygen concentration was recorded.

3.3.3 FTIR characterization

Fourier transform infrared (FTIR) spectroscopy was employed for the identification of the polymeric materials and the surface functional groups of the fresh and modified MPs using Varian 640 FTIR, operated in the attenuated total reflectance mode (ATR PRO450-S). A sample, sufficient enough to cover the diamond crystal, was introduced and measured with 64 counts in

the range of 4000 – 600 cm^{-1} at 4 cm^{-1} resolution. The spectra data were pretreated in three steps using Matplotlib, Pandas, Pybaselines and NumPy libraries in a Python environment. Firstly, the baselines were individually corrected by the asymmetric least squares (AsLS) model. Followed by picking of responses of reference band (1470, 1376, 1450 and 1353 cm^{-1} for PE, PP, PS and PVC, respectively). Lastly, the spectra were normalized by dividing responses with their respective reference bands. The spectra were plotted and bands were interpreted.

3.3.4 Crystallinity

Thermal characteristics of the fresh and UV-aged MPs were determined using a DSC-60 (Shimadzu) Differential Scanning Calorimeter (DSC) device. The DSC measurements were performed using aluminum seal in helium atmosphere with a flow rate of 30 ml/min and at heating rates of 10 °C/min. The weight of the examined samples was between 3.56–4.85 mg and two parallel measurements were carried out in all cases. The crystallinity, X_c (%), of the polymer samples was determined using Equation 10:

$$X_c\ (\%) = \frac{\Delta H_f}{\Delta H_c} \times 100 \qquad \text{Equation 10}$$

where ΔH_f is the heat of fusion of the samples obtained from the DSC analyzes and ΔH_c is the heat fusion of of the polymers with 100% crystalline (PE = 293 J/g ([Inoue, 1963](#)) and PP = 165 J/g ([Wunderlich, 2013](#))).

3.3.5 Zeta potential

The electric potential at the microplastics-liquid surface (fresh and modified MPs) was measured using a Malvern zetasizer (Nano ZS90). About 10 mg of each MP was weighed into a test tube and 10 mL of SFW of pH 6.54 was added and mixed thoroughly. A-1 mL aliquot was pipetted into a 1 mL cuvette measured and measured at 25 °C and attenuator of between 8 and 10.

3.3.6 pH at the Point of zero charge (pHpzc)

The pH at the point of zero charges (pHpzc) of the fresh and modified MPs was determined from measurements of zeta potential at pH ranging from 2 to 10. The procedure of zeta potential

measurement was repeated with the pH adjusted to 2, 4, 6, 8 and 10 with HCl and NaOH. The zeta potential was plotted against the pH and the intercept was recorded as the pHpzc.

3.4 Sorption experiments

The sorption experiments are designed to evaluate the adsorption and desorption characteristics of SMX and DCF on various types of microplastics. This section outlines the detailed procedures for conducting these experiments, including the setup, experimental conditions, and the specific steps followed to ensure accurate and reproducible results. In this section, the procedure for simulating Lake Paranoá and the biological fluids and the methodologies for measuring adsorption rates, capacities, and desorption rates are thoroughly explained, providing a clear understanding of the experimental approach.

3.4.1 Preparation of simulated freshwater

Lake Paranoá water was simulated for this study. Lake Paranoá is one of the 32 notable lakes in Brazil and is located in the urban area of Brasília, Federal District, Brazil. It was artificially dammed from the Paranoá River during the 41-month between 1956 and 1960. It receives water from WWTPs located around it. Over decades, Lake Paranoá has been a hub of various activities including but not limited to fishing, sports, relaxation and scientific research (Barbosa et al., 2021). Sodré and Sampaio (2020) accessed 35 organic pollutants in drinking water produced from the lake and found SMX and DCF at concentrations of 4.5, 5.1 and 2.63 ng/L, respectively. The concentrations of the major ions reported by Costa (2014) in the lake were used to prepare the SFW and they are presented in Table 5.

Table 5. Obtained and adjusted concentrations of major ions in Lake Paranoá

Ion	Determined Concentration		Adjustment factor (µeq/L)	Balanced Conc. (µeq/L)
	µmol/L	µeq/L		
Na+	56	56	2	58
Ca2+	63	126	5	131
Mg2+	10	21		21
K+	4	4		4
S.CZ+	134	207	7	214
Cl⁻	31	31	1	30
NO3-	13	13	1	12
SO42-	13	26	1	25
HCO3-	150	150	2	148
S.AZ-	206	219	5	214

Na^+ = sodium ion, Ca^{2+} = calcium ion, Mg^{2+} = magnesium ion, K^+ = potassium ion, $S.C^{Z+}$ = the sum of cations in PL, Cl^- = chloride, NO_3^- = nitrate, SO_4^{2-} = sulfate, HCO_3^- = bicarbonate, and $S.A^{Z-}$ = the sum of anions in PL

The SFW was prepared using the synthetic soft water model described by Smith et al. (2002). To check if the water is electronically neutral, the molar concentrations of the ions were converted to equivalent (µeq/L) using Equation 11.

$$Eq = M \times Q$$
<div align="right">Equation 11</div>

where Eq is the equivalent, M is the molar concentration of the ions and Q is the charge

Since the chemical composition of water is typically determined through analytical methods, the precise balance of cations and anions in its concentrations often deviates slightly, then small adjustments were made using the adjustment factor (Table 5) to achieve the balance. Salts selected by Smith et al. (2002) were used because of their solubility. Some amounts of measured ions were used to determine the amount of each salt as presented in Table 6. The measured concentrations of Mg_2^+, NO_3^-, K^+ and SO_4^{2-} were used to calculate the amounts of $MgCl_2$, $Ca(NO_3)_2$, $KHCO_3$ and Na_2SO_4 required, respectively. The required amounts of $CaCl_2$, $CaCO_3$ and $NaHCO_3$ were balanced with Cl^-, Ca^{2+} and Na^+, respectively. Three separate stock solutions (S₁, S₂ and S₃) were prepared at elevated concentrations (x1000, x1.1 and x1000, respectively) to minimize potential errors due to weighing and ensure that the ions are relatively

stable in the solution. A specific stock solution, S$_2$, was prepared to overcome the low solubility of $CaCO_3$, an essential component in the SFW. Also, air was bubbled into the stock for 24 h before mixing it with other stocks as $CaCO_3$ is only sparingly soluble in water under normal of temperature and atmospheric conditions.

Table 6. Matrix of ions contributing required salts

Ion (µeq/L)	Cl^-	NO_3^-	SO_4^{2-}	C_T	$S.C^{Z+}$
Na^+			25	33	58
Ca^{2+}	9	12		110	131
Mg^{2+}	21				21
K^+				4	4
$S.A^{Z-}$	30	12	25	148	214

C_TT = sum of the concentrations of HCO_3^- and CO_3^{2-}

Table 7 presents the necessary concentrations of individual salts (mg/L) for the lake water formulation, and provides the corresponding masses required to prepare suitable volumes of stock solutions and simulated water. The SFW was filtered using a 0.22 µm syringe filter and kept at room temperature. The pH, total dissolved solids and electrical conductivity of SFW were measured using the HANNA HI 9829 multiparameter analyzer coupled with the HANNA HI 7609829-3 and HI 7698194-1 (for pH), and the results were 17 mg/L, 0.034 mS/cm and 6.54, respectively. These results indicate that the SFW has a pH within the typical range for lake water, but lower than usual levels of total dissolved solids and electrical conductivity, probably due to the absence of dissolved organic matter.

Table 7. Concentrations and volumes of salts used for SFW formulation

Stock solution	µeq/L	Final required concentration (mg/L)		Mass of salt (g)	Concentration factor	Dilution factor (mL)
		C^{Z+}	A^{Z-}			
S_1				1 L	x1000	5.0
$MgCl_2$	21	0.25	0.74	2.12		
$CaCl_2 \cdot 2H_2O$	9	0.18	0.33	1.01		
$Ca(NO_3)_2 \cdot 6H_2O$	12	0.24	1.10	1.39		
S_2				5 L	x1.1	4545.0
$CaCO_3$)	110	2.21	3.31	0.03		
S_3				1 L	x1000	5.0
Na_2SO_4	25	0.28	1.18	1.75		
$KHCO_3$	4	0.16	0.25	0.42		
$NaHCO_3$	33	0.76	2.02	2.78		
Milli-Q						445
Total Volume						5000

C^{Z+} = cationic concentration required, A^{Z-} = anionic concentration required

3.4.2 Preliminary experiments

All sorption experiments were carried out using the batch equilibrium method and in duplicate runs. The working solution was prepared with simulated freshwater (Elizalde-Velázquez et al., 2020). Stability tests were conducted to confirm the possible retention of analytes during the filtration process and to ensure their stability in simulated freshwater and biological fluids. Prior to testing DCF, the preliminary test was carried out with triclosan, but more than 90% of the analyte was lost to the filtration procedure (see details in Appendix A). To assess potential analyte loss during filtration, a 500 µg/L solution of SMX and DCF was individually filtered through a 0.22 μm syringe filter. 0.95 mL of the filtrates were transferred into 1.5 mL vials containing 0.05 mL internal standard (sulfamethoxazole-D4 and $^{13}C6$-diclofenac) and analyzed using LC-MS/MS. The percentage losses were then calculated. For stability in simulated fluids, solutions of 500 µg/L SMX and DCF in simulated freshwater were individually prepared and agitated for 48 hours using a tube homogenizer before analysis with LC-MS/MS. The percentage losses were calculated, and

the procedure was repeated with solutions in artificial gastric fluid and artificial intestinal fluid for 24 h. Figure 11 presents an image of the ALB 260 H tube homogenizer, loaded with samples.

Figure 11. ALB 260 H tube homogenizer loaded with samples during adsorption experiment

Before the sorption experiment, the sorptive capacity of fresh and modified MPs was investigated. A portion of 30 mg individual MP was weighed into 15 mL glass test tubes, and a 12 mL working solution of 1000 μg/L of individual analyte was added to each tube, capped and homogenized with ALB 260 H tube homogenizer at the maximum speed for 48 h. about 2 mL were withdrawn and filtered through a 0.22 μm PVDF syringe filter and 0.95 mL were transferred into a 1.5 mL vial containing internal standard before the LC-MS/MS analysis.

3.4.3 LC-MS/MS analysis

The filtrates were analyzed using the Agilent 1290 Infinity II liquid chromatography (LC) system, which is equipped with a micro vacuum degasser, a quaternary pump (G7104A, 1290 Infinity II Flexible Pump), an automatic sampler, and a column compartment featuring a thermostat. The LC is coupled with a mass spectrometry system, Agilent 6470B, equipped with a triple quadrupole (QqQ) mass analyzer and electrospray ionization (ESI) as depicted in Figure 12.

Figure 12. Agilent 1290 Infinity II liquid chromatograph coupled to Agilent 6470B mass spectrometer, equipped with QqQ and ESI

In the LC system, a Zorbax Eclipse Plus C18 column with dimensions of 50 mm in length and 2.1 mm in internal diameter, and packed with particles of size 1.8 µm (Agilent Technologies) was used for chromatographic separation at 55.0 °C. The elution of the target substances was accomplished using a mobile phase consisting of a mixture of pH-modified ultrapure water (MIlli-Q) and methanol (MeOH) with 0.1% formic acid and 5 mmol/L ammonium formate, and 0.1% formic acid, respectively. The injection volume and the flow rate were set to 5.0 µL and 0.25 mL/min, respectively. Gradient elution was achieved by increasing the relative organic solvent concentration from 5% (initial condition) to 98% within 0.5 min, starting at 0.5 min into the run. It was then maintained at 98% for 4 min before being readjusted to the initial conditions within 0.5 min and held there for an additional 1.5 min to re-equilibrate the system. To ensure a complete re-equilibration of the column and pressure, a 3-min post-run was set before the next injection, bringing the total analytical run time to 10 min.

The ESI parameters used include nitrogen as the curtain gas (CUR) at 50 psi and nebulizer gas at 35 psi. The ESI interface was operated at 300 °C with capillary voltages of 3500 V for both positive and negative modes. The concentrations of CECs were determined using the mass analyzer in the multiple reaction monitoring (MRM) acquisition mode. The MRM parameters were obtained from the Veterinary Drug tMRM Database for Triple Quadrupole LC/MS (G1735CA) and literature. Compound parameters such as fragmental and collision energies were manually

optimized. The precursor ion of the analytes monitored in the quadrupole analyser was the protonated $[M+H]^+$, with an m/z ratio of 254.1 for SMX and 296 for DCF amu. To produce selective fragmentation of the precursor ions to two product ions, nitrogen was used as collision gas with collision energies for both identifier and quantifier (CE) of 12 and 24 (SMX), and 8 and 48 (DCF), respectively. From the two daughter ions, the one producing the highest intensity was used for quantification and they are m/z 92.1 and 250 amu while m/z 156 and 179.1 amu were used to identify SMX and DCF, respectively.

The linearity of spectrometric techniques was evaluated by examining the quality of linear regression applied to the analytical curves utilizing the least squares approach. The coefficients for slope (b) and intercept (a) of $y = a + bx$, where x denotes the independent variable (calibrator concentration) and y signifies the dependent variable (equipment response), were used to interpolate concentrations of the analytes measured by the LC-MS/MS. The analytical curves for measuring the analytes are presented in Figure 13.
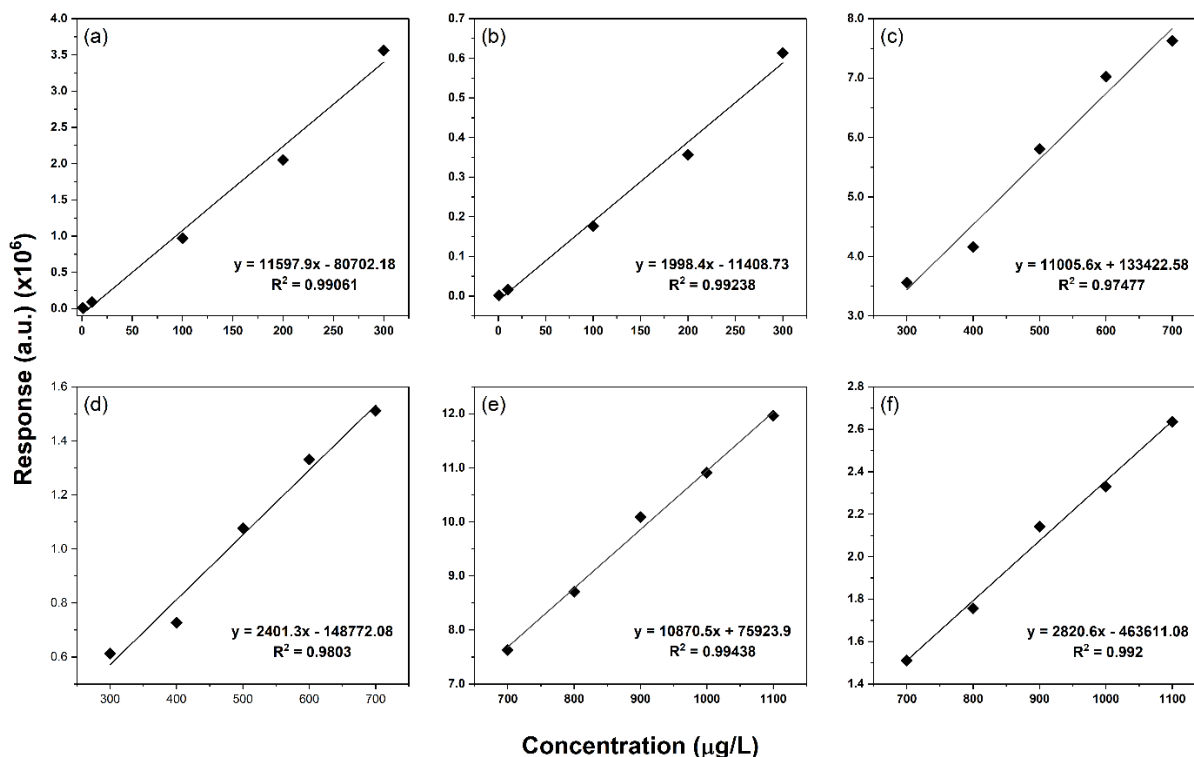
Figure 13. Analytical curves for measuring (a) lower range SMX, (b) lower range DCF, (c) medium range SMX, (d) medium range DCF, (e) higher range SMX and (f) higher range DCF

The LOQ of the method was determined as the lowest concentration of the analyte on the analytical curve, given a signal-to-noise ratio of approximately 10. The LOD was obtained using LOQ divided by 3.3. The LOQ and the LOD are, therefore, 1.00 and 0.30 µg/L, respectively.

3.4.4 Sorption

The sorption section delves into the process by which the analytes interact with and sorb to different types of MPs under different modifications. This investigation is critical for understanding the efficiency and capacity of each type of microplastic in transferring pollutants in aquatic environments. The section is divided into subsections that explore different aspects of sorption, starting with the kinetics study, which examines the rate at which adsorption occurs and identifies the underlying mechanisms governing this process. The isotherm study, on the other hand, analyzes the relationship between the concentration of the contaminants in solution and their equilibrium adsorption capacity on the microplastics.

Kinetics study

In a kinetic sorption experiment, 30 mg of individual MP was weighed into a 15 mL glass test tube, filled with 12 mL solution of 500 µg/L SMX, capped and then homogenized with ALB 260 H tube homogenizer at the maximum speed for 0, 0.5, 1, 2, 4, 8, 12, 24 and 48 h. At the corresponding time, about 2 mL were withdrawn and filtered through a 0.22 µm PVDF syringe filter and 0.95 mL were transferred into a 1.5 mL vial containing 0.05 mL sulfamethoxazole-D_4 internal standard and analyzed for the SMX using LC-MS/MS. The experiment was repeated for DCF using $^{13}C_6$-diclofenac internal standard. The amount of the analytes adsorbed (mg/g) at each time t, q_t (mg/g), was calculated according to Equation 16:

$$q_t = \frac{(C_i - C_t)V}{m} \qquad \text{Equation 12}$$

where C_i is the initial concentration (mg/L), C_t is the concentration (mg/L) of the solution at time t, V is the solution volume (L), and m is the adsorbent mass (g).

Kinetics models

Time is one of the important experimental parameters. The evolution process, from the beginning up to (or near) a true equilibrium in sorption phenomena is explained by kinetics (Moussout et al., 2018). The kinetics data were modelled using both pseudo-first- and pseudo-second-order kinetic models. For each MP and analyte, isotherm models were fitted by plotting the amount of the analyte adsorbed, q_t (mg/g), at time t against time, t (h). The models are explained below.

Pseudo-first-order model

The non-linear form of the pseudo-first-order kinetic model is widely used to describe the rate of adsorption in systems where the rate of occupation of adsorption sites is proportional to the number of unoccupied sites. This model provides a more accurate representation of adsorption kinetics by directly fitting the experimental data without linearization. The expression for the pseudo-first-order kinetic model is given in Equation 13 (Lagergren, 1898).

$$q_t = q_e(1 - e^{-k_1 t})$$ Equation 13

where q_t (mg/g) is the amount of analyte adsorbed at equilibrium and k_1 (1/min) is the pseudo-first-order rate constant.

Pseudo-second-order model

The non-linear form of the pseudo-second-order kinetic model is extensively utilized to describe adsorption processes where the rate of adsorption is dependent on the square of the number of unoccupied sites. This model assumes that the adsorption mechanism involves chemisorption, where valence forces through the sharing or exchange of electrons between adsorbent and adsorbate dominate. The non-linear pseudo-second-order kinetic equation provides a direct fit to the experimental data, enhancing the accuracy of kinetic parameter estimation. The expression for the pseudo-second-order kinetic model is given in Equation 14 (Ho & McKay, 1999).

$$q_t = \frac{q_e^2 k_2 t}{1 + q_e k_2 t}$$ Equation 14

where q_t (mg/g) is the amount of adsorbate adsorbed at time t, q_e (mg/g) is the equilibrium adsorption capacity, k_2 (g/mg·h) is the pseudo-second-order rate constant, and t is the contact time (h). The initial adsorption rate, k_0 (mg/g/h), at t → 0, can be calculated using Equation 15 (Mane et al., 2007).

$$k_0 = k_2 q_e^2$$ Equation 15

Isotherm study

The batch equilibrium sorption experiment was carried out by weighing a portion of 30 mg PE into 15 mL glass test tubes, and 12 mL working solution of 0, 100, 200, 400, 500, 600, 800 and 1000 µg/L SMX were added to each tube, capped and homogenized with ALB 260 H tube homogenizer at the maximum speed for 48 h. about 2 mL were withdrawn and filtered through a 0.22 µm PVDF syringe filter and 0.95 mL were transferred into a 1.5 mL vial containing internal standard before the LC-MS/MS analysis. The experiment was repeated for DCF and with the PP, PS and PVC (Guo & Wang, 2019; Siri et al., 2021). The amount of adsorbed analyte at equilibrium, q_e (mg/g), was calculated using Equation 16.

$$q_{e,} = \frac{(C_i - C_e)V}{m}$$ Equation 16

where C_i is the initial concentration (mg/L), C_e is the concentration (mg/L) of the solution at equilibrium, V is the solution volume (L), and m is the adsorbent mass (g).

Isotherm models

Isotherms are essential tools to describe and interpret the dynamics and capacity of adsorbents in the adsorption phenomenon. They explain the feasibility and efficiency of adsorbents to establish relationships with adsorbates under various conditions. As earlier described, this study considers two variables, which are the impacts of fresh and modified microplastics. One linear (Henry) and four non-linear (Langmuir, Frundlich, Langmuir-Freundlich and Dubinin-Radushkevich) isotherm models were employed to explain the roles of these variables in the interactions of MPs with organic pollutants of both hydrophobic and hydrophilic nature.

Henry model

The Henry model, derived from Henry's law, is a fundamental adsorption isotherm model frequently used to describe the adsorption behaviour of gases on solid surfaces at low concentrations. Initially formulated by Henry (1803), it posits a proportional relationship between the solubility of a gas in a liquid and the partial pressure of that gas above the liquid. Over time, this law was adapted to describe adsorption processes on solid adsorbents, assuming that the solute follows Henry's law in infinitely dilute solutions, establishing a linear relationship between the adsorbed amount of adsorbate and its concentration in the bulk solution, as expressed in Equation 17. The adsorption mechanisms in this model involve electrostatic, van der Waals, and hydrophobic interactions, encapsulated by the partition coefficient K_d, which is a physical constant (Chen et al., 2022).

$$Q_e = K_d \times C_e \hspace{3cm} \text{Equation 17}$$

where K_d (L/mg) is the linear sorption coefficient.

Langmuir Model

The Langmuir model assumes monolayer adsorption and the occurrence of adsorption at homogeneous definite localized sites (Langmuir, 1918; Sena et al., 2018). The model assumes that the sites are identical and equivalent, without any lateral interactions or steric hindrance between the adsorbed molecules. It also assumes that each molecule possesses constant enthalpies and sorption activation energy, which indicates an equal affinity for the adsorbate (Foo & Hameed, 2010). It is mathematically expressed as Equation 18.

$$q_e = \frac{q_m K_L C_e}{1 + K_L C_e} \hspace{3cm} \text{Equation 18}$$

where q_m is the maximum adsorption capacity of the adsorbent (mg/g) and K_L is the Langmuir constant (L/mg), related to the affinity of the binding sites (Anah & Astrini, 2018) and energy of adsorption (Sena et al., 2018).

Freundlich Model

The Freundlich model describes adsorption phenomena on heterogeneous adsorbent surfaces characterized by a non-uniform distribution of adsorption heat and affinities across the

surface. This model implies that the formation of multilayer adsorption is possible. The model presumes that each bonding site possesses a unique bonding energy and that the ratio of adsorbate molecules binding to a specific mass of adsorbent varies with different solution concentrations. In this context, the total amount of adsorbate adsorbed is cumulative adsorption across all available sites, and the sites with stronger binding energies are the first to be occupied and continue until the adsorption energy exponentially decreases upon completion (Foo & Hameed, 2010). It is usually described by Equation 19.

$$q_e = K_F C_e^{1/n}$$

<div align="right">Equation 19</div>

where K_F (mg/g) is the Freundlich constant that indicates the overall adsorption capacity and n is the Freundlich isotherm exponent that determines the adsorption intensity, the surface heterogeneity or the non-linearity of the sorption process (Elizalde-Velazquez et al., 2020; Sena et al., 2018). The value of n ranges between 0 and 1, and as it approaches 0, the surface of the adsorbent becomes increasingly heterogeneous (Foo & Hameed, 2010). The reciprocal of the n can be estimated and when it drops below unity, it implies a chemisorption process, while a value above 1 indicates physisorption adsorption (Foo & Hameed, 2010).

 Langmuir-Freundlich model

The Langmuir-Freundlich model combines aspects of both the Langmuir and Freundlich adsorption isotherms, allowing for more flexibility in describing adsorption on heterogeneous surfaces (Sips, 1948). Unlike the Langmuir model, which assumes monolayer adsorption on a homogeneous surface with identical adsorption sites, the Langmuir-Freundlich model considers that the surface may have varying degrees of heterogeneity in adsorption energies and site capacities. The general form of the Langmuir-Freundlich isotherm equation is presented in Equation 20 (Jeppu & Clement, 2012).

$$q_e = \frac{Q_m(K_a C_e)^n}{1 + (K_a C_e)^n}$$

<div align="right">Equation 20</div>

where q_e is the adsorbed amount at equilibrium (mg/g), Q_m is the maximum adsorption capacity (mg/g), K_a is the affinity constant (L/mg), C_e is the aqueous phase concentration at equilibrium (mg/L) and n is the index of heterogeneity.

Dubinin-Radushkevich Model

The Dubinin-Radushkevich isotherm is an empirical model used to describe the adsorption mechanism on heterogeneous surfaces, assuming that the distribution of pores in adsorbents conforms to Gaussian energy distribution (Piccin et al., 2011; Saleh, 2022). It is expressed mathematically as Equation 21:

$$q_e = q_s e^{-K_D \varepsilon^2}$$
<div align="right">Equation 21</div>

where q_s represents the theoretical isotherm saturation capacity (mg/g); ε is the Polany potential described as $\varepsilon = RTln(1 + 1/C_e)$ having R and T to represent the gas constant (8.314 J/mol K) and absolute temperature (K), respectively, and K_D is the Dubinin–Radushkevich isotherm constant (mol²/kJ²) related to the mean free energy (Sena et al., 2018). The mean free energy of adsorption, E, is calculated by Equation 22 and indicates the free energy involved in the transfer of 1 mol of sorbate from the solution to the adsorbent surface:

$$E = \frac{1}{\sqrt{2K_D}}$$
<div align="right">Equation 22</div>

3.4.5 Desorption

The method for desorption experiments in freshwater and biological fluid(s) that mimic the internal fluid(s) of an aquatic organism as described by Siri et al. (2021) was adopted in this study with slight modification. Desorption processes play a critical role in understanding the overall dynamics of contaminant interactions with microplastics. This section examines the factors influencing the release of adsorbed contaminants back into the environment and gastrointestinal fluids. By exploring desorption, we can gain insights into the potential environmental impact and mobility of pollutants previously adsorbed onto microplastics.

Preparation of biological fluids

Two gastrointestinal fluids, artificial gastric fluid (AGF) and artificial intestinal fluid (AIF), mimicking stomach and intestine fluids will be prepared in the laboratory. The fluids will be produced from a buffer solution composed of 8819.6 mg/L of $NaCl$, 224.4 mg/L of KCl, 108.8 mg/L of $MgSO_4$, 148.2 mg/L of $CaCl_2$, 912 mg/L of D-glucose and 558.6 mg/L of Na-pyruvate.

To prepare the AGF solution, 1000 mL buffer solution will be adjusted to pH = 2 with 32% HCl, and then, 1 mL of 1000 mg/L of pepsin was added. The AIF solution will be prepared by mixing 4 mg of porcine bile extract powder, 2 mg of pancreatin powder, 0.84 mg of $NaHCO_3$ salt, and 20 µL of HEPES (1 M) solution in a 1000 mL volumetric flask. The volume was made up to the mark with the buffer solution and stirred for 45 min.

Desorption setup

Here, each analyte was first adsorbed onto the MPs. 1 g of each MP was transferred into 15 mL different test tubes with 10 mL of 10 mg/L analyte and homogenized with ALB 260 H tube homogenizer for 96 h. The high concentration of analyte and the elongated time were to ensure that enough analyte was sorbed on the microplastics. Then, the sample was filtered, and the filtrate was analyzed with LC-MS/MS and the adsorbed concentration (mg/g) was calculated using Equation 23. The microplastics were gently rinsed with 50 mL ultrapure to remove aqueous pharmaceuticals, collected by filtration, and dried in an oven at 40 °C for 1 h (Siri et al., 2021).

$$q_{e,\ ads} = \frac{(C_i - C_e)V}{m}$$
<div align="right">Equation 23</div>

where C_i is the initial concentration (mg/L), C_e is the concentration (mg/L) of the solution at equilibrium, V is the solution volume (L), and m is the mass (g).

The kinetics of desorption involved weighing 30 mg of individual analyte-laden MP into a 15 mL test tube containing 12 mL of simulated freshwater and homogenized with ALB 260 H tube homogenizer at the maximum speed for 0, 1.0, 2.0, 4.0, 8.0, 12.0, and 24.0 h. At the corresponding time, about 1.5 mL were withdrawn and filtered through a 0.22 µm syringe filter and 0.95 mL were transferred into a 1.5 mL vial containing 0.05 mL internal standard and analyzed for the desorbed analyte using LC-MS/MS, and the desorbed capacity (mg/g) was calculated using Equation 24. Then, the percentage desorption was calculated using Equation 25. The experiment was carried out in duplicates and repeated with artificial gastric fluid and artificial intestinal fluid as the desorbing media.

$$q_{e,\ des} = \frac{C_t V}{m}$$
<div align="right">Equation 24</div>

where C_t is the concentration (mg/L) of the solution at time t, V is the solution volume (L), and m is the mass of loaded MP (g). Then, the percentage desorbed (D_C) was calculated using Equation 25.

$$D_C = \frac{q_{e,\ ads}}{q_{e,\ des}} * 100 \qquad \text{Equation 25}$$

The experiments were carried out in duplicates and repeated with artificial gastric fluid and artificial intestinal fluid as desorbing media.

4 RESULTS AND DISCUSSION

This chapter presents the findings of the study and provides an in-depth discussion of the results obtained from the various experiments conducted. The initial section focuses on the characterization of the microplastics used, detailing their physical and chemical properties. This characterization is crucial for understanding the subsequent adsorption and desorption behaviours observed in the experiments. Following this, the chapter delves into the results of the adsorption and desorption studies, comparing the performance of fresh, UV-aged, and HA-coated microplastics. The discussion integrates these findings with existing literature to draw meaningful conclusions and highlight the implications of the study.

4.1 Characterization of microplastics

The characterization of microplastics is a critical step in understanding their behaviour in adsorption and desorption processes. This section provides detailed analyses of the physical and chemical properties of the microplastics used in the study. These properties include aspects such as thermal stability, decomposition behaviour, surface morphology, and chemical composition. Understanding these characteristics is essential for interpreting the results of the adsorption and desorption experiments conducted with fresh, UV-aged, and humic acid-coated microplastics, as well as the results of desorption of the analytes in simulated water and biological fluids.

4.1.1 Thermal stability and decomposition behaviour analysis of fresh MPs

Thermogravimetric Analysis was used to investigate the decomposition behavior of the fresh microplastics at elevated temperatures to verify that the materials acquired for this study are PE, PP, PS, and PVC. The results are presented in Figure 14. From the Figure, PE, PP and PS decomposed at just a stage at specific temperature ranges: 400–499, 337–483 and 322–460 °C, respectively. PVC exhibits a two-stage decomposition process, occurring at 226–367 and 400–528 °C. The initial stage of PVC decomposition is ascribed to dehydrochlorination, resulting in the release of hydrogen chloride. In the final stage, as well as in the case of the other polymers (PE, PP, and PS), decomposition proceeds through random scission of the main chain, liberating small aliphatic chains and leaving behind no residue (Cruz et al., 2021; Dümichen et al., 2015).
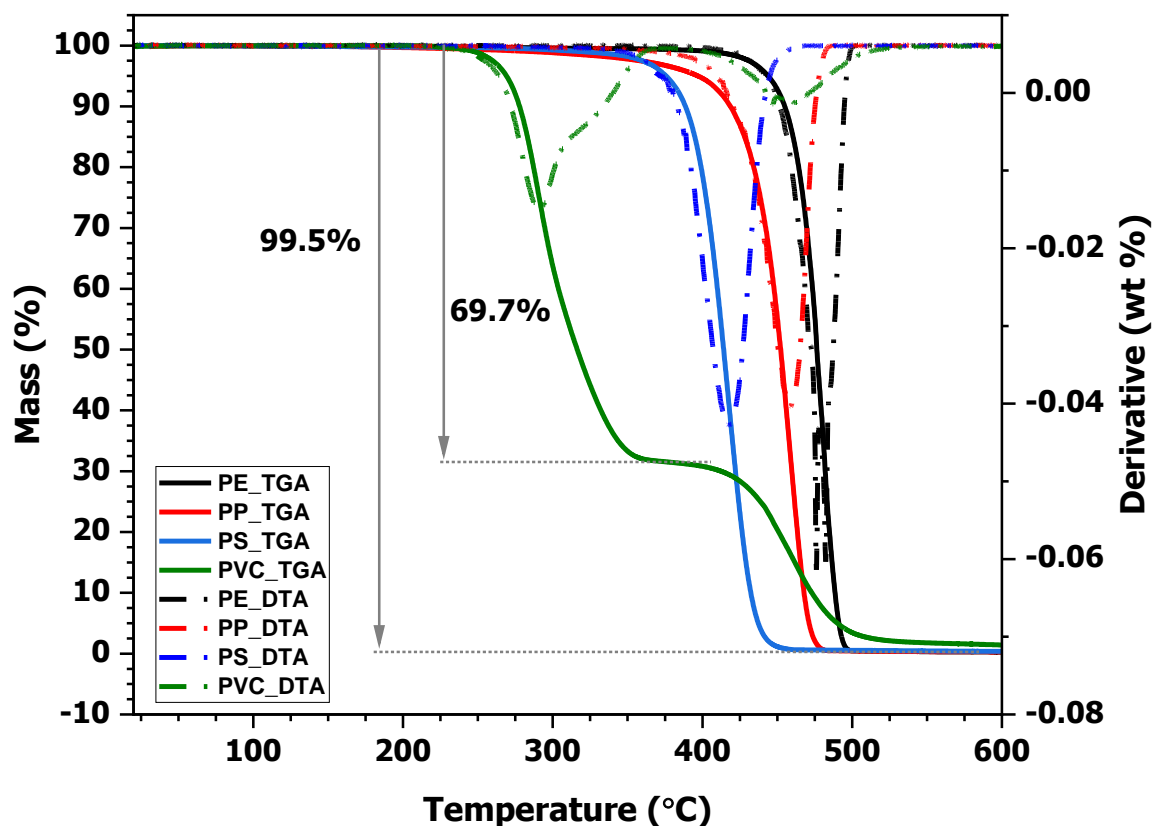
Figure 14. Thermogravimetric analysis results of fresh PE, PP, PS and PVC

The Differential Thermal Analysis (DTA) part of the Figure 14, represented by the black (PE), red (PP), blue (PS) and green (PVC) dashed lines, reveals critical insights into the thermal stability and decomposition behavior of the materials. The curves aligns well with established findings in polymer science. The peaks around 460, 450, 400, and 440 °C correspond the breaking of the polymer chains of PE, PP, PS and PVC, respectively, and the formation of volatile degradation products (Vasile, 2000). PVC shown a peak around 260 °C which corresponds to the dehydrochlorination process, where HCl is released, leading to the formation of polyenes, which further degraded at higher temperatures (Yassin & Sabaa, 1990). The thermal deposition of polymers may be influenced by their chemical structure and the presence of stabilizing additives. For instance, PE's higher decomposition temperature can be attributed to its simpler and more stable molecular structure, while the presence of chlorine atoms in PVC promotes its earlier thermal decomposition (Yu et al., 2016). These thermal behaviour are consistent with literature and indicated that the materials acquired for this study are PE, PP, PS and PVC.

4.1.2 Visual inspection of modified microplastics

Figure 15 shows images of the fresh, UV-aged, and HA-coated microplastics. Among other physicochemical changes induced by UV and HA treatments, the colour alteration was notable. UV irradiation caused the most intense colour change in PVC, followed by PS, whereas the colour of UV-aged PE and PP was not significantly affected. Plastics gradually change colour with UV exposure; initially, they may discolour or whiten if tinted. Over time, they shift from white to yellow and eventually to brown due to the production of chromophoric substances through oxidation (Zhao et al., 2022). The UV-aged PS turned yellowish after 20 minutes of irradiation, while PVC became brownish, indicating different reactions to UV radiation. The olefins (PE and PP), which are semicrystalline and rubbery polymers, are more resistant to UV-induced discolouration. Conversely, the two amorphous microplastics form chromophoric substances when exposed to UV light. All microplastics turned brownish after 48 hours of HA exposure, indicating coating by natural organic matter.
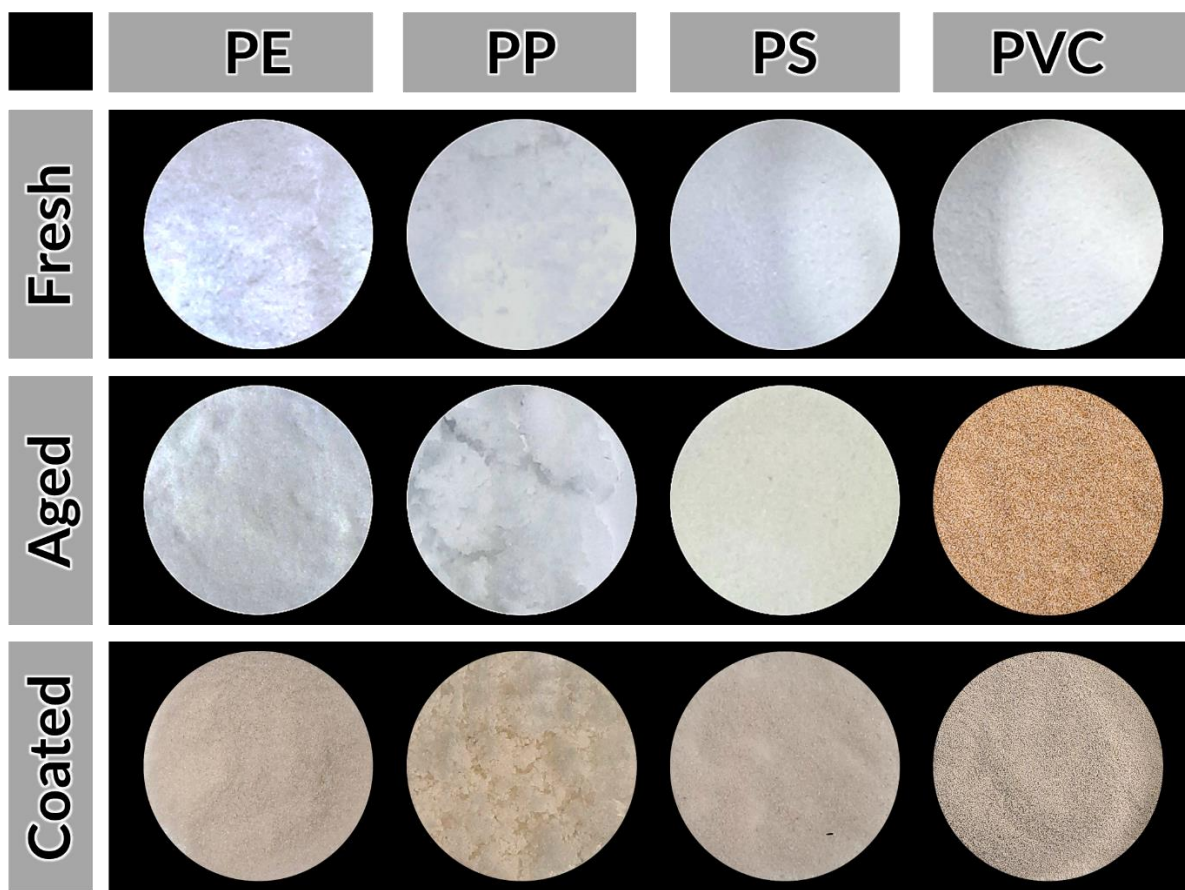
Figure 15. Images of fresh, UV-aged and HA-coated MPs

4.1.3 Crystallinity

To evaluate the change in the crystallinity due to UV exposure of the microplastics, the crystallinity of the fresh and UV-aged MPs was investigated using DSC. Figure 16 shows the glass transition temperature (T_g) and the melting temperature (T_m) of the materials.
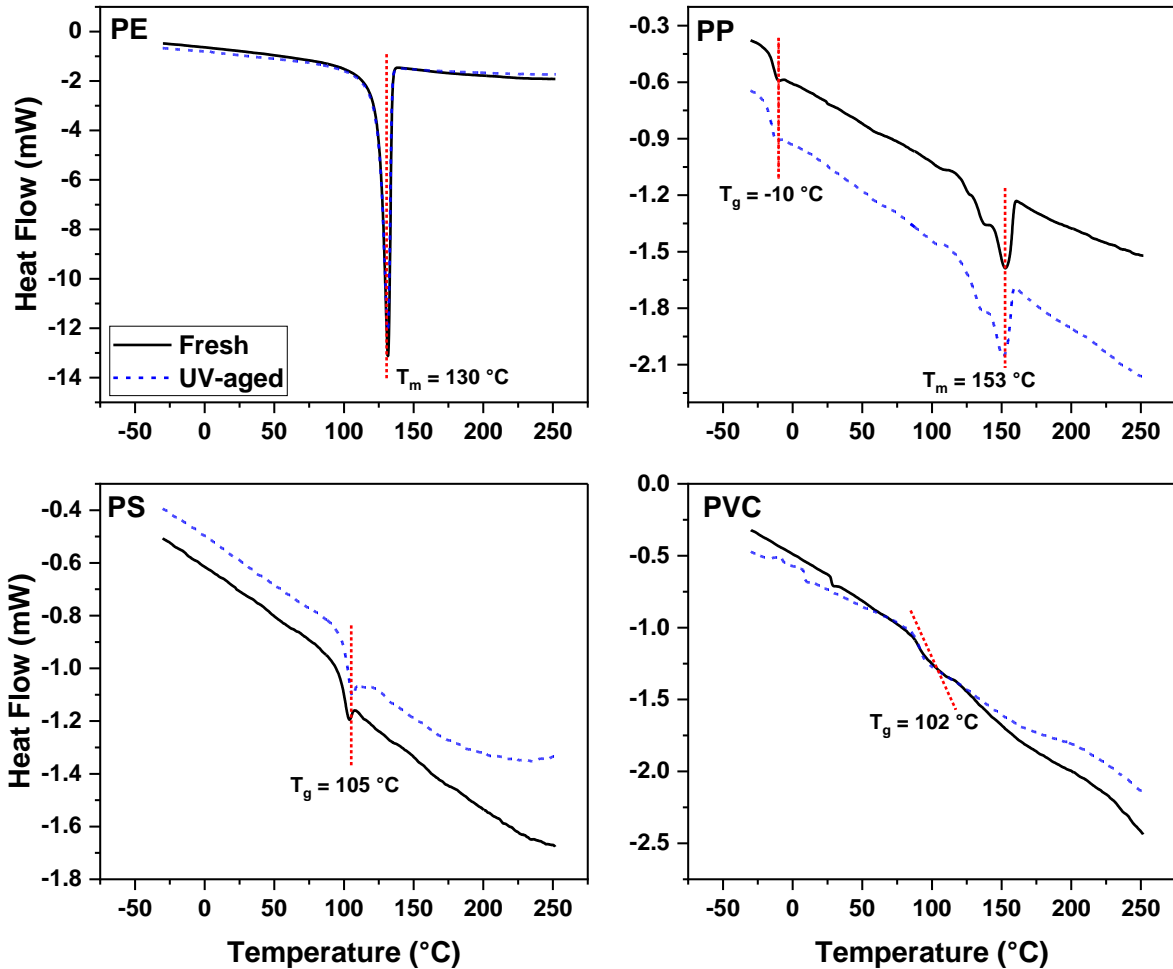
Figure 16. DSC curves of fresh and UV-aged microplastics

From the figure, the T_g of PP, PS and PVC are -10, 105 and 102 °C. The T_g of PE usually occur between -120 – -52 which is below the recorded temperature range in this study. T_m from DSC is associated with the heat of fusion and was only observed from PE and PP thermograms and they are 130 and 153 °C, respectively. The absence of T_m in the themograms of PS and PVC suggests that they are amorphous materials. The crystallinity which was determined using Equation 10 and slightly declined from 50.3% in fresh PE to 49.03 in UV-aged PE. Likewise, the crystallinity of PP decreased from 7.19% in fresh to 6.85 % upon UV exposure for 20 min. The

decrease in the crystallinity indicates a slight increase in the amorphous regions of the materials upon ageing, and thereby possibly increase their brittleness. An insertion of oxygen groups into the polymeric chains is possible upon UV exposure, and they can interrupt both the amorphous and crystalline domains of the polymer's chain, truncating the polymer chains or introducing bulky oxygen groups that do not fit well within the tightly packed crystalline pattern and subsequently lowering the polymeric crystallinity (Sarkar et al., 2021). A downward change in the crystallinity of polyurethane was reported by Wu et al. (2020) with chemical oxidation.

Contrarily, photo-oxidation may increase crystallinity in polymers because the amorphous regions within the plastic are more susceptible to photo-degradation. These regions are less tightly packed and more accessible to light than the crystalline regions. Consequently, chain scission occurs, resulting in a decrease in the molar mass of the macromolecules (de la Orden et al., 2015). In this study, a slight decrease in crystallinity was observed, indicating that the ageing process effectively promoted a more flexible molecular chain arrangement (Guo et al., 2012; Wu et al., 2020). Consequently, the UV-aged microplastics had a greater proportion of amorphous regions and were likely more brittle and hydrophilic than the fresh samples.

4.1.4 FTIR characterisation

FTIR was used to investigate the chemical composition and structural changes of fresh, aged, and coated microplastics and their spectra are presented in Figure 17. The peaks at 1470, 1376, 1454 and 1427 cm^{-1} are normal peaks of PE, PP, PS and PVC, respectively, and they were used to normalize their respective spectra. For the olefins, the two peaks in the region of 3000 - 2850 cm^{-1} (2918 and 2847 cm^{-1} for PE and 2955 22929, 2870 and 2840 cm^{-1} for PP) are characteristic symmetric and asymmetric stretching vibrations of CH$_2$ and CH$_3$ (Kong et al., 2021; Smith, 2021). For PS, the CH$_3$ and CH$_2$ stretching of aromatic were recorded at 3060 and 3027 cm^{-1} and for aliphatic at 2920 and 2850 cm^{-1}. The PVC's characteristics bands at 2910 and 620 for aliphatic C–H stretching and C–Cl stretching, respectively, were observed. These bands also confirmed the nature of the purchased microplastics in this study.
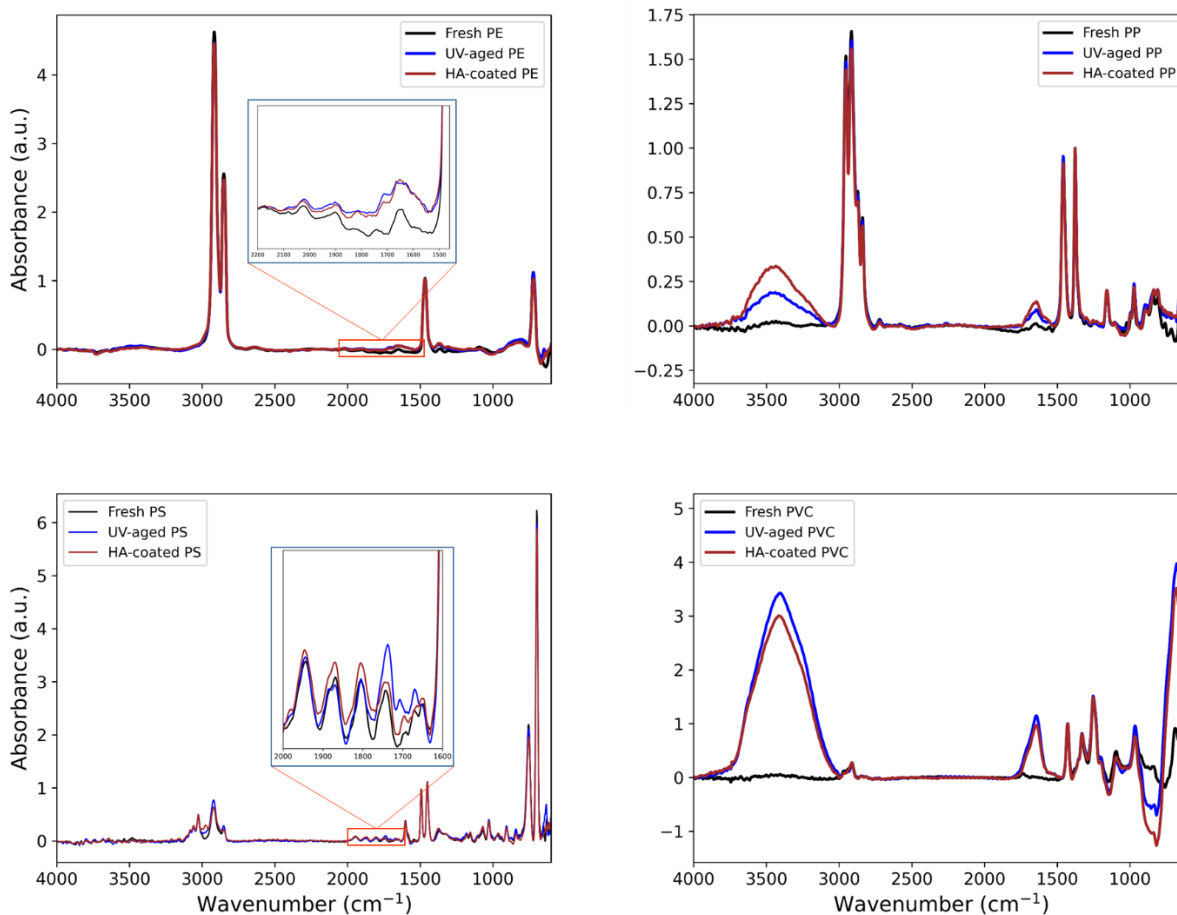
Figure 17. FTIR spectra of fresh, UV-aged and HA-coated PE, PP, PS and PVC

Hydroxyl (3800–3100 cm^{-1}) and carbonyl (1800–1600 cm^{-1}) groups have been extensively used to explain various types of microplastic ageing. Hydroxyl groups, such as those found in alcohols and phenols, and carbonyl groups, such as those in esters, ketones, lactones, and amides, are commonly introduced during the plastics UV ageing (Bredács et al., 2023; Changmai et al., 2018; Gulmine & Akcelrud, 2006; Harshvardhan & Jha, 2013). Ali et al. (2024) observed that biomolecules of various functional groups (e.g., -COOH, -OH, -NH$_2$, -NH$_3$, -HSO$_3$) can stick on the surface of MPs by various interaction forces, including hydrophobic interactions, electrostatic, π–π interactions.

The faint bands observed at 2100–1540 cm^{-1}, 1682–1588 cm^{-1} and 1973–1633 cm^{-1} in the fresh PE, PP and PS, respectively, suggested the presence of carbonyl impurities. For PE and PS, these bands increased slightly upon exposure to ultraviolet light and humic acid, indicating a possible enhancement in the concentration of these groups. In the case of PP and PVC, photoageing

and acidic coating introduced significant amounts of carbonyl and hydroxyl compounds. This is evidenced by the intense peaks at 1740–1590 cm^{-1} and 1810–1568 cm^{-1}, and the broad bands at 3650–3097 cm^{-1} and 3740–2980 cm^{-1}, respectively, in the UV-aged and humic acid-coated samples of PP and PVC.

These results suggest that 20 min of UV irradiation and 48 hours of acidic coating effectively modified the chemical composition of the microplastics, along with other physical alterations. This study underscores the significance of analyzing specific functional groups to comprehend the chemical transformations in microplastics resulting from ageing processes and environmental exposure. It was anticipated that these modifications would enhance the adsorption performance of the microplastics for both hydrophilic and hydrophobic pollutants, which our findings confirm. Detailed discussions and analyses are subsequently presented in this section.

4.1.5 Surface morphology

The surface morphology of fresh, aged, and coated microplastics was analyzed to investigate changes in their texture and surface roughness using SEM, and the morphological images are depicted in Figure 18. Fresh PE, PP and PS had relatively smooth surfaces with some characteristic details, such as microfractures in PE; flakes, wrinkles and microfractures in PP, and a few flakes in PS; which must have introduced during cryogenic milling. Fresh PVC was more rough with cracks and pores.
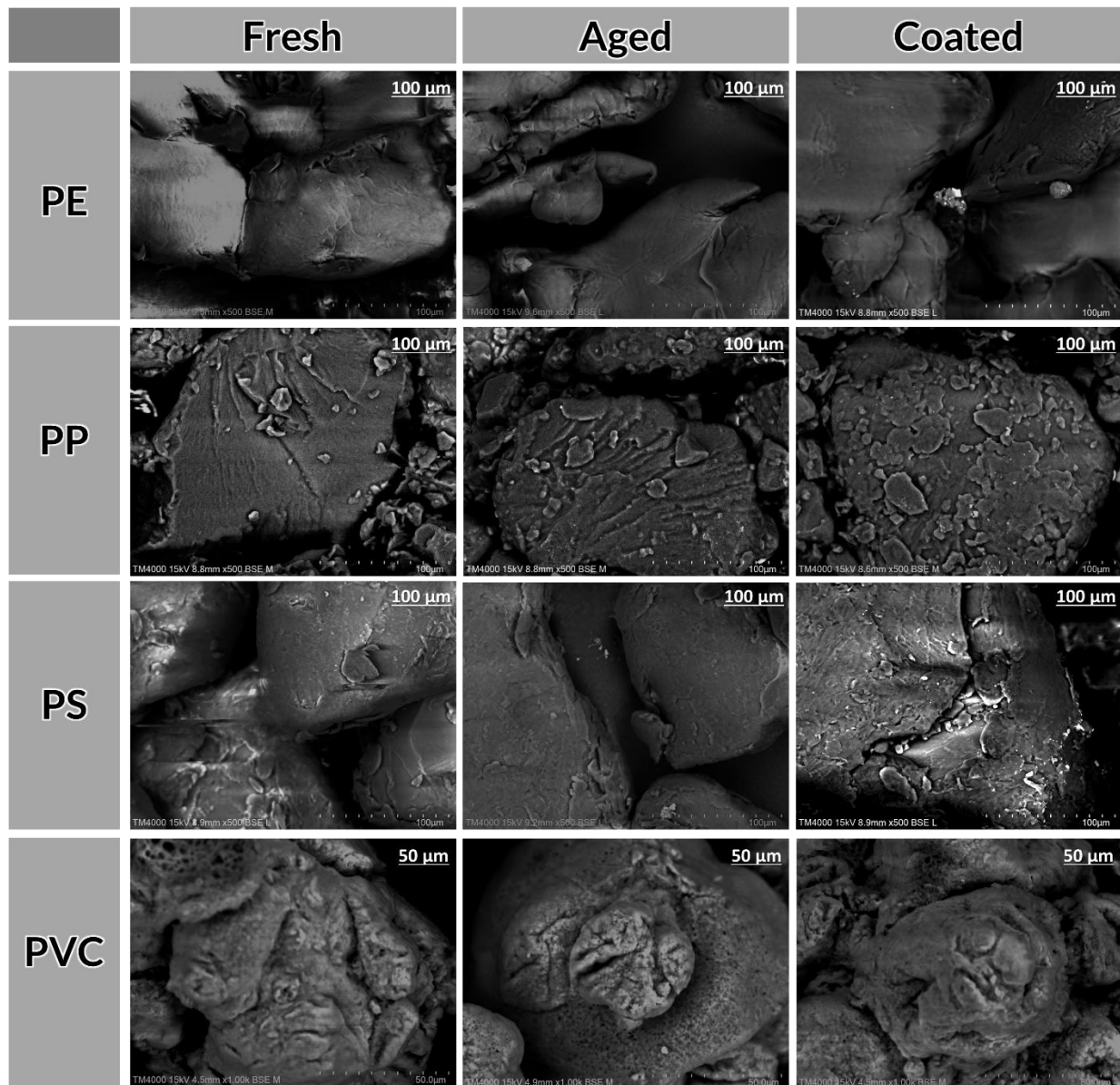
Figure 18. SEM images of fresh, UV-aged and HA-coated PE, PP, PS and PVC

UV ageing and eco-coronation of microplastics lead to a range of morphological changes, such as wrinkles, cracks, bulges, folds, pores, crumples, and flakes (Gao et al., 2021; Li et al., 2024; Luo et al., 2022; Wang et al., 2021a). After 20 min of UV-C exposure, surface features of PE, PS and PVC were smoother while PP had some crumples. The smoother surface is likely a result of the removal of small surface features and irregularities, while the crumples may arise from internal fractures or localized compressive stresses, leading to crumpled areas instead of a uniform smoothness. In the case of the HA-coated MPs, the surface of the PE exhibited swelling, while the PP and PS showed the presence of scales. Additionally, the PVC had its pores covered,

along with swelling. The various surface changes could stem from the intricate nature of humic acid and the distinct polymeric properties of the materials. The morphological transformations observed during treatment suggest that the surface modification of the microplastics may have resulted from their exposure to UV-C for 20 min and interaction with humic acid for 48 h.

4.1.6 Oxygen content

The percentage of oxygen in the microplastics was investigated using scanning electron microscopy coupled with energy dispersive x-ray spectroscopy (SEM-EDS) and the results are presented in Figure 19.
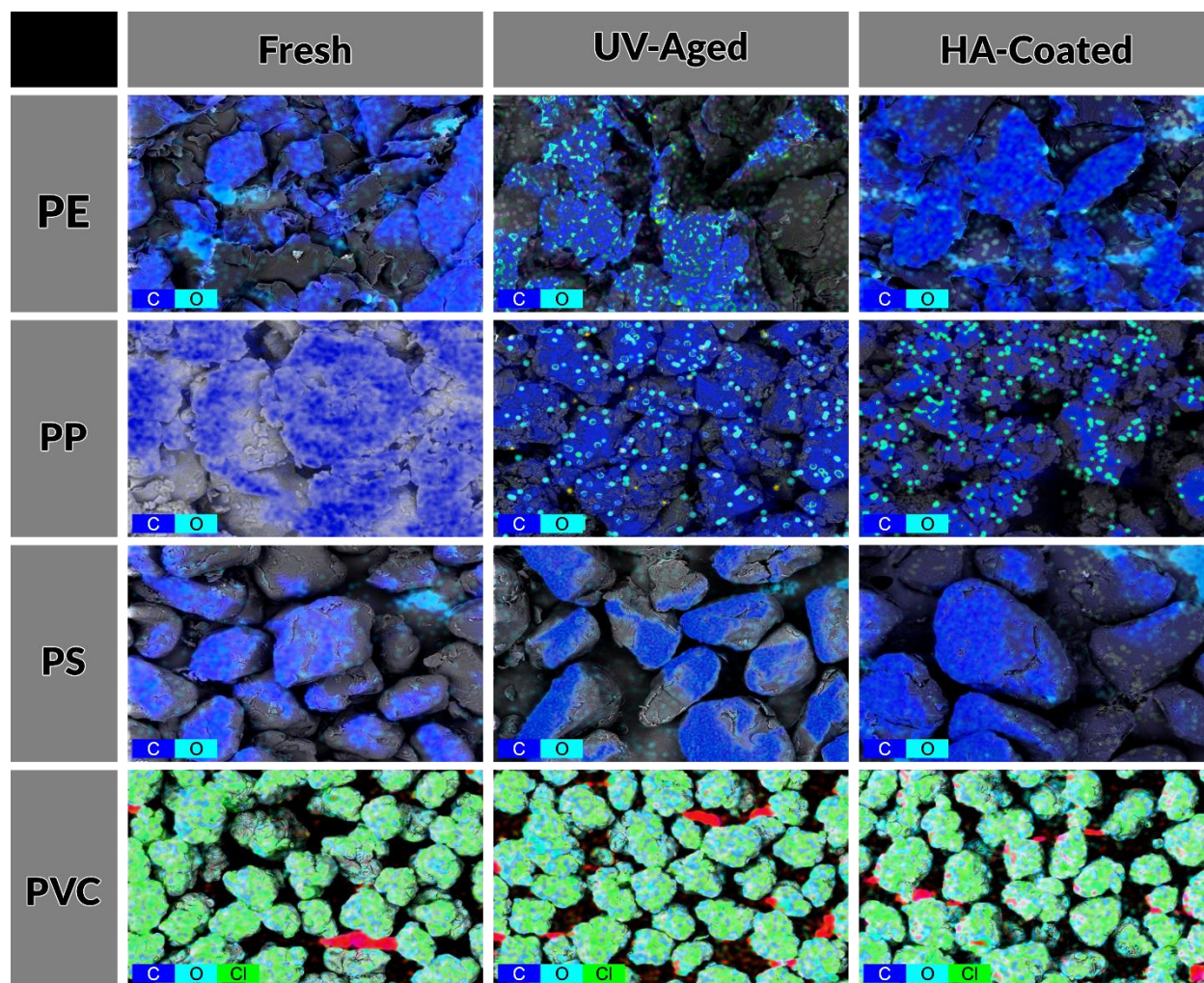
Figure 19. SEM-EDS images of fresh, aged and coated PE, PP, PS and PVC

The oxygen content of the fresh microplastics ranged from 1.33 to 2.90% and is relatively low compared to the UV-aged and HA-coated microplastics, indicating a minimal oxo species,

probably impurities, are present in the fresh microplastics. Upon ageing, there is a modest increase in the oxygen concentration, most noticeable in PE (5.45%), followed by PVC (4.35%), PS (3.58%) and PP (3.17%), indicating mild oxidation by the photooxidation process.

Similarly, coating with humic acid enhanced oxygen content, however, the extent differed between microplastics. The highest percentage was found by HA-coated PP (7.96%), followed by PE (5.46%), PS (4.98%), and PVC (4.97%). The increase in oxygen content implies that the treatments must have created more oxygen-containing functional groups such as hydroxyl, carbonyl, and carboxyl groups on the coated microplastics, which could improve their surface hydrophilicity (Huang et al., 2024).

4.1.7 Zeta potential

Zeta potential, a measure of the electrostatic potential at the slipping plane of a particle in a suspension, provides valuable insights into the stability of colloidal dispersions. It was measured in this study to determine the suspension ability of fresh, UV-aged, and HA-coated microplastic. Zeta potentials of materials are usually grouped with potentials ranging from 0 to ±5 mV been classified as having the potential to coagulate or flocculate rapidly, ±10 to ±30 mV as incipient instability, ±30 to ±40 mV as moderate stability, ±40 to ±60 mV as good stability, and more than ±61 mV as excellent stability (Alsharef et al., 2017). According to Clogston and Patri (2011b), particles with zeta potential ranging from 0 to ±10 mV are approximately neutral, while those greater than +30 mV or less than -30 mV are strongly cationic and anionic, respectively.

The zeta potential of fresh and treated microplastics is presented in Table 8. Fresh microplastics, excluding PE, exhibited zeta potentials in the range of 0 to ±10 mV, suggesting that fresh PP, PS, and PVC are not stable in water at a pH of 6.54. In contrast, PE presented a zeta potential of –14 mV, indicating that the repulsive and attractive forces between PE particles are nearly balanced. Consequently, PE particles may stabilize or destabilize with minor changes in the surrounding media conditions, such as slight pH adjustments (Alsharef et al., 2017).

Table 8. Zeta potential of fresh, UV-aged and HA-coated PE, PP, PS and PVC

MP	Fresh	UV-aged	HA-coated
PE	-14.5	-6.46	-15.65
PP	-8.78	-12.2	-9.26
PS	-8.355	-14.8	-10.325
PVC	-4.16	-18.8	-18.75

Upon ageing, the zeta potential of the microplastics decreased to less than –10 mV, except for PE, which saw an increase from –14 mV to –6.46 mV. This increase in aged PE's zeta potential suggests a reduction in stability. Coating the microplastics with humic acid significantly reduced their zeta potential, particularly in the case of PVC. Humic acid, being rich in oxygen-containing groups, can introduce these functional groups to the surface of the microplastics, thereby altering their surface charge and enhancing their stability.

For most microplastics, except aged PE and coated PP, treatment appears to have enhanced their stability in water. Negative zeta potential values indicate the presence of cationic material in the liquid, while positive values suggest anionic material (Clogston & Patri, 2011b). Additionally, a zeta potential further from zero indicates higher ionic concentration. Thus, all microplastics tested carried a negative charge in water at pH 6.54, which could significantly impact their interactions with the CECs. This finding suggests that negatively charged microplastics may have specific interactions with various CECs due to electrostatic forces, potentially influencing their transport and fate in aquatic environments.

4.1.8 pH at the Point of zero charge

The pHpzc is the pH at which the surface of a material carries no net electrical charge. At this specific pH, the number of positive charges on the surface equals the number of negative charges, resulting in a neutral surface. This parameter is crucial in understanding and predicting the interactions between microplastic particles and their environment, especially in aqueous solutions (Wang et al., 2022). Figure 20 illustrates the pHpzc for both fresh and treated microplastics. The PCZ of PE ranged from 4.57 to 5.10 in SFW, AGF and AIF, 3.71 to 5.01 for PP, 5.05 to 5.33 for PS, and 4.66 to 5.65 for PVC. The results showed that the zeta potential

materials reduced with increasing pH, and were consistent with the results for PVC, PS and PET by Du et al. (2022).
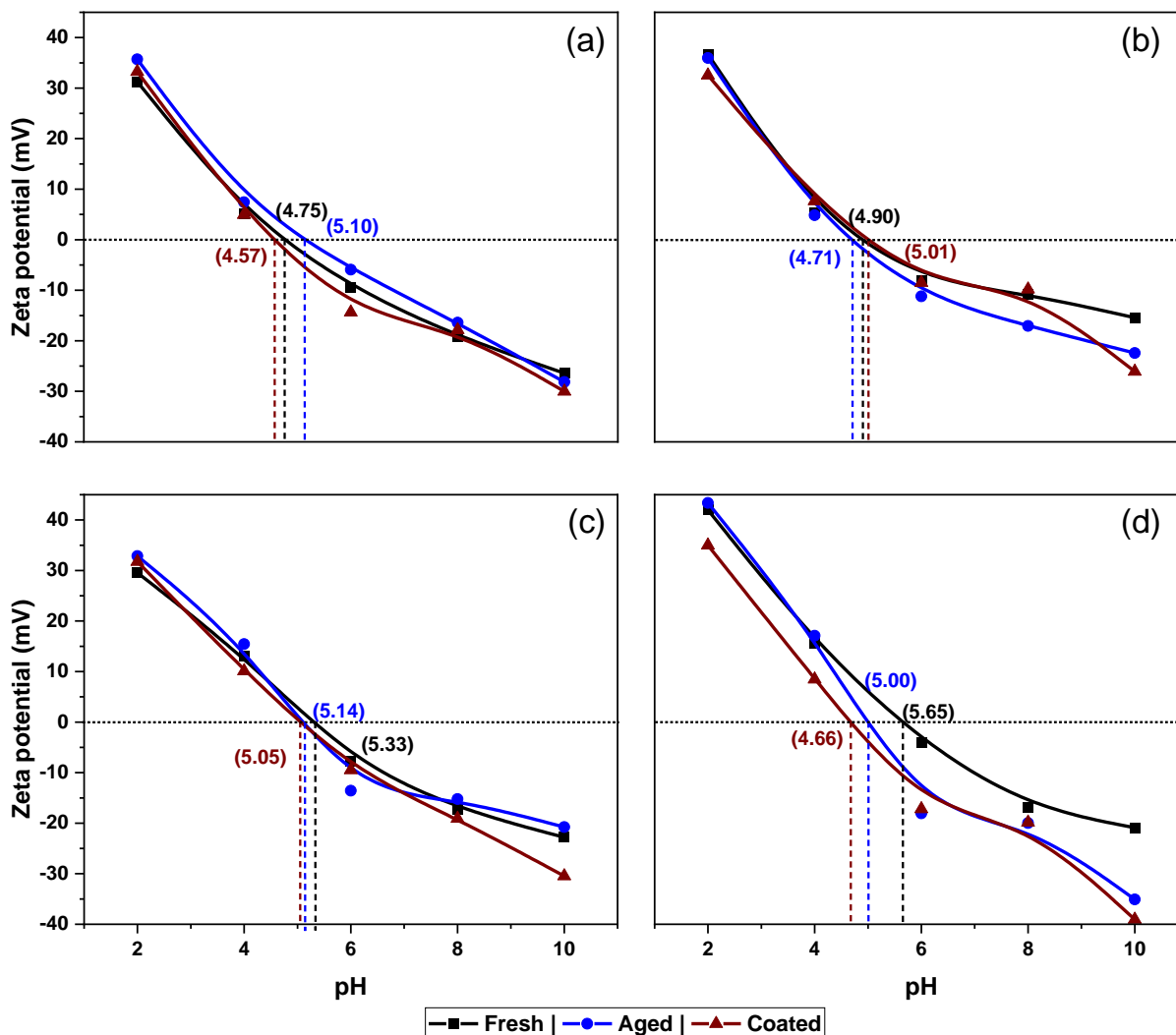
Figure 20. pH at the Point of zero charge (pHpzc) of fresh and modified PE (a), PP (b), PS (c) and PVC (d)

In this study, all sorption experiments were conducted in solutions with a pH above the pHpzc of the microplastics. This indicates that the surface of the microplastics carried a net negative charge during the sorption process (Agboola & Benson, 2021). The negative surface charge of the microplastics would favour the adsorption of positively charged species through electrostatic attraction, while potentially repelling negatively charged species. Considering the hydrophilic contaminant, sulfamethoxazole, and the hydrophobic one, diclofenac, investigated, the adsorption would likely be influenced by the surface charge of the microplastics.

Sulfamethoxazole, being neutral or negatively charged in typical environmental pH ranges, as well as diclofenac which can exist as a negatively charged species, might experience repulsion (Chen et al., 2011; Zhao et al., 2017).

4.1.9 Summary of characteristics of fresh and modified microplastics

The thermal stability and decomposition behaviour of fresh microplastics (PE, PP, PS, and PVC) were investigated using Thermogravimetric Analysis (TGA), revealing distinct decomposition stages for each polymer. PE, PP, and PS decomposed in a single stage at temperature ranges of 400–499, 337–483, and 322–460 °C, respectively. In contrast, PVC exhibited a two-stage decomposition process at 226–367 and 400–528 °C, with the initial stage involving dehydrochlorination and the final stage involving random scission of the main polymer chain. The UV and humic acid treatments significantly altered the microplastics' physicochemical properties, including colour changes. UV irradiation caused the most pronounced colour changes in PVC, followed by PS, while PE and PP were more resistant to UV-induced discolouration. The crystallinity index of the MPs also changed upon UV ageing, with PE and PP showing decreased crystallinity.

The UV and humic acid treatments also altered the chemical composition, surface morphology, and water suspension of the microplastics. FTIR analysis showed increased carbonyl and hydroxyl groups into the materials upon treatments. SEM images revealed that the UV-aged microplastics became smoother, except for UV-aged polypropylene, where crumples were observed. Additionally, the humic acid coating led to surface swelling, scaling, and pore filling. The oxygen content on the MPs increased with the UV and humic acid treatments, suggesting the formation of oxygen-containing functional groups. Zeta potential measurements indicated that the UV and humic acid treatments generally enhanced the stability of the MPs in water, except for aged PE, which became less stable. These results indicate that the MPs must have been UV-aged and humic acid-coated, which may consequently reduce their hydrophobicity and impact their adsorption performance for pollutants.

4.2 Preliminary experiments

4.2.1 Analyte stability

To ensure the stability of analytes in simulated freshwater and biological fluids, and to verify that they were not lost during the filtration process, a stability test was conducted. The results of the analyte stability test are presented in Table 9.

Table 9. Results of analytes stability test in filter material, SFW, AGF and AIF

Control	Concentration (µg/L)		Loss (%)	
	SMX	DCF	SMX	DCF
S_{FIL}	491.19 ± 1.65	489.24 ± 2.39	1.8	2.2
S_{SFW}	478.96 ± 4.18	476.95 ± 1.23	4.2	4.6
S_{AGF}	484.3 ± 2.40	472.15 ± 5.14	3.14	5.57
S_{AIF}	475.4 ± 3.63	459.8 ± 5.31	4.92	8.04

S_{FIL}, S_{SFW}, S_{AGF}, and S_{AIF} represent stability tests of the analytes in the filtration process, simulated freshwater, artificial gastric fluid and artificial intestinal fluid.

A possible loss of analytes to the filter materials was investigated, and the results indicated that only 1.8% of SMX and 2.2% of DCF were lost to the filter material. Hydrophilic polyvinylidene fluoride (PVDF) was chosen for this study due to its low extractability and high porosity, which favours high flow rates. Likewise, the stability of the two retained analytes, SMX and DCF, which were not significantly affected by the filtration process, was tested in the simulated media (simulated freshwater, artificial gastric fluid, and artificial intestinal fluid). Over 95% of both analytes were successfully accounted for in the simulated freshwater. For the gastrointestinal fluids, only about 3-5% of SMX and 5-8% of DCF were not accounted for after 24 hours of agitation, suggesting that the enzymes in the biological fluids did not degrade the analytes, thereby allowing the desorption experiment to proceed in these media. These results indicated that SMX and DCF were stable in both the adsorbing and desorbing media, with SMX being more stable in the biological media.

4.2.2 Preliminary sorption experiments

Adsorption experiments have been used to understand the interactions of both hydrophobic and hydrophilic pollutants with microplastics in freshwater systems (Guo et al., 2019; Tseng et al., 2022). In this study, the batch adsorption study was carried out and the equilibrium concentrations

were calculated. The absorption of a particular pollutant onto a particular microplastic primarily correlates with the properties of the pollutant and the microplastic.

To gain an insight into the sorptive capacities of the microplastics, both before and after treatment, the equilibrium concentrations, when the initial concentrations were 1000 μg/L, were compared. The sorptive uptake of SMX by the microplastics differs with the treatment of the microplastics (Figure 21). The fresh PS uptake SMX more than the other fresh microplastics having adsorbed about 25% of the initial concentration (1000 μg/L) of the adsorbent followed by the fresh PVC (19%) while others adsorbed SMX similarly (about 17%), probably due to their similar chemical nature.
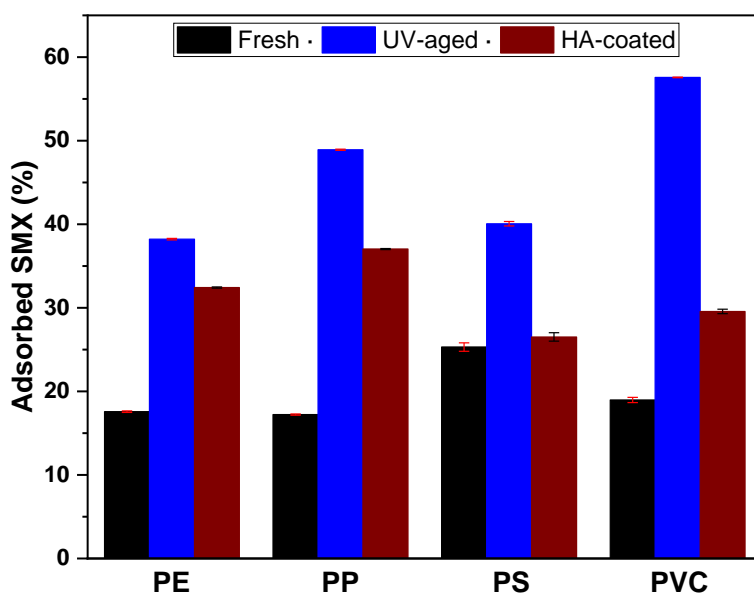
Figure 21. Percentage SMX uptake by fresh, UV-aged and HA-coated microplastics when the initial concentration was 1000 μg/L

The humic acid-coated microplastics appreciably adsorbed more SMX than the fresh ones, except for PS which increased by only 1.2% while PP increased by about 19.8%. SMX uptake by the aged microplastics was generally improved. The aged PVC adsorbed more than half (57.6%) of initial SMX, followed by PP, PS and PE with 48.9%, 40.1% and 38.2%, respectively. These indicate that both treatment approaches may have enhanced the adsorption capacity of the microplastics and corroborate previous results. A similar result has been reported by Kong et al. (2021) that humic acid coating of microplastics increased the adsorption capacity of SMX on

80

polylactic acid, polyethylene terephthalate and PP by up to 57.7%. Ageing processes have been reported to be transforming the surface structure of microplastics, which include the formation of oxygen-containing functional groups and increasing of specific surface area and porosity, among others, thereby enhancing their capacity to adsorb organic substances (Guo & Wang, 2019; Kowalski et al., 2016). Microplastic hydrophobicity has also been reported altered by ageing, increasing their water tolerance and enhancing interaction with polar substances (Liu et al., 2019).

Figure 22 presents the percentage uptake of DCF by the fresh, aged and coated microplastics. The percentage uptake was calculated based on the 1000 μg/L initial concentration of DCF, and it was notable that the percentage uptake of DCF varies among different types of microplastics and under different conditions.
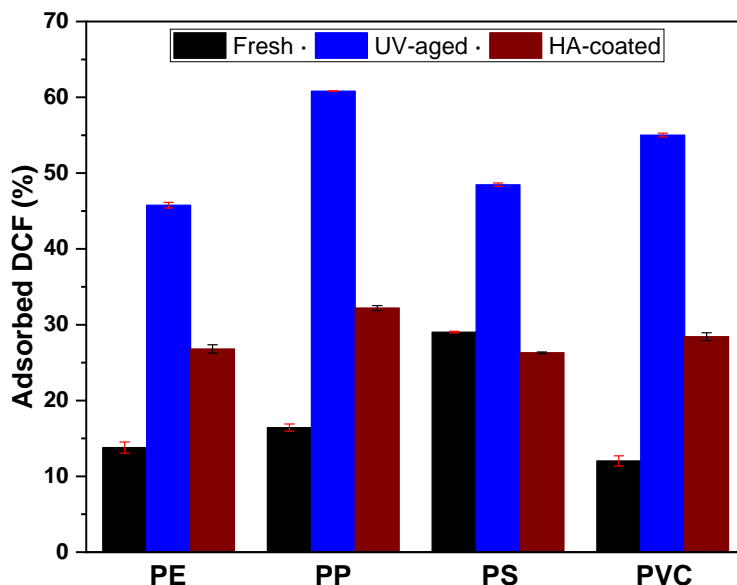
Figure 22. Percentage DCF uptake by fresh, UV-aged and HA-coated microplastics when the initial concentration was 1000 μg/L

Similar to SMX uptake, fresh PS exhibits the highest sorptive capacity for DCF (29.03%), followed by PVC (17.03%), PP (16.44%), and PE (13.8%). Similar results were obtained by Tseng et al. (2022). Coating the microplastics with humic acid leads to varied effects on DCF adsorption. The percentage uptake of DCF by coated microplastics generally increased except for PS. The coated PE and PP adsorbed about half more compared to the fresh PE and PP while PS decreased by about 3%. The ageing process significantly impacts the adsorption behaviour of DCF onto the

81

microplastics as the percentage uptake substantially increases after ageing. Generally, the adsorption was tripled compared to the fresh microplastics, except for PS. The aged PP and PVC adsorbed more than half of the initial concentration (60.82 and 55.02%, respectively) followed by PS (48.47%) and PE (45.77). Again, both treatments show a significant impact on the adsorption of the hydrophobic pharmaceutical, DCF, onto the microplastics.

In examining the sorptive capacities of microplastics for SMX and DCF, the surface properties of the adsorbent, as well as the physicochemical properties of the adsorbates, are good determinants. Fresh microplastics, particularly PS, exhibit notable sorptive capabilities for both SMX and DCF, which diminish slightly upon humic acid coating but generally increase after UV ageing. The sorptive uptake of SMX is highest in fresh PS (25%) and fresh PVC (19%), suggesting their chemical nature plays a crucial role. The humic acid coating enhances SMX adsorption, notably in PP (19.8%) and minimally in PS (1.2%). The UV-C exposure substantially improvements the uptake of SMX, particularly by PVC (57.6%) and PP (48.9%). Similar trends were also observed for DCF. These findings underscore the complex interplay of surface transformation that possibly reduced the surface hydrophobicity of the MPs and altering their adsorptive performance for pharmaceutical contaminants.

4.3 Kinetics Studies

The adsorption kinetics of SMX and DCF on the PE, PP, PS and PVC microplastics before and after 2 different treatments were investigated. Adsorption kinetics is a paramount factor dictating the pace at which solutes are adsorbed, thereby profoundly influencing adsorption efficiency. The analytes individually interacted with the microplastics at different times ranging from 0 to 48 h, and their adsorption rates were not exactly identical. Generally, adsorption equilibrium was attained within 24 h agitations. The non-linear form of pseudo-first- and pseudo-second-order models were fitted to elucidate the behaviour of the acquired empirical data.

4.3.1 SMX with fresh microplastics

The amount of sulfamethoxazole adsorbed on the fresh microplastics (PE, PP, PS and PVC) as a function of contact time is presented in Figure 23.
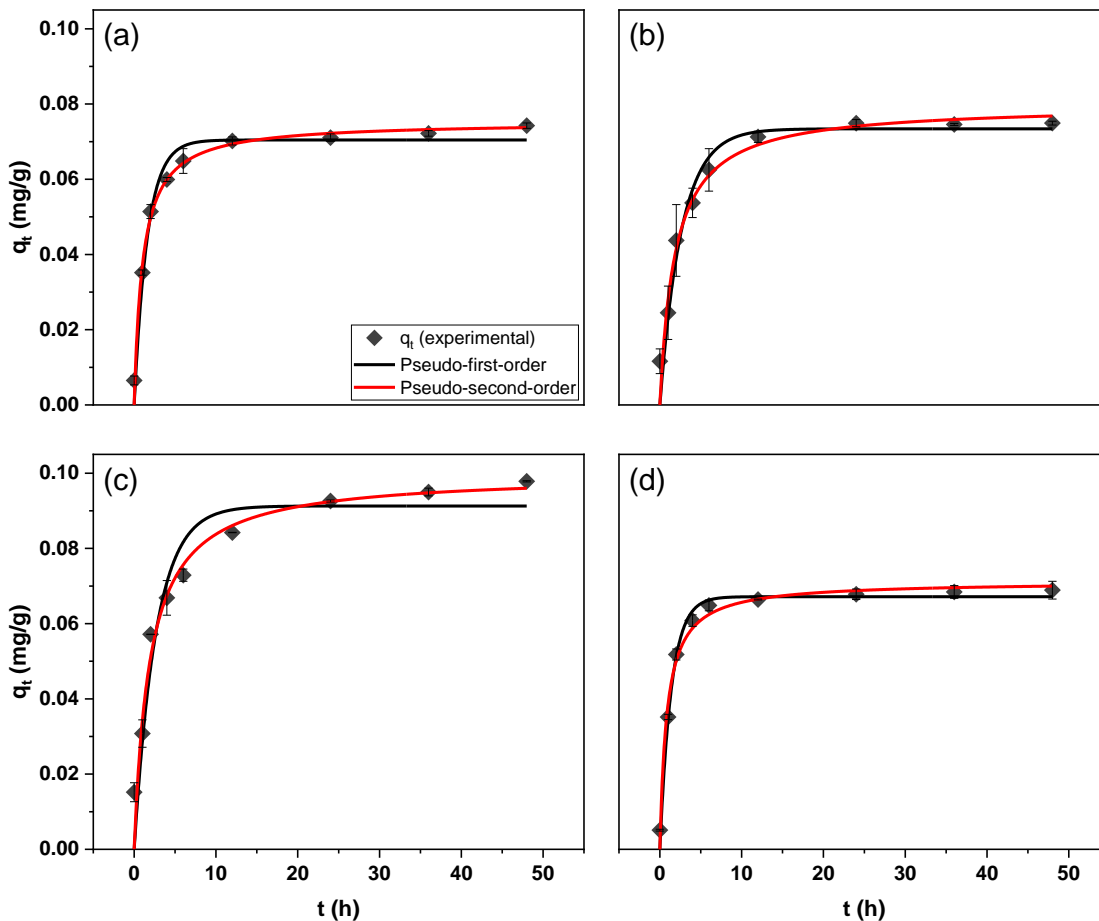
Figure 23. Sorption kinetics of SMX on fresh (a) PE, (b) PP, (c) PS and (d) PVC

The fresh microplastics were prepared from commercial plastic pellets through cryogenic milling and sieving using mesh sizes 50 and 100. The rate of the adsorption was initially high for all the fresh microplastics until around 4 h. Thereafter, a moderate rate was observed until an equilibrium was reached. For fresh PE, PP and PVC, the adsorption equilibrium was attained after 12 h (Kong et al., 2021). Subsequently, the data dispersion reaches a plateau or shows signs of stabilisation, likely due to a decrease in available binding sites. The kinetics of pharmaceutical sorption have been previously investigated. Guo et al. (2019) found that the sorption of SMX on PE, PP, PS, PVC, polyamide and poly(ethylene terephthalate) reached equilibrium within 12 h, whereas Guo et al. (2018) reported that sorption of tylosin attained 80% on the same set of MPs in 8 h. It could be concluded that SMX initially shows a high affinity for MPs, but as adsorption rates decrease over time, the reduced availability of sites and increasing repulsive forces make it more challenging for SMX to occupy them (Sena et al., 2018).

Figure 23 and Table 10 present the fitted pseudo-first and pseudo-second-order models along with their corresponding parameters and correlation coefficient (R^2).

Table 10. Sorption kinetics parameters of pseudo-first-order and pseudo-second-order models for the adsorption of SMX on FMPs

MP	$q_{e,exp}$ (mg/g)	Pseudo-first order			Pseudo-second order			
		$q_{e,cal}$ (mg/g)	k_1 (1/h)	R^2	$q_{e,cal}$ (mg/g)	k_2 (g/mg/h)	k_0 (mg/g/h)	R^2
PE	0.074	0.07 ± 0.002	0.62 ± 0.07	0.974	0.08 ± 0.002	12.87 ± 1.8	0.073	0.987
PP	0.075	0.07 ± 0.003	0.38 ± 0.05	0.957	0.08 ± 0.003	6.80 ± 1.5	0.043	0.963
PS	0.098	0.09 ± 0.004	0.38 ± 0.07	0.926	0.10 ± 0.004	5.22 ± 1.2	0.052	0.956
PVC	0.069	0.07 ± 0.001	0.72 ± 0.06	0.989	0.07 ± 0.002	16.60 ± 2.6	0.084	0.985

$q_{e,exp}$ is the experimental analyte adsorbed at equilibrium; $q_{e,cal}$ is the estimated analyte adsorbed at equilibrium; k_1 is the pseudo-first-order rate constant; k_2 is the pseudo-second-order rate constant; k_0 is the initial adsorption rate.

The initial rate (k_0) of the adsorption process was calculated from $k_2 q_e^2$ and the results are in the order PP<PS<PE<PVC, suggesting that the PVC possesses higher active sites and the PP with the lowest (Sena et al., 2018). Both pseudo-first-order and pseudo-second-order models effectively describe the adsorption process of SMX onto the microplastics, as indicated by an R^2 > 0.92. The pseudo-second-order model provided the best fit for the empirical data regarding SMX adsorption on PE, PP, and PS, with higher R^2 values ranging from 0.963 to 0.987, and the calculated and experimental adsorption capacities ($q_{e, exp.}$ and $q_{e, cal.}$) closely aligned. The SEM images revealed that the surfaces of fresh MPs are not entirely smooth, with microfractures, wrinkles, and flakes present in PE, PP, and PS, which might have originated from the cryogenic milling, potentially contributing to complex adsorption behaviour.

In contrast, for SMX on PVC, the pseudo-first-order model gave the best fit, as indicated by an R^2 of 0.989 and the $q_{e, exp.}$ value closer to the experimental one. A similar study by Kong et al. (2021) reported pseudo-first-order model described an adsorption of SMX onto pristine PP, poly(ethylene terephthalate), and poly(lactic acid). The fresh PVC, being a hydrophilic polymer and likely supplied as virgin microplastic, underwent no further processing before the experiment. This could explain its unique adsorption behaviour with SMX, which is also hydrophilic.

4.3.2 SMX with UV-aged MPs

In this study, the surface of the microplastics was modified by ultraviolet irradiation to simulate ageing caused by sunlight. Plastic ageing is recognized for inducing cracks, pores, and streaks, as well as increasing the presence of oxygenated functional groups, particularly carbonyl and hydroxyl groups, while also augmenting the crystalline structure of the polymer. This, thereby, impacts how microplastics interact with other matter in the environment (Bhagat et al., 2022). Given that the surfaces of the MPs were successfully modified by the UV exposure (see Section 4.1) an enhanced adsorption behaviour is expected. The graphs of the kinetics fittings for SMX on UV-aged MPs are shown in Figure 24.
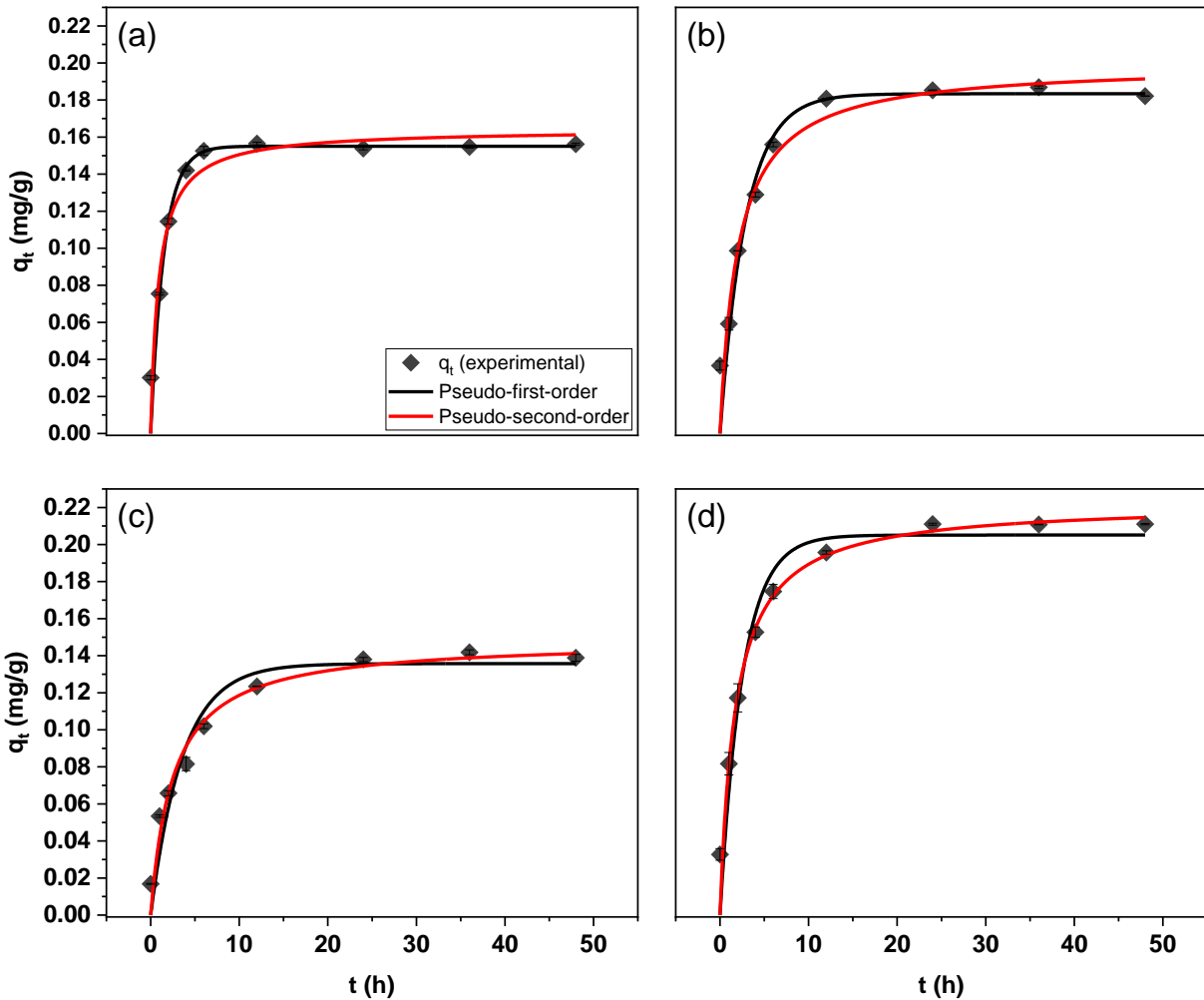
Figure 24. Sorption kinetics of SMX on aged (a) PE, (b) PP, (c) PS and (d) PVC

Similar to results obtained for fresh microplastics, a high rate of adsorption was observed within the first 4 h for SMX on all the UV-aged microplastics and equilibrium was reached after 12 h. The result is similar to that of (Kong et al., 2021). Again, there exists an initial rate of adsorption between SMX and the UV-aged microplastics in the first 4 h, and the adsorption rates tend to decrease over time until the plateau where further adsorption of SMX becomes very repulsive. Table 11 presents the model parameters of the pseudo-first- and pseudo-second-order kinetics fitting for the empirical data.

Table 11. Sorption kinetics parameters of pseudo-first-order and pseudo-second-order models for the adsorption of SMX on UV-aged MPs

MP	$q_{e,exp}$ (mg/g)	Pseudo-first order			Pseudo-second order			
		$q_{e,cal}$ (mg/g)	k_1 (1/h)	R^2	$q_{e,cal}$ (mg/g)	k_2 (g/mg/h)	k_0 (mg/g/h)	R^2
PE	0.16	0.16 ± 0.005	0.66 ± 0.11	0.944	0.16 ± 0.008	6.68 ± 2.1	0.18	0.922
PP	0.19	0.18 ± 0.007	0.34 ± 0.05	0.943	0.20 ± 0.0102	2.46 ± 0.7	0.10	0.939
PS	0.14	0.14 ± 0.006	0.28 ± 0.05	0.934	0.15 ± 0.006	2.66 ± 0.6	0.06	0.966
PVC	0.21	0.21 ± 0.008	0.39 ± 0.06	0.949	0.22 ± 0.008	2.58 ± 0.5	0.13	0.966

$q_{e,exp}$ is the experimental analyte adsorbed at equilibrium; $q_{e,cal}$ is the estimated analyte adsorbed at equilibrium; k_1 is the pseudo-first-order rate constant; k_2 is the pseudo-second-order rate constant; k_0 is the initial adsorption rate.

The initial active sites, as suggested by the initial adsorption rate (k_0), on the aged microplastics were in the ranged of 0.06–0.18 mg/g/h, in the order of UV-age PE>PVC>PP>PS, and higher than those obtained for fresh MPs with SMX. Both models presented calculated equilibrium concentrations similar to the experimental one. The pseudo-first-order model demonstrated the best fit for SMX on the UV-aged polyolefins (PE and PP) with R^2 of 0.944 and 0.943, respectively. This outcome may be due to the shift in surface properties from hydrophobic to hydrophilic, along with other physicochemical changes induced by UV ageing. On the other hand, the adsorption process of SMX onto UV-aged PS and PVC was favoubly fitted by pseudo-second-order kinetics model higher R^2 value (0.966). The adsorption rate constants for the pseudo-first-order and pseudo-second-order models showed a significant increase of 30–67% and a decline of 48–84%, respectively, after UV ageing. This is likely due to the increase in active sites on the surface of the microplastics, which enhanced the adsorption conditions. For instance, the ageing process, which altered the morphological properties and increased the hydrophilicity of the materials by introducing oxygen-containing functional groups, likely created a more favourable sorption environment for the hydrophilic SMX. These findings are consistent with the results of

Chen and Sweetman (2024), Kong et al. (2021) and Wu et al. (2020), who reported that UV ageing improved conditions for organic contaminant adsorption. Therefore, regardless of the polymer types, ageing elevates the risk of microplastics transporting hydrophilic contaminants of emerging concern within freshwater ecosystems.

4.3.3 SMX with HA-coated MPs

The surface of the microplastics was also modified by interacting them with humic acid to simulate the "eco-corona," where natural organic matter coats co-existing particles in the environment. Coating microplastics decreases their hydrophobicity and buoyancy, increases their toxicity and may enhance or deplete their interaction with pollutants in aquatic bodies (Arowojolu et al., 2023). More so, eco-corona can dictate the biological and chemical reactivity of MPs (Junaid & Wang, 2021). The fresh MPs were coated with humic acid to produce HA-coated microplastics and were exposed to SMX by the adsorption process. Figure 25 presents the graph of their kinetics fitting.
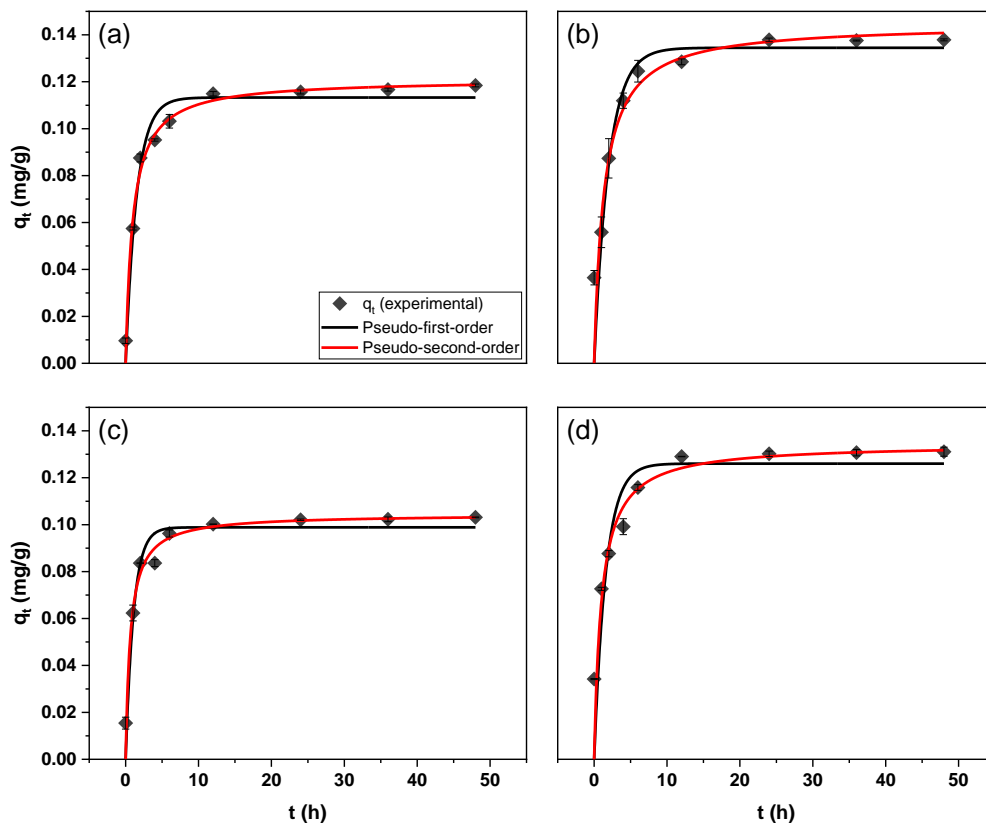
Figure 25. Sorption kinetics of SMX on humic acid coated (a) PE, (b) PP, (c) PS and (d) PVC

87

A significantly rapid adsorption rate was noted within the initial 2 hours with equilibrium being achieved approximately at the 12-hour mark. Furthermore, an initial affinity between SMX and the coated MPs is evident, with adsorption rates declining gradually over time until reaching a plateau, where additional SMX adsorption becomes highly repulsive. These results are similar to what we obtained for the fresh and the UV-aged MPs. The pseudo-first- and pseudo-second-order kinetics fitted parameters adsorption of SMX and the coated microplastics are presented in Table 12.

Table 12. Sorption kinetics parameters of pseudo-first-order and pseudo-second-order models for the adsorption of SMX on HA-coated MPs

MP	$q_{e,exp}$ (mg/g)	Pseudo-first order			Pseudo-second order			
		$q_{e,cal}$ (mg/g)	k_1 (1/h)	R^2	$q_{e,cal}$ (mg/g)	k_2 (g/mg/h)	k_0 (mg/g/h)	R^2
PE	0.18	0.11 ± 0.003	0.66 ± 0.09	0.969	0.12 ± 0.003	8.51 ± 1.30	0.12	0.985
PP	0.14	0.13 ± 0.007	0.50 ± 0.11	0.876	0.14 ± 0.009	5.17 ± 1.88	0.11	0.876
PS	0.10	0.10 ± 0.003	0.92 ± 0.18	0.931	0.10 ± 0.004	14.90 ± 4.07	0.16	0.954
PVC	0.13	0.13 ± 0.007	0.62 ± 0.17	0.804	0.13 ± 0.008	7.45 ± 2.90	0.13	0.856

$q_{e,exp}$ is the experimental analyte adsorbed at equilibrium; $q_{e,cal}$ is the estimated analyte adsorbed at equilibrium; k_1 is the pseudo-first-order rate constant; k_2 is the pseudo-second-order rate constant; k_0 is the initial adsorption rate.

The number of active sites on the microplastics as described by the k_0 values in the pseudo-second-order model was in the ranged of 0.1–0.16 mg/g/h and was in the order of HA-coated PP<PE<PVC<PS. The $q_{e,\,cal.}$ values from both models are closer to the $q_{e,\,exp.}$ values; but, the pseudo-second-order model provided a better fit for the experimental data with coefficient of determination of $0.856 < R^2 < 0.985$. The SEM images of the HA-coated MPs, morphological details like scales formation, pore covering and swelling were suggested induced by the interactions with humic acid. Also, the FTIR spectra proposed increase in oxygen-containing functional groups. These results suggested that the surface of the adsorbents have been modified and more hydrophilic, potentially increased adsorption sites on the materials and stirred a complex adsorption behaviour with the hydrophilic SMX. This could be supported further by the increase and decrease of the adsorption rate constants of pseudo-first-order and pseudo-second-order, respectively.

4.3.4 DCF with fresh MPs

To advance the understanding of the interaction of analytes with microplastics in the freshwater environment, a hydrophobic contaminant was also sorbed onto the fresh, aged and coated microplastics. Generally, hydrophobic substances tend to partition between water and organic phases, with a somewhat less affinity for water due to their *log K_{ow}* values that are far from 0, mostly $\geq$ 2. Diclofenac, with *log K_{ow}* of 4.5, was used as the representative hydrophobic contaminants of emerging concern. It is anticipated that the DCF will engage with the MPs distinctly from the hydrophilic SMX.

Studying the potential adsorption interactions between fresh MPs and hydrophobic DCF indicates (as depicted in Figure 26) a rapid adsorption rate within the initial 2 h for all the microplastic types, reaching equilibrium around 12 h.
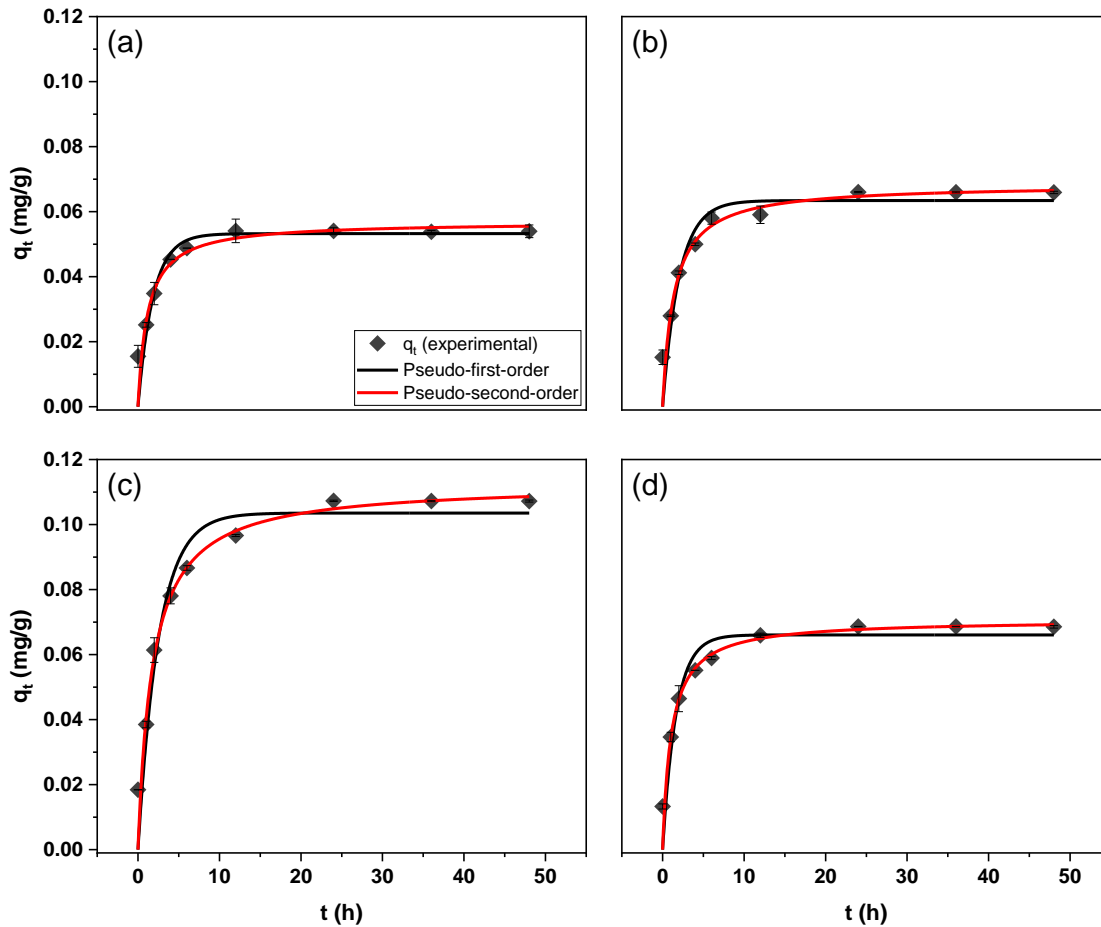
Figure 26. Sorption kinetics of DCF on fresh (a) PE, (b) PP, (c) PS and (d) PVC

The initial strong affinity, exceeding that seen with SMX and fresh microplastics, may be attributed to the hydrophobic nature of both substances. Furthermore, adsorption rates tend to diminish over time until reaching a plateau, potentially indicating a decrease in available active sites, leading to the subsequent repulsive nature of further DCF adsorption.

Table 13 depicts the parameters of the fitted kinetic models for the empirical data. The initial adsorption rates, represented by the k_0 values (ranging from 0.048 to 0.066 mg/g/h), follow the order fresh PVC > PS > PP > PE, indicating that fresh PVC offers more initial interactive sites for DCF adsorption than the other polymer types. Quantitatively, the amounts of DCF adsorbed onto the MPs were 0.11, 0.07, 0.07, and 0.05 mg/g for fresh PS, PP, PVC, and PE, respectively, indicting the superiority adsorption performance of PS for DCF. These findings demonstrate that the adsorption behaviour of the MPs aligns with their inherent physicochemical properties, as these properties are known to influence adsorption behaviour (Liang et al., 2023). The SEM images revealed slight differences in the surface morphology of the MPs, with fresh PVC exhibiting pores that were likely filled by the adsorbate. Additionally, the FTIR analysis suggested the presence of minute oxygenated impurities in fresh PE, PP, and PS, which may affect their interactions with hydrophobic DCF.

Table 13. Sorption kinetics parameters of pseudo-first-order and pseudo-second-order models for the adsorption of DCF on fresh MPs

MP	$q_{e,exp}$ (mg/g)	Pseudo-first order			Pseudo-second order			
		$q_{e,cal}$ (mg/g)	k_1 (1/h)	R^2	$q_{e,cal}$ (mg/g)	k_2 (g/mg/h)	k_0 (mg/g/h)	R^2
PE	0.05	0.05 ± 0.003	0.54 ± 0.1	0.843	0.06 ± 0.004	14.98 ± 5.9	0.048	0.847
PP	0.07	0.06 ± 0.003	0.49 ± 0.1	0.885	0.07 ± 0.004	10.62 ± 3.4	0.050	0.908
PS	0.11	0.10 ± 0.004	0.39 ± 0.1	0.936	0.11 ± 0.005	4.97 ± 1.1	0.063	0.957
PVC	0.07	0.07 ± 0.003	0.60 ± 0.1	0.906	0.07 ± 0.003	13.29 ± 3.64	0.066	0.937

Both the pseudo-first-order and pseudo-second-order models adequately described the empirical data, with R^2 values exceeding 0.84. Considerably, the pseudo-second-order model demonstrated superior R^2 values (ranging from 0.847 to 0.957) for all microplastics compared to the pseudo-first-order model. Additionally, the pseudo-second-order model's calculated q_e closely matched the experimental q_e, making it the best representation of the empirical data. Theoretically,

the pseudo-second-order model reflects a more complex adsorption process, where the adsorption rate is proportional to the square of the number of unoccupied sites (Hubbe et al., 2019). Given the physicochemical properties, including surface morphology and functional groups, of the fresh MPs, the adherence of DCF to them is likely driven by a combination of adsorption processes.

4.3.5 DCF with UV-aged MPs

To assess the effect of UV-induced surface transformations on MPs and their influence on the adsorption kinetics of DCF, both pseudo-first-order and pseudo-second-order models were applied and their plots are shown in Figure 27. Similar to the adsorption DCF onto fresh microplastics, a rapid initial adsorption was again obtained within 2 h and reduced until equilibrium at around 12 h, where a plateau was observed.
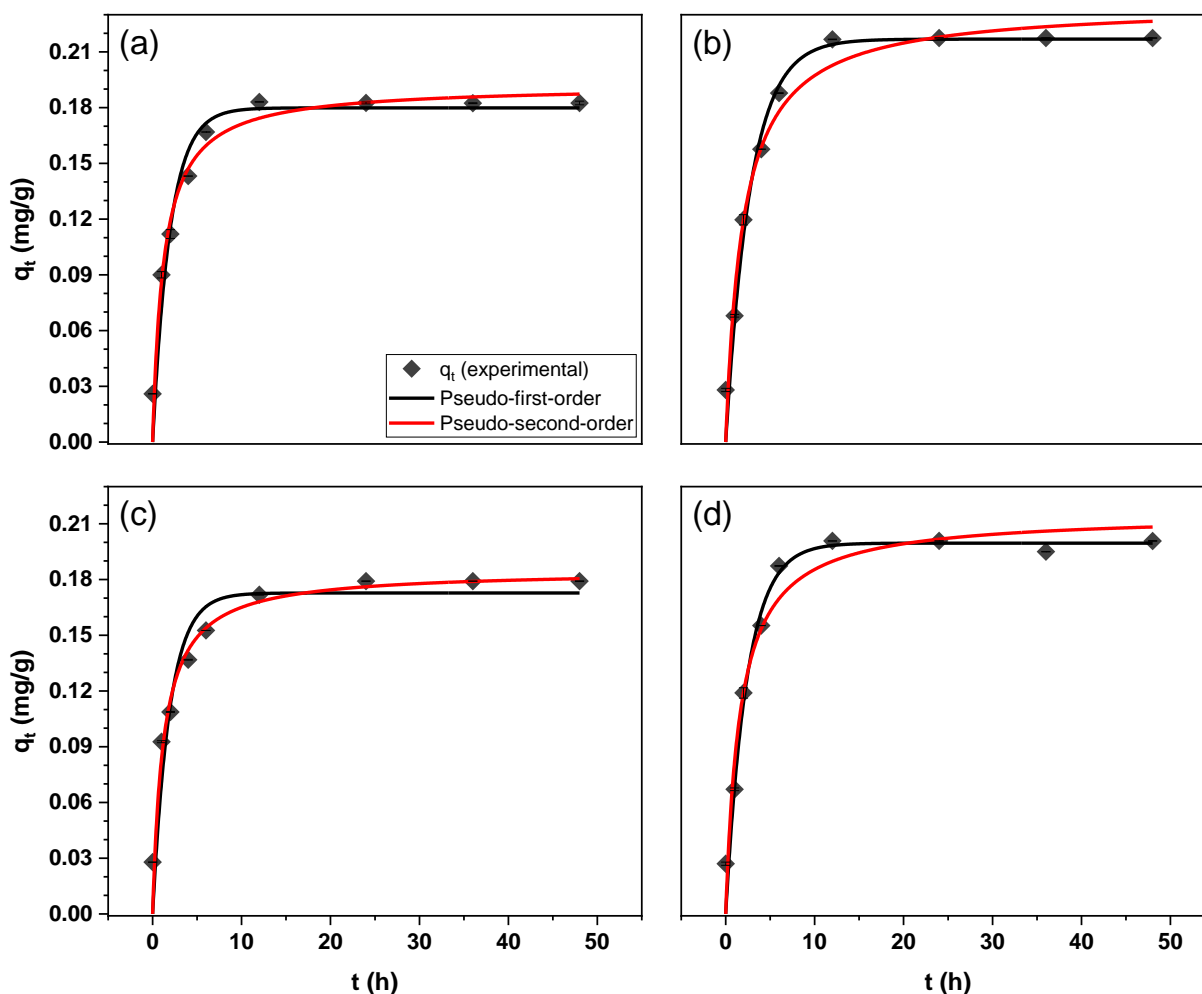
Figure 27. Sorption kinetics of DCF on UV-aged (a) PE, (b) PP, (c) PS and (d) PVC

The fitted kinetics parameters of DCF and UV-aged MPs are shown in Table 14. Both models favourably described the empirical data, with R^2 values exceeding 0.9. The rate constant, k_0 (0.12–0.16), was noticeably higher than that observed for DCF and fresh MPs, indicating an increase in active sites in the aged microplastics. In the pseudo-first-order kinetics model, UV-aged PE and PS displayed calculated q_e values closer to the experimental q_e, with higher R^2 values of 0.962 and 0.955, respectively. Conversely, the pseudo-second-order kinetics model provided calculated q_e values closer to the experimental q_e for UV-aged PP and PVC, with higher R^2 values of 0.977 and 0.975, respectively. The empirical data for DCF adsorption onto UV-aged PE and PS aligned most accurately with the pseudo-first-order model, whereas PP and PVC demonstrated a better fit with the pseudo-second-order model. The rate constants for pseudo-first-order and pseudo-second-order kinetics respectively increased and decreased, suggesting that the surface transformations of the MPs enhanced adsorption behaviour.

Table 14. Sorption kinetics parameters of pseudo-first-order and pseudo-second-order models for the adsorption of DCF on UV-aged MPs

MP	qe, exp (mg/g)	Pseudo-first order			Pseudo-second order			
		$q_{e,cal}$ (mg/g)	k_1 (1/h)	R^2	$q_{e,cal}$ (mg/g)	k_2 (g/mg/h)	k_0 (mg/g/h)	R^2
PE	0.18	0.18 ± 0.006	0.51 ± 0.08	962	0.18 ± 0.007	4.26 ± 0.95	0.16	0.949
PP	0.22	0.22 ± 0.006	0.36 ± 0.04	0.968	0.24 ± 0.009	2.18 ± 0.46	0.12	0.977
PS	0.18	0.17 ± 0.007	0.53 ± 0.10	0.955	0.18 ± 0.007	4.47 ± 1.05	0.16	0.917
PVC	0.20	0.20 ± 0.005	0.42 ± 0.05	0.954	0.22 ± 0.009	2.88 ± 0.73	0.13	0.975

$q_{e,exp}$ is the experimental analyte adsorbed at equilibrium; $q_{e,cal}$ is the estimated analyte adsorbed at equilibrium; k_1 is the pseudo-first-order rate constant; k_2 is the pseudo-second-order rate constant; k_0 is the initial adsorption rate.

The SEM images shown that the surfaces of the MPs got smoother upon UV-C exposure, except PP where crumbles were noticed. Smoother surface likely suggests a homogeneous layer which may be favoured by a simple adsorption by the pseudo-first-order model. Peculiar to UV ageing is the formation of oxygen-containing groups on the surface of the aged MPs, tending the surface towards hydrophilicity (Wang et al., 2024). Thus, irrespective of the polymer types, ageing increases the likelihood of microplastics transporting hydrophobic contaminants of emerging concern through freshwater ecosystems.

4.3.6 DCF with HA-coated MPs

To evaluate the impact of surface changes on MPs promoted by humic acid and their influence on the adsorption kinetics of DCF, both non-linear pseudo-first-order and pseudo-second-order models were fitted (Figure 28). An initial high adsorption rate was observed within 2 h and attained equilibrium in less than 12 h, except for HA-coated PP, similar to those of fresh and UV-aged MPs with DCF.
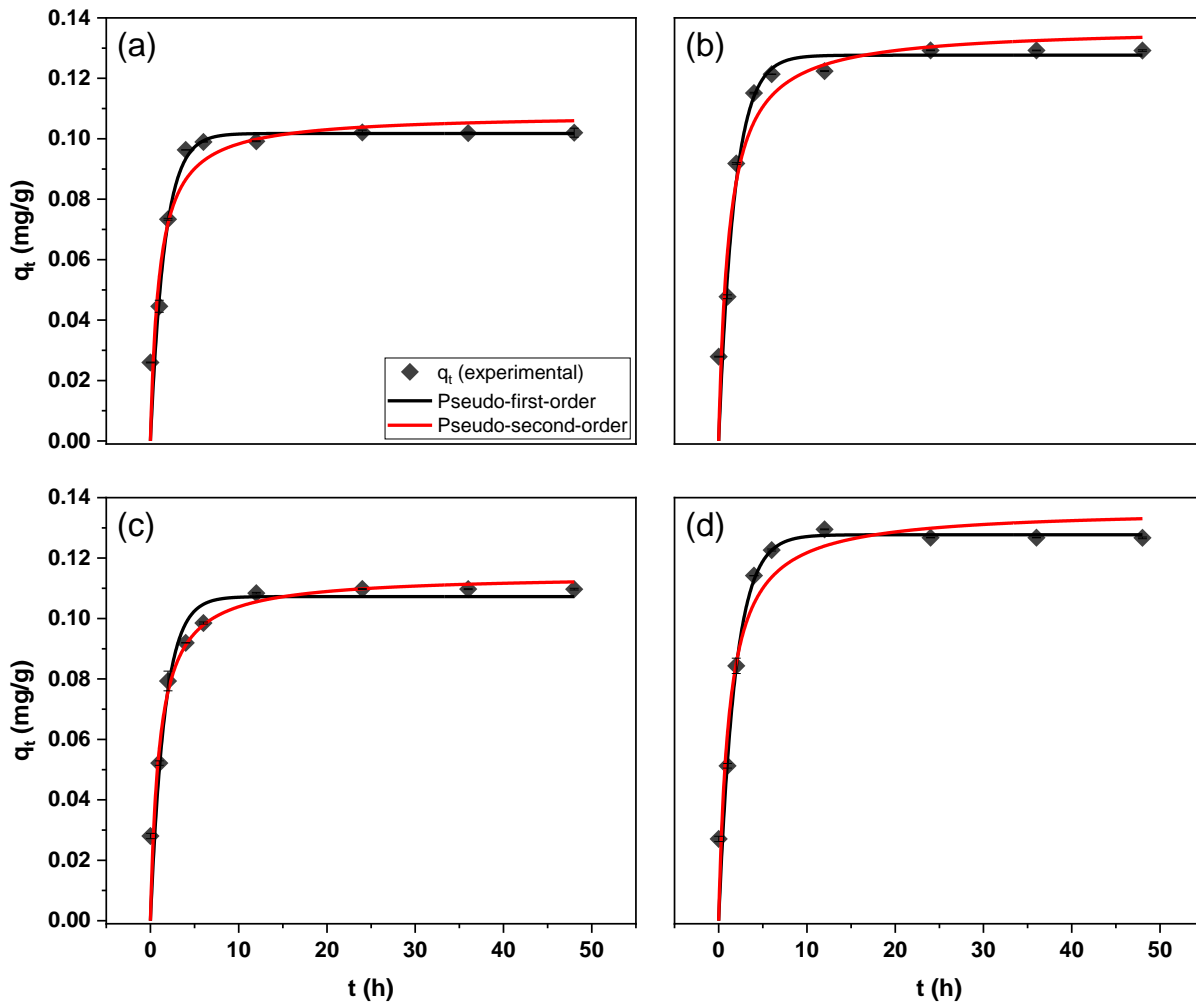
Figure 28. Sorption kinetics of DCF on HA-coated (a) PE, (b) PP, (c) PS and (d) PVC

Both models described the empirical data of DCF and HA-coated MPs, with R^2 values approximately ≥ 0.9, and Table 15 portrays their fitted parameters. The values of k_0 (0.11–0.12) are roughly consistent; they are higher than those obtained for DCF on fresh MPs but lower than those for UV-aged MPs. This suggests a uniform coating of the MPs that has slightly enhanced

their adsorptive rates. The pseudo-first-order model demonstrated calculated equilibrium adsorbed DCF ($q_{e,\,cal}$) values that were closer to the experimental equilibrium q_e. It yielded higher R^2 values of 0.894, 0.923, and 0.936 for HA-coated PE, PP, and PVC, respectively, thereby fitting the empirical data well. In contrast, the pseudo-second-order kinetics achieved a higher R^2 value of 0.879 for HA-coated PVC and most effectively described the empirical data. These results suggest that the MPs were modified by humic acid in a manner that favours adsorption processes, where the rate of occupation of adsorption sites is proportional to the number of unoccupied sites. However, this trend did not apply to PS, which possesses a phenolic group in its backbone.

Table 15. Sorption kinetics parameters of pseudo-first-order and pseudo-second-order models for the adsorption of DCF on HA-coated MPs

MP	$q_{e,exp}$ (mg/g)	Pseudo-first order			Pseudo-second order			
		$q_{e,cal}$ (mg/g)	k_1 (1/h)	R^2	$q_{e,cal}$ (mg/g)	k_2 (g/mg/h)	k_0 (mg/g/h)	R^2
PE	0.10	0.10 ± 0.005	0.62 ± 0.13	0.894	0.11 ± 0.007	9.21 ± 3.8	0.11	0.856
PP	0.13	0.13 ± 0.005	0.56 ± 0.10	0.923	0.14 ± 0.008	6.14 ± 2.2	0.12	0.897
PS	0.11	0.11 ± 0.005	0.62 ± 0.14	0.870	0.11 ± 0.006	8.54 ± 3.1	0.11	0.879
PVC	0.13	0.13 ± 0.005	0.54 ± 0.09	0.936	0.14 ± 0.007	6.12 ± 2.1	0.11	0.904

$q_{e,exp}$ is the experimental analyte adsorbed at equilibrium; $q_{e,cal}$ is the estimated analyte adsorbed at equilibrium; k_1 is the pseudo-first-order rate constant; k_2 is the pseudo-second-order rate constant; k_0 is the initial adsorption rate.

4.3.7 Comparison of the sorption rates between treatments

The adsorption rates of both hydrophilic and hydrophobic organic contaminants onto fresh, UV-aged, and HA-coated MPs were influenced by their physicochemical and surface characteristics. The initial rates were impacted by the hydrophobic nature of the adsorbate, with SMX adsorbing rapidly within the first 4 h and DCF at an even faster rate within the first 2 h, indicating the crucial role played by the hydrophobicity of MPs. Both non-linear pseudo-first-order and pseudo-second-order models fit the empirical data well, with $R^2 > 0.8$. The initial adsorption, derived from the k_0 values of the pseudo-second-order model, demonstrated that DCF interacted favourably with the adsorptive sites of the MPs than SMX. Additionally, the surface physicochemical properties significantly affected the adsorption process. The presence of oxygen-containing groups on the surface of fresh PE, PP, and PVC altered the expected behaviour of simple adsorption, which typically aligns with the pseudo-first-order model. These properties increased with surface modifications, particularly following UV irradiation. Therefore,

irrespective of the polymer type or the hydrophobicity of the contaminants, the adherence of organic pollutants onto MPs is likely driven by a combination of adsorption mechanisms. Furthermore, ageing enhances the risk of MPs transporting contaminants of emerging concern within freshwater ecosystems.

4.4 Sorption isotherms

To investigate the adsorption capacity and affinity, as well as the adsorption mechanisms and interactions, five isotherm models (Henry, Langmuir, Freundlich, Langmuir-Freundlich, and Dubinin–Radushkevich) were fitted for data obtained from the batch equilibrium sorption experiment of SMX and DCF on microplastics with different treatment. It is believed that adopting multiple models offers supplementary information which enhances understanding of the interactions between adsorbates and adsorbents. Interactions between the analytes and the microplastics, including those treated, were explored in this section.

4.4.1 SMX with fresh microplastics

To investigate the interactions between SMX and fresh microplastics, isotherm models were applied to the empirical data. The resulting plots are shown in Figure 29. The data exhibit type-C behaviour, indicating that adsorption is facilitated by a constant partitioning of the adsorbate between the adsorbent and the solvent, suggesting that linear models are expected to fit the data. All models showed coefficients of determination (R^2) greater than 0.9, and their parameters, which differed across the various types of MPs, help to explain the adsorption behaviour. This variation also highlighted the influence of microplastic composition, adsorbent properties, and the characteristics of the adsorbing medium on the adsorption processes.
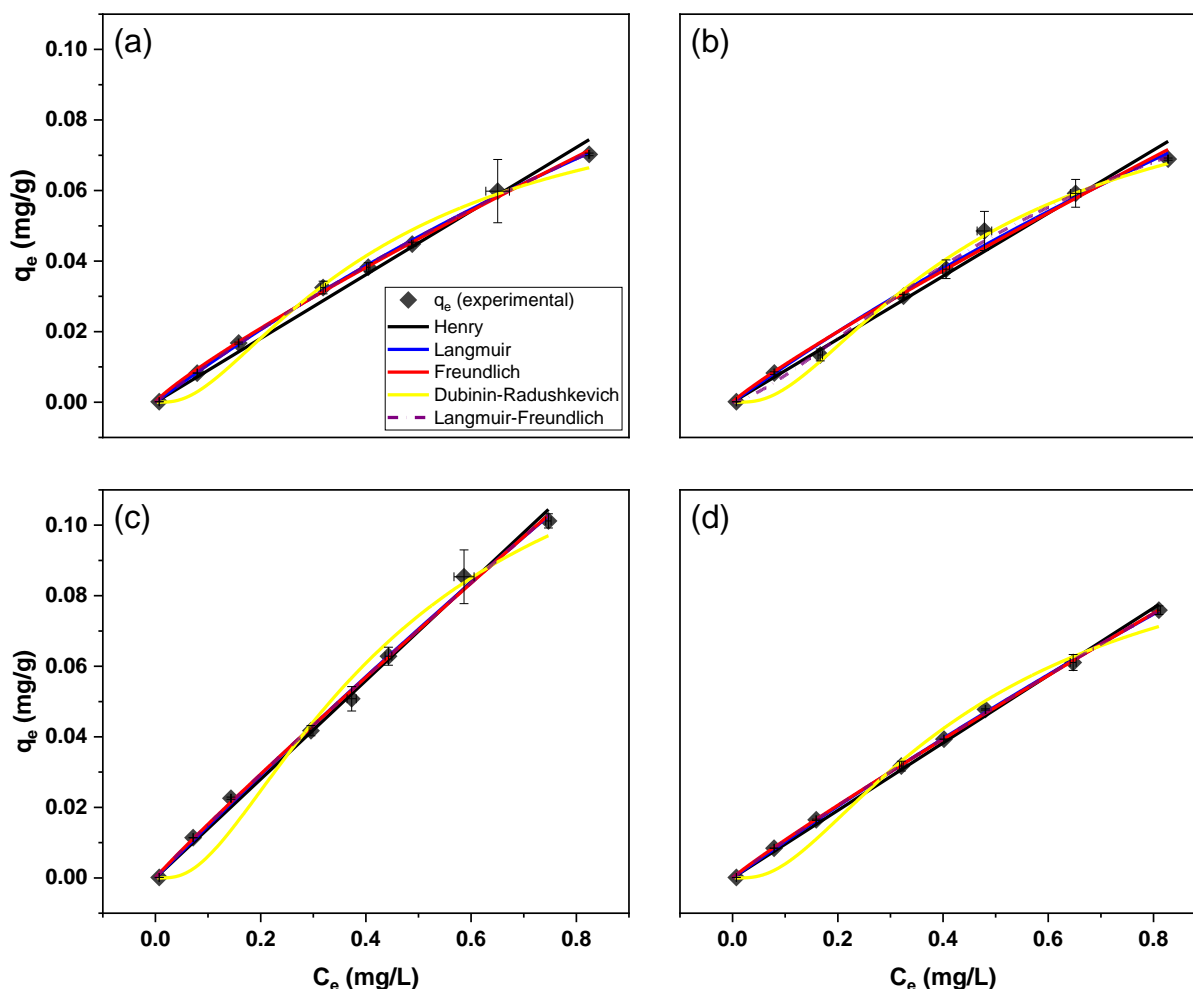
Figure 29. Adsorption isotherms of SMX on fresh (a) PE, (b) PP, (c) PS and (d) PVC

Table 16 presents the regression parameters of the models obtained from each model. All the fitted models described the empirical data well with a determination coefficient ($R^2 > 0.9$). For all the microplastic types, both the Henry's, Langmuir and Langmuir-Freundlich models yielded the highest determination coefficients (R^2 ranging from 0.972 to 0.999) with the Freundlich model coming next (R^2 ranging from 0.987 to 0.994), and finally the Dubinin-Radushkevich model (R^2 ranging from 0.97 to 0.99). The Langmuir-Freundlich equation was very suitable for fitting the empirical data of PE and PVC ($R^2 = 0.999$). The Langmuir-Freundlich model's n parameter for PE was greater than 1 (1.19) and may have impend the model to adequately explain the interaction between the adsorbents (fresh PE, PP, PS and PVC) and SMX.

Table 16. Parameters of Henry, Langmuir, Freundlich, Langmuir-Freundlich and Dubinin–Radushkevich equations for adsorption of SMX on fresh PE, PP, PS and PVC

Model	Parameter	PE	PP	PS	PVC
Henry	K (L/mg)	0.09 ± 0.002	0.09 ± 0.002	0.14 ± 0.002	0.08 ± 0.002
	R^2	0.992	0.995	0.994	0.992
Langmuir	q_m (mg/g)	0.32 ± 0.1	0.37 ± 0.2	1.29 ± 0.9	0.70 ± 0.1
	K_L (L/mg)	0.34 ± 0.06	0.29 ± 0.1	0.12 ± 0.1	0.15 ± 0.03
	R^2	0.972	0.992	0.997	0.999
Freundlich	K_F (mg/g)	0.08 ± 0.001	0.08 ± 0.003	0.14 ± 0.003	0.09 ± 0.001
	n	1.2 ± 0.03	1.1 ± 0.08	1.1 ± 0.04	1.1 ± 0.01
	R^2	0.989	0.989	0.994	0.987
Langmuir-Freundlich	Q_m (mg/g)	0.34 ± 0.20	0.13 ± 0.04	3.31 ± 24.33	1.18 ± 1.37
	K_a	0.36 ± 0.27	1.35 ± 0.52	0.04 ± 0.32	0.08 ± 0.11
	n	1.19 ± 0.09	1.38 ± 0.21	0.97 ± 0.14	0.97 ± 0.05
	R^2	0.999	0.995	0.997	0.999
Dubinin–Radushkevich	q_s (mg/g)	0.12 ± 0.01	0.10 ± 0.01	0.14 ± 0.01	0.10 ± 0.01
	E (kJ/mol)	2.4 ± 0.3	2.3 ± 0.2	2.3 ± 0.3	2.3 ± 0.3
	R^2	0.98	0.99	0.97	0.98

K_d is the linear sorption coefficient; q_m is the maximum adsorption capacity of the adsorbent; K_L is the Langmuir constant related to the affinity of the binding sites; K_F is the Freundlich constant that indicates the overall adsorption capacity; n is the index heterogeneity; Q_m is the maximum adsorption capacity, K_a is the affinity constant for adsorption; q_s represents the theoretical isotherm saturation capacity; E is the mean free energy of adsorption.

The ideal n-values for isothermal consideration are typically range between 0 and 1 (Dong et al., 2020). For PVC, the model's n-value is approximately 1, indicating that the Langmuir model may be suitable to describe the data. The Henry (linear) equation best described the adsorption of SMX on fresh PE and PP with R^2 0.992 and 0.995, respectively, indicating that a simple partitioning of the solute between the adsorbent and the solution predominated (Wang et al., 2015). Having best described by the Langmuir equation with R^2 of 0.997 and 0.999, the monolayer adsorption of SMX on fresh PS and PVC, respectively, must have occurred on a homogeneous surface. The fresh PS, a supposedly hydrophobic MP, was assumed to exhibit a higher content of oxygen-containing moieties compared to other MPs, as indicated by the FTIR spectra. This would have enhanced the surface hydrophilicity of the MP. The presence of chlorine atoms in the PVC backbone, which pull electron density towards themselves (Meng et al., 2024), promotes the hydrophilicity of fresh MP, facilitating the formation of hydrogen bonds between PVC and water.

Given the hydrophilic surfaces of fresh PS and PVC, the aqueous medium would likely have interacted more with their adsorptive sites, particularly through specific functional groups, than adsorbate. This indicates that competitive adsorption likely occurred between the fresh PS and PVC with SMX, consistent with the Langmuir model fit.Isotherm models' parameters (q_m, K_F and q_s of Langmuir, Freundlich and Dubinin–Radushkevich, respectively), derived from the fitted of empirical data, are commonly employed to compare the potential adsorption capacities of various adsorbents (Sena et al., 2018). The values for q_m range from 0.32 to 1.29 mg/g, for K_F from 0.08 to 0.14 mg/g, and for q_s from 0.1 to 0.14 mg/g. The highest values were recorded for PS, followed by PVC, PP, and PE, indicating that fresh PS adsorbed SMX more effectively than the other MPs, with PE showing the lowest adsorption capacity. The affinity between adsorbate and adsorbent is usually predicted using the K and the K_L parameters of the Henry's and Langmuir models, respectively; the higher the value of these parameters, the higher/stronger the affinity (Zeng et al., 2014; Zhu et al., 2010); and in the present study, they range from 0.08 to 0.14 for and 0.12 to 0.34 L/mg, respectively. These models' parameters were higher in fresh PS and PP, suggesting having a higher affinity for SMX.

Physical properties of environmental pollutant dynamics play significant roles in understanding interactions of organic pollutants with MPs. Brittle properties of microplastics can play a significant role in their interactions with organic pollutants (Guo et al., 2023; Wang et al., 2015). PE and PP are less brittle microplastics due to their low T_g and PS and PVC, with T_g above room temperature (25 °C), are more brittle microplastics. Brittle microplastics, subjected to mechanical stress, develop fractures and surface irregularities, creating additional active sites for adsorption. This increased surface area enhances their adsorption capacity for organic pollutants. This might explain why PS and PVC adsorbed more SMX than PE and PP. This result is in line with (Guo et al., 2019) that less brittle microplastics adsorbed less SMX.

Hydrophobic interactions, electrostatic attraction, van der Waals forces, π–π interactions, and hydrogen bonding are the major mechanisms driving the interactions between organic pollutants and microplastics (Agboola & Benson, 2021). At an experimental pH above 6, SMX exists as an anion in solution, and all microplastics exhibit a net negative surface charge due to their pHpzc (Figure 20) (Xu et al., 2018b). Consequently, electrostatic repulsion occurs between the species, ruling out electrostatic attraction as a contributor to the sorption process. Both SMX

and PVC are hydrophilic substances because SMX has a low logK$_{ow}$ value, and PVC contains chlorine atoms in its structure. van der Waals forces which are common to all the microplastics due to temporary dipoles from electron movement, as well as the significant permanent dipole moment from the electronegativity difference between chlorine and carbon (0.61) in PVC, must have contributed to the overall interactions between SMX and the fresh microplastics, particularly fresh PVC. Despite its hydrophilicity, PVC did not demonstrate the highest sorption capacity for SMX, instead, PS, which is the most hydrophobic microplastic among the four, exhibited the highest sorption capacity. Given that both SMX and PS contain aromatic moieties, π–π interactions likely play a significant role in the high affinity between SMX and PS. Additionally, van der Waals forces may account for the sorption of the hydrophilic sulfamethoxazole on PE and PP. These results are consistent with the findings of Hüffer and Hofmann (2016) and Yu et al. (2020).

Partitioning and surface sorption have been reported as the main mechanisms of the sorption of organic substances, pollutants in particular on microplastics, and the n-value derived from Freundlich fitting has been used to predict sorption mechanisms. An n-value less than 1 represents a linear isotherm which is a proof of partitioning mechanism while greater than 1 suggests an adsorption mechanism from a nonlinear isotherm (Siri et al., 2021). The obtained n-values for SMX and the microplastics were all slightly greater than 1, suggesting competitive adsorption, which is in addition to the partitioning mechanism proposed for PE and PP. The mean free energy of sorption (E), calculated from the Dubinin-Radushkevich isotherm parameter, has been used to estimate the adsorption mechanism. Values of E less than 8 kJ/mol are associated with physisorption, while values between 8 and 16 kJ/mol indicate chemisorption (Sena et al., 2018). In this study, the values of E are less than 8 kJ/mol, indicating that the adsorption mechanism is physisorption.

Crystallinity is a characteristic of the structure that influences the surface and bulk properties of semi-crystalline polymers (Kołbuk et al., 2022), and have been employed in adsorption mechanism determination (Siri et al., 2021). The DSC results suggested that both the PE and PP are semi-crystalline microplastics, having less accessible pollutant sites due to fixed polymer chains requiring more energy for adsorption. This may explain the predominant partitioning adsorption mechanism for fresh PE and PP with SMX. In contrast, amorphous polymers, fresh PS and PVC, have greater chain mobility and accessible free volume, offering

more adsorption sites at lower energy due to their less rigid structure than fresh PE and PP. Therefore, the sorption of SMX onto PE and PP is dominated by the partitioning mechanism while adsorption is predominant for PS and PVC. The interaction of SMX on the fresh PE, PP and PVC must have been by van der Waals interaction. For fresh PS, π–π interactions are likely while hydrophilic factors might have contributed to the adsorption of SMX on PVC.

4.4.2 SMX with UV-aged microplastics

An equilibrium experiment was conducted between aged microplastics and SMX, with the isotherm plots shown in Figure 30.
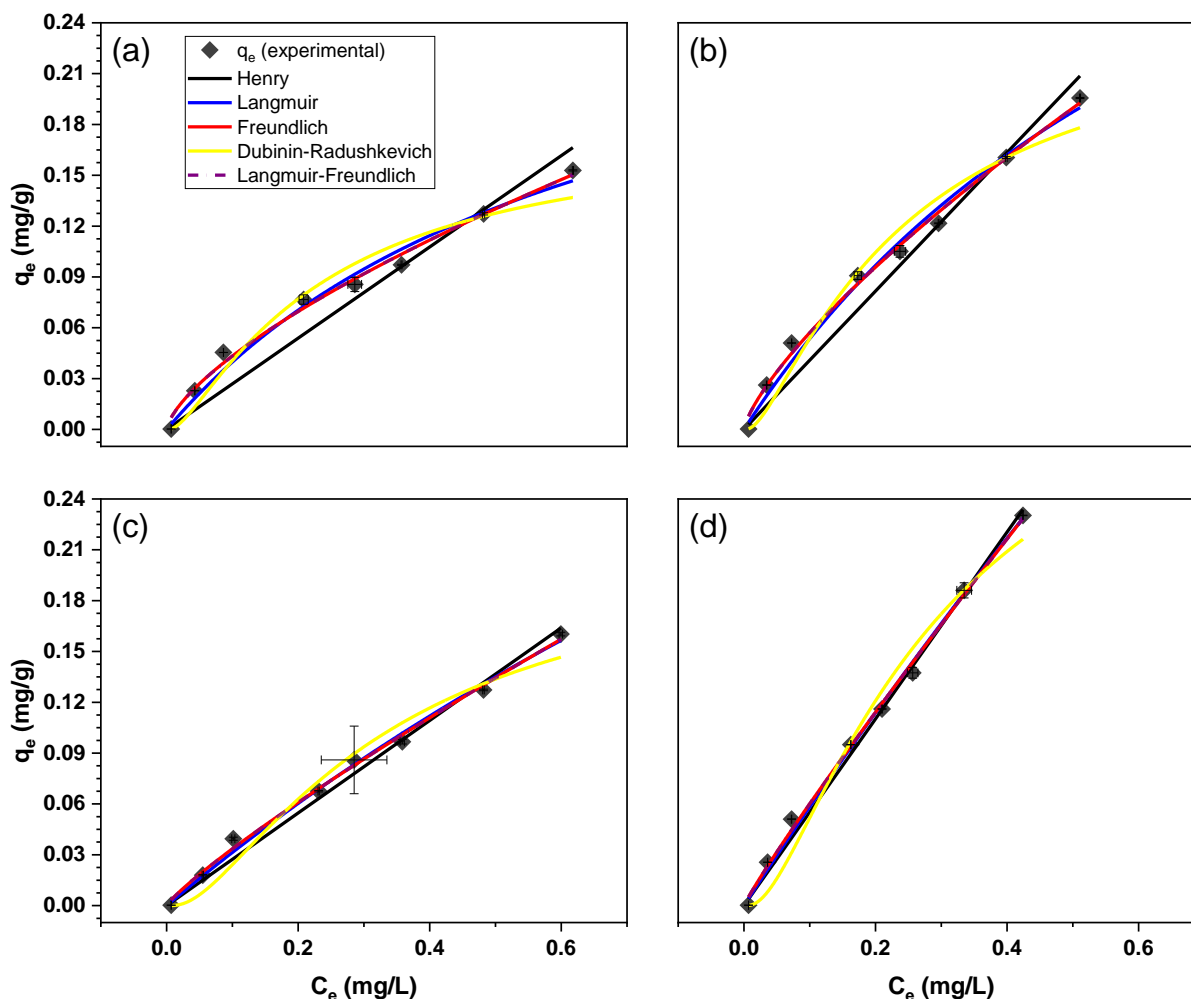
Figure 30. Sorption isotherm of SMX on aged (a) PE, (b) PP, (c) PS and (d) PVC

The empirical data consistently exhibited Type-C behaviour, with UV-aged PE and PP tending towards Type-L, suggesting partial competitive adsorption between the MPs and SMX. Compared to fresh microplastics, improved sorption behaviour is anticipated for UV-aged microplastics. The sorptive capacity of SMX on microplastics, presented in Figure 21 and the reported changes by the physicochemical characterization, like increased oxygen contents and cracks among others, suggest an enhanced adsorption capacity. This subsection explores how UV modification impacts the sorptive capacity and the extent of these changes.

The fitted parameters are depicted in Table 17. The Freundlich model yielded the highest coefficient of determination (R^2), ranging from 0.994 to 0.998, followed by the Langmuir-Freundlich model (0.991 to 0.997), the Langmuir model (0.984 to 0.997), the Henry model (0.979 to 0.997), and finally the Dubinin-Radushkevich model (0.96 to 0.97).

Table 17. Parameters of Henry, Langmuir, Freundlich and Dubinin–Radushkevich equations for adsorption of SMX on UV-aged PE, PP, PS and PVC

Model	Parameter	PE	PP	PS	PVC
Henry	K (L/mg)	0.27 ± 0.002	0.41 ± 0.017	0.27 ± 0.002	0.55 ± 0.008
	R^2	0.979	0.988	0.996	0.997
Langmuir	q_m (mg/g)	0.30 ± 0.06	0.50 ± 0.11	0.77 ± 0.27	2.52 ± 0.17
	K_L (L/mg)	1.51 ± 0.47	1.21 ± 0.38	0.42 ± 0.18	0.52 ± 0.14
	R^2	0.984	0.989	0.994	0.997
Freundlich	K_F (mg/g)	0.21 ± 0.008	0.31 ± 0.011	0.24 ± 0.008	0.50 ± 0.019
	n	1.5 ± 0.08	1.4 ± 0.06	1.2 ± 0.05	1.1 ± 0.04
	R^2	0.994	0.996	0.996	0.998
Langmuir-Freundlich	Q_m (mg/g)	1.00 ± 0.27	1.97 ± 0.3	1.89 ± 0.04	4.63 ± 0.19
	K_a	0.004 ± 0.2	0.004 ± 0.2	0.007 ± 0.3	0.008 ± 0.1
	n	0.69 ± 0.18	0.73 ± 0.14	0.87 ± 0.16	0.93 ± 0.14
	R^2	0.991	0.996	0.996	0.997
Dubinin–Radushkevich	q_s (mg/g)	0.17 ± 0.02	0.24 ± 0.02	0.21 ± 0.02	0.35 ± 0.04
	E (kJ/mol)	3.5 ± 0.6	3.4 ± 0.6	2.8 ± 0.3	3.0 ± 0.4
	R^2	0.96	0.96	0.97	0.97

K_d is the linear sorption coefficient; q_m is the maximum adsorption capacity of the adsorbent; K_L is the Langmuir constant related to the affinity of the binding sites; K_F is the Freundlich constant that indicates the overall adsorption capacity; n is the index heterogeneity; Q_m is the maximum adsorption capacity, K_a is the affinity constant for adsorption; q_s represents the theoretical isotherm saturation capacity; E is the mean free energy of adsorption.

The Freundlich model best fitted all empirical data for SMX on aged microplastics, suggesting that multilayer adsorption on heterogeneous surfaces occurred. Similar results were reported by (Wang et al., 2022). The values of q_m, K_F and q_s range from 0.30 to 2.52 mg/g, 0.21 to 0.50 mg/g, and 0.17 to 0.35 mg/g, respectively. The highest values were obtained from PVC, while the lowest were from PE. The Freundlich model, which best fitted the data, indicated that aged PVC and PP microplastics have a higher sorption capacity for SMX. This increased capacity may be attributed to the higher oxygen-containing functional groups identified by FTIR.

For the K and K_L parameters, UV-aged PVC and PE exhibited the highest affinity for SMX with 0.55 and 1.51 L/mg, respectively. The K value for PS, initially the lowest, became the highest after ageing, while PVC, initially the highest, became the lowest. For K_L, the order of affinity remained consistent even after 20 min of UV-C exposure. Despite the higher affinity suggested by the Langmuir model, aged PE showed the lowest capacity for SMX, highlighting the complexities surrounding the sorption of the pollutant on microplastics due to factors like surface area, surface chemistry, pore size distribution, adsorption energy, competitive adsorption, and physical structure (da Costa et al., 2024).

Several factors contribute to the improved sorption capacities of UV-aged microplastics. Photoageing, a combined physical and chemical process, is known to introduce oxygen and induce cracking, which increases surface area and active sites (Liu et al., 2019). Additionally, it reduces surface hydrophobicity and enhances water wettability, thereby facilitating interactions with water and dissolved particles, especially hydrophilic substances (Sodré et al., 2023). SMX is a weak acid that can exist in different protonation states depending on the pH of freshwater. It contains functional groups with different pKa values: the sulfonamide group (pKa = 1.6) and the amino group (pKa = 5.6). At pH values below 1.6, sulfamethoxazole predominantly exists in its protonated form (positively charged), and above pH 5.6, it predominantly exists in its deprotonated form (neutral or negatively charged). Additionally, the introduction of oxygen-containing functional groups increases the negative charge of the microplastics, especially when the pH of the medium is higher than the pHpzc of the microplastics (Huang et al., 2024). Therefore, electrostatic attraction may not be the primary interaction between these species. Similarly, the oxygen-containing groups increase the surface polarity of the microplastics, thereby potentially suppressing hydrophobic interactions between SMX and the aged microplastics.

Conversely, the introduced oxygen-containing groups can lead to hydrogen bonding interactions in the sorption process. The sulfonamide group contains both hydrogen donors (NH group) and acceptors (sulfonyl oxygen), while the amino group is a hydrogen donor. These groups can form hydrogen bonds with oxygen-containing functional groups such as hydroxyls and carbonyls, enhancing the interaction between SMX and UV-aged microplastics (Kong et al., 2021). Therefore, the sorption mechanism and interaction of SMX with the aged microplastics might be predominately be by hydrogen bonding.

4.4.3 SMX with HA-coated microplastics

To investigate how natural organic matter influences interactions between microplastics and hydrophilic pollutants in freshwater environments, we coated the microplastics with humic acids and conducted adsorption experiments with SMX. Previous studies (Kong et al., 2021; Song et al., 2022) have extensively documented these interactions and the impact of humic acid on them. Song et al. (2022) and Luo et al. (2022) studied the adsorption of humic acid on microplastics, revealing interactions primarily through physisorption involving the aromatic structure of humic acid, which is reversible. Kong et al. (2021) simultaneously investigated the adsorption of SMX and humic acid on microplastics, observing dual effects where humic acid both hindered and enhanced sorption performance for the pollutant. We assumed that some pre-adsorbed humic acid may be reintroduced into the adsorption medium and compete with SMX, but this aspect was not monitored in our study. Our focus was to explore how pre-coated humic acid affects the adsorption capacity of microplastics for SMX.

Figure 31 presents the isotherm plots for adsorption experiments of SMX on HA-coated PE, PP, PS, and PVC. All empirical data followed type-C behaviour, proposing that SMX continues to preferentially bind to specific sites on the microplastics even after coating. Meanwhile, the plots show a tendency towards type-L, indicating that the moieties of humic acid might have competed with the MPs' surface for SMX. It is visually obvious that the adsorptive performance of the microplastics was improved after coating. This can be attributed to the formation of oxygen-containing functional groups on the surface of the microplastics.
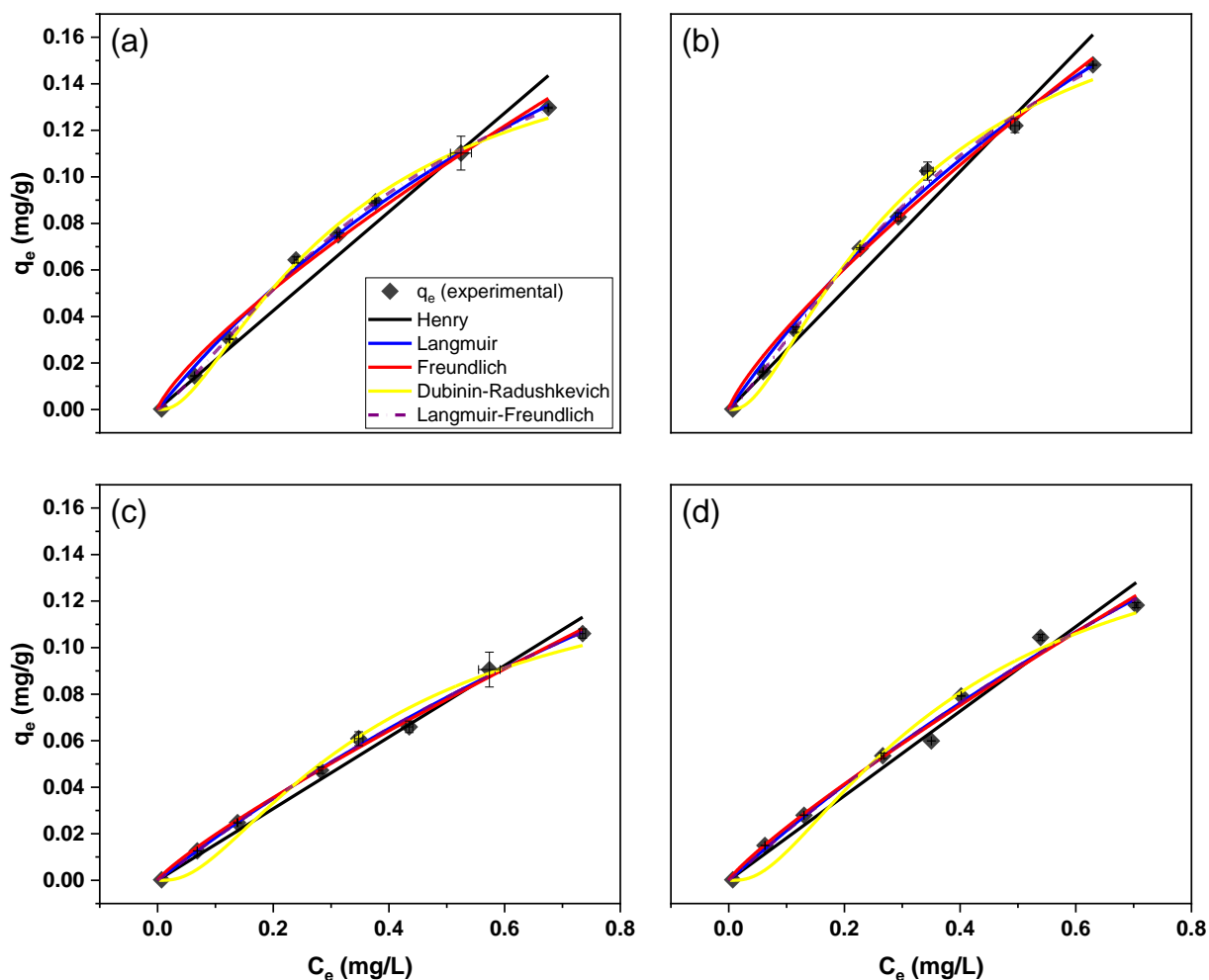
Figure 31. Sorption isotherm of SMX on humic acid coated (a) PE, (b) PP, (c) PS and (d) PVC

The fitted parameters are presented in Table 18. The models all demonstrated a good fit to the data, with R^2 values exceeding 0.9. Notably, Langmuir exhibited the best fit for coated PE, PP, and PVC, with $R^2 \geq 0.996$, indicating dominant monolayer sorption on a homogeneous surface. Both Langmuir and Freundlich presented R^2 of 0.996 for SMX on coated PS, and judging from the n-value of the Langmuir-Frreundlich model which is approximately 1, the Langmuir model could be considered the best fit for the data. The oxygen-containing functional groups in the humic acid altered the surfaces of the MPs, as indicated by the physicochemical characterisation, making them more hydrophilic. This promoted favourable interactions with the hydrophilic SMX, likely in a monolayer form.

Table 18. Parameters of Henry, Langmuir, Freundlich and Dubinin–Radushkevich equations for adsorption of SMX on HA-coated MPs

Model	Parameter	PE	PP	PS	PVC
Henry	K (L/mg)	0.21 ± 0.009	0.26 ± 0.010	0.15 ± 0.004	0.19 ± 0.004
	R^2	0.988	0.989	0.995	0.994
Langmuir	q_m (mg/g)	0.36 ± 0.05	0.43 ± 0.07	0.45 ± 0.10	0.54 ± 0.22
	K_L (L/mg)	0.86 ± 0.15	0.82 ± 0.18	0.43 ± 0.12	0.41 ± 0.20
	R^2	0.996	0.996	0.996	0.997
Freundlich	K_F (mg/g)	0.18 ± 0.008	0.22 ± 0.010	0.14 ± 0.004	0.20 ± 0.010
	n	1.3 ± 0.08	1.3 ± 0.08	1.2 ± 0.05	1.0 ± 0.06
	R^2	0.991	0.991	0.996	0.989
Langmuir-Freundlich	Q_m (mg/g)	0.22 ± 0.02	0.27 ± 0.06	0.42 ± 0.34	0.50 ± 0.71
	K_a	2.0 ± 0.4	1.8 ± 0.6	0.5 ± 0.6	0.5 ± 0.9
	n	1.3 ± 0.1	1.2 ± 0.1	1.0 ± 0.2	1.0 ± 0.3
	R^2	0.999	0.997	0.996	0.99
Dubinin–Radushkevich	q_s (mg/g)	0.17 ± 0.01	0.20 ± 0.01	0.14 ± 0.01	0.21 ± 0.03
	E (kJ/mol)	2.9 ± 0.2	2.9 ± 0.2	2.6 ± 0.3	2.2 ± 0.2
	R^2	0.99	0.99	0.98	0.97

K_d is the linear sorption coefficient; q_m is the maximum adsorption capacity of the adsorbent; K_L is the Langmuir constant related to the affinity of the binding sites; K_F is the Freundlich constant that indicates the overall adsorption capacity; n is the index heterogeneity; Q_m is the maximum adsorption capacity, K_a is the affinity constant for adsorption; q_s represents the theoretical isotherm saturation capacity; E is the mean free energy of adsorption.

The values of q_m, K_F and q_s range from 0.36 to 0.54 mg/g, 0.14 to 0.22 mg/g, and 0.17 to 0.21 mg/g; the highest values were obtained from PVC, PP and PVC while the lowest were from PE, PS and PE, respectively. While for the K and K_L parameters, PS and PVC exhibited the highest affinity for SMX with 0.26 and 0.17 L/mg, respectively. Compared to the fresh microplastics, the sorption capacity decreased according to q_m, unchanged according to K_F, and partially improved according to q_s upon coating. Meanwhile, their affinity increased, indicating that the coating process impacted the interactions of microplastics and SMX.

Although not monitored in this study, the dynamics of interactions between microplastics and humic acid are crucial to understanding how SMX interacts with coated microplastics. Humic acid's heterogeneity and complexity can lead to varying effects on these interactions, hindering or enhancing them. This complexity arises from the various functional groups in humic acid that

serve as interaction points with mineral surfaces. At the study's pH of 7, humic acid remains ionically active due to the presence of both acidic (e.g., carboxyl) and basic (e.g., phenolic) groups (Schlautman & Morgan, 1994). These properties may influence the interactions between microplastics and contaminants of emerging concern. This increased capacity may be attributed to the higher oxygen-containing functional groups identified by FTIR.

4.4.4 DCF with fresh microplastics

An equilibrium experiment was also conducted between fresh microplastics and the hydrophobic analyte, DCF, and the isotherm plots presented in Figure 32. Similar to the results for SMX on fresh microplastics, the data exhibited type-C behaviour, indicating that adsorption was likely facilitated by a constant partitioning of the adsorbate between the adsorbent and solvent.
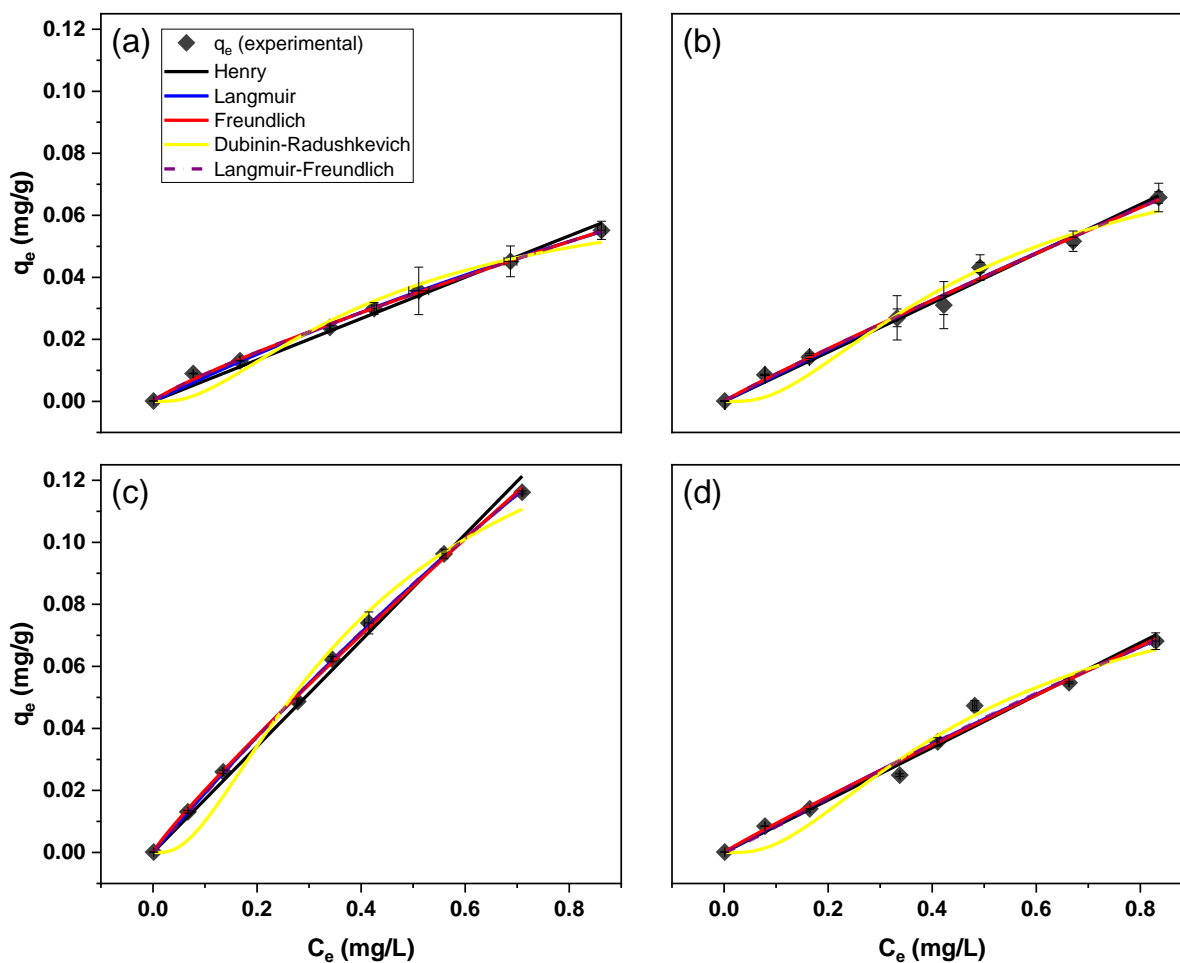
Figure 32. Adsorption isotherms of DCF on fresh (a) PE, (b) PP, (c) PS and (d) PVC

Table 19 presents the regression parameters of the models obtained from each model. Judging from the isotherm plots (Figure 32) it is expected that data be modelled linearly but all the models were fitted well with determination coefficients (R^2) higher than 0.9.

Table 19. Parameters of Henry, Langmuir, Freundlich and Dubinin–Radushkevich equations for adsorption of DCF on fresh PE, PP, PS and PVC

Model	Parameter	PE	PP	PS	PVC
Henry	K (L/mg)	0.07 ± 0.002	0.08 ± 0.002	0.17 ± 0.003	0.08 ± 0.002
	R^2	0.996	0.997	0.998	0.994
Langmuir	q_m (mg/g)	0.26 ± 0.1	0.80 ± 0.9	0.71 ± 0.1	0.67 ± 0.8
	K_L (L/mg)	0.32 ± 0.1	0.11 ± 0.1	0.28 ± 0.1	0.14 ± 0.2
	R^2	0.998	0.992	0.999	0.985
Freundlich	K_F (mg/g)	0.06 ± 0.001	0.08 ± 0.003	0.16 ± 0.002	0.08 ± 0.004
	n	1.2 ± 0.04	1.1 ± 0.06	1.1 ± 0.02	1.1 ± 0.09
	R^2	0.996	0.992	0.999	0.985
Langmuir-Freundlich	Q_m (mg/g)	2.15 ± 0.03	11.21 ± 0.12	0.59 ± 0.26	0.29 ± 0.45
	K_a	0.04 ± 0.06	0.01 ± 0.39	0.36 ± 0.22	0.45 ± 1.00
	n	0.85 ± 0.12	0.84 ± 0.25	1.03 ± 0.04	1.12 ± 0.35
	R^2	0.998	0.992	0.999	0.985
Dubinin–Radushkevich	q_s (mg/g)	0.07 ± 0.01	0.09 ± 0.01	0.16 ± 0.01	0.10 ± 0.01
	E (kJ/mol)	2.4 ± 0.4	2.3 ± 0.4	2.5 ± 0.3	2.2 ± 0.3
	R^2	0.96	0.96	0.98	0.97

K_d is the linear sorption coefficient; q_m is the maximum adsorption capacity of the adsorbent; K_L is the Langmuir constant related to the affinity of the binding sites; K_F is the Freundlich constant that indicates the overall adsorption capacity; n is the index heterogeneity; Q_m is the maximum adsorption capacity, K_a is the affinity constant for adsorption; q_s represents the theoretical isotherm saturation capacity; E is the mean free energy of adsorption.

The sorption of DCF on the fresh PP and PVC were best fitted by the Henry model with R^2 of 0.997 and 0.994, respectively, indicating an adsorption process characterized by a constant partitioning of the adsorbate between the adsorbent and the solvent and a consistent adsorption capacity across different concentrations of the adsorbate. The fresh PP exhibited a faint peak between 1682 and 1588 cm⁻¹ (Figure 17), corresponding to carbonyl groups. These carbonyl species must have been sufficient to render the MP somewhat hydrophilic, thereby influenced the adsorption of DCF. Therefore, the hydrophilic surfaces of PP and PVC may have contributed to the partitioning of DCF onto the surfaces of the MPs and into the aqueous medium, as suggested

by Henry's model. The Langmuir equation, with R^2 values of 0.998 for fresh PE and 0.999 for fresh PS, best describes the monolayer sorption of DCF, indicating that it occurs on a homogeneous surface for both materials.

The adsorption capacity parameters vary depending on the type of microplastics, ranging from 0.26 to 0.80 mg/g for q_m, 0.06 to 0.16 mg/g for K_F and 0.07 to 0.16 mg/g for q_s. The highest values were observed in fresh PP, PS and PS, respectively, while the lowest were consistently found in fresh PE. This trend indicates that fresh PS, known for its highest hydrophobicity among the microplastics studied, exhibited the greatest adsorption capacity for DCF, and this is likely due to hydrophobic interactions. The affinity parameters (K for Henry's model and K_L for Langmuir model) provide insight into the interaction strength between DCF and microplastics, ranging from 0.07 (PE) to 0.17 (PS) for K and 0.11 (PE) to 0.32 (PP) for K_L. Notably, fresh PS showed a high K_L value, supporting hydrophobic interactions as the predominant interaction in DCF sorption onto the fresh microplastics. This finding aligns with previous results in the literature, which concluded that the adsorption of DCF on microplastics is mainly driven by hydrophobic interactions and depends on the distribution of the sorbate between the adsorbent and the surrounding solution (Hüffer & Hofmann, 2016; Munoz et al., 2021).

Moreso, π–π interactions likely contribute to the strong adsorption capacity and affinity of fresh PS for DCF, given its aromaticity. Meanwhile, van der Waals forces, arising from the dipoles caused by electron movement in the microplastics, also potentially contribute to their interactions with DCF. The n-values for DCF and the microplastics were approximately 1, except for fresh PE at 1.2, indicating a slightly favourable and uniform adsorption process on an equivalent surface.

Likewise, DCF's ability to form non-covalent interactions, such as hydrogen bonds facilitated by its carboxylic or amino groups, may also explain the unexpectedly higher adsorption capacity observed in hydrophilic microplastics like PVC, as well as the reported oxygen-containing impurities in PP compared to PE, due to the latter's hydrophobic nature (Elizalde-Velazquez et al., 2020). Overall, hydrophobic, hydrogen bonding, π–π, and van der Waals interactions collectively contribute to the adsorption of DCF on fresh microplastics.

4.4.5 DCF with UV-aged microplastics

To investigate how photoaging affects the interactions of microplastics with hydrophobic substances, an adsorption experiment was conducted, and the isotherm fittings are presented in Figure 33. The empirical data generally exhibited type-C behaviour, despite the equilibrium concentration (q_e) nearly doubling. Meanwhile, the data for UV-aged PE, PS and PVC showed a tendency towards Type-L behaviour, implying partial competition for adsorption sites between the MPs and DCF.

UV-aged microplastics are expected to demonstrate enhanced sorption behaviour compared to fresh microplastics due to the complex alterations that occur during photoaging. Literature suggests that particle size decreases with this type of ageing, which increases their porosity and modifies other properties, several of which are documented in this study.
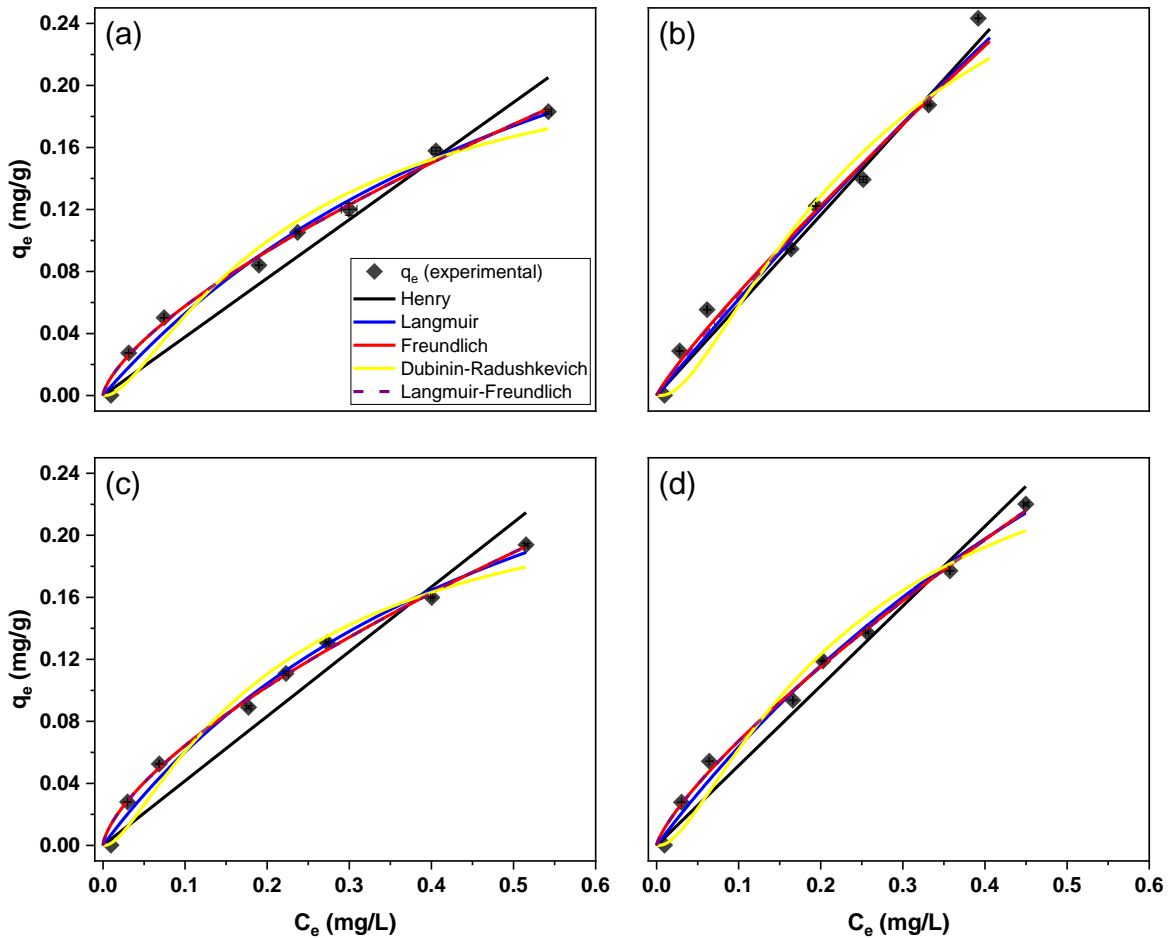
Figure 33. Sorption isotherm of SMX on aged (a) PE, (b) PP, (c) PS and (d) PVC

The fitted parameters are presented in Table 20. The Freundlich model yielded the highest coefficients of determination (R^2 = 0.996, 0.997, and 0.997) for UV-aged PE, PS, and PVC, indicating multilayer adsorption on heterogeneous surfaces. The Henry model best fitted the empirical data for DCF on UV-aged PP, with an R^2 of 0.999, suggesting constant sorption energy independent of adsorbate concentration.

Table 20. Parameters of Henry, Langmuir, Freundlich and Dubinin–Radushkevich equations for adsorption of DCF on aged PE, PP, PS and PVC

Model	Parameter	PE	PP	PS	PVC
Henry	K (L/mg)	0.38 ± 0.019	0.58 ± 0.016	0.42 ± 0.023	0.51 ± 0.018
	R^2	0.982	0.999	0.989	0.996
Langmuir	q_m (mg/g)	0.40 ± 0.06	2.04 ± 0.26	0.39 ± 0.05	0.67 ± 0.16
	K_L (L/mg)	1.51 ± 0.37	0.31 ± 0.36	1.8 ± 0.38	1.05 ± 0.33
	R^2	0.991	0.986	0.992	0.992
Freundlich	K_F (mg/g)	0.28 ± 0.009	0.51 ± 0.041	0.30 ± 0.008	0.40 ± 0.015
	n	1.5 ± 0.06	1.3 ± 0.08	1.5 ± 0.05	1.3 ± 0.05
	R^2	0.996	0.989	0.998	0.997
Langmuir-Freundlich	Q_m (mg/g)	1.43 ± 0.70	2.09 ± 0.31	1.92 ± 0.42	2.26 ± 0.61
	K_a	0.12 ± 0.02	0.89 ± 0.25	0.64 ± 0.02	1.45 ± 0.05
	n	0.69 ± 0.12	1.22 ± 0.15	0.67 ± 0.10	0.78 ± 0.13
	R^2	0.996	0.997	0.998	0.997
Dubinin–Radushkevich	q_s (mg/g)	0.23 ± 0.02	0.35 ± 0.05	0.24 ± 0.02	0.29 ± 0.03
	E (kJ/mol)	3.4 ± 0.3	3.1 ± 0.2	3.6 ± 0.3	3.3 ± 0.03
	R^2	0.97	0.95	0.97	0.97

K_d is the linear sorption coefficient; q_m is the maximum adsorption capacity of the adsorbent; K_L is the Langmuir constant related to the affinity of the binding sites; K_F is the Freundlich constant that indicates the overall adsorption capacity; n is the index heterogeneity; Q_m is the maximum adsorption capacity, K_a is the affinity constant for adsorption; q_s represents the theoretical isotherm saturation capacity; E is the mean free energy of adsorption.

The values of q_m, K_F and q_s range from 0.36 to 2.04 mg/g, 0.28 to 0.51 mg/g, and 0.23 to 0.35 mg/g, respectively. The highest values were consistently obtained from PP, while the lowest were from PS, PE, and PE, respectively. For K and K_L parameters, PP and PS exhibited the highest affinity for DCF, with 0.58 and 1.80 L/mg, respectively. The study identified that initially, fresh PS, being highly hydrophobic, demonstrated the highest adsorption capacity and affinity for DCF. However, these characteristics diminished with ageing, indicating that the adsorption of

hydrophobic substances onto hydrophobic microplastics decreases after photoageing due to surface oxidation and reduced hydrophobicity. This study aligns with Munoz et al. (2021) on adsorption of DCF and hydrophilic metronidazole onto four hydrophobic micplastics (PE, PP, PS and polyethylene terephthalate).

Additionally, upon photo-ageing, the adsorption capacity and affinity of microplastics for DCF increased. This is likely because photo-ageing led to the formation of oxygen-containing groups on the surface of microplastics, and these groups facilitated hydrogen bonding with the amino and carboxylic groups of DCF. PVC, which is the most hydrophilic among the microplastics studied, showed a significantly higher sorption capacity and affinity for the hydrophobic DCF after ageing. The FTIR (Figure 17) analysis showed an increase in hydroxyl and carbonyl groups, and an increase in amorphous regions in UV-aged PP and PVC, respectively, supported these findings. This is consistent with Elizalde-Velazquez et al. (2020), who found that the adsorption potential of the microplastics for DCF was enhanced due to the ability to interact with various chemical groups through proton donation or acceptance. Therefore, the study demonstrates that UV-ageing significantly alters the adsorption characteristics of the microplastics. While hydrophobic interactions decrease due to surface oxidation, the formation of new functional groups enhances adsorption capacity and affinity through hydrogen bonding.

4.4.6 DCF with HA-coated microplastics

To assess the impact of humic acid on the interactions between microplastics and hydrophobic pollutants in freshwater environments, the HA-coated microplastics were used in adsorption experiments with DCF. Figure 33 shows the isotherm plots for the adsorption experiments of SMX on HA-coated PE, PP, PS, and PVC. All empirical data exhibited type-C behaviour, indicating a preferential partitioning of DCF between the microplastics and adsorbing solution after coating. It is evident from the figure that the adsorptive performance of the microplastics improved post-coating, probably facilitated by the introduced Oxygen-bearing moieties on the surface of the microplastics.
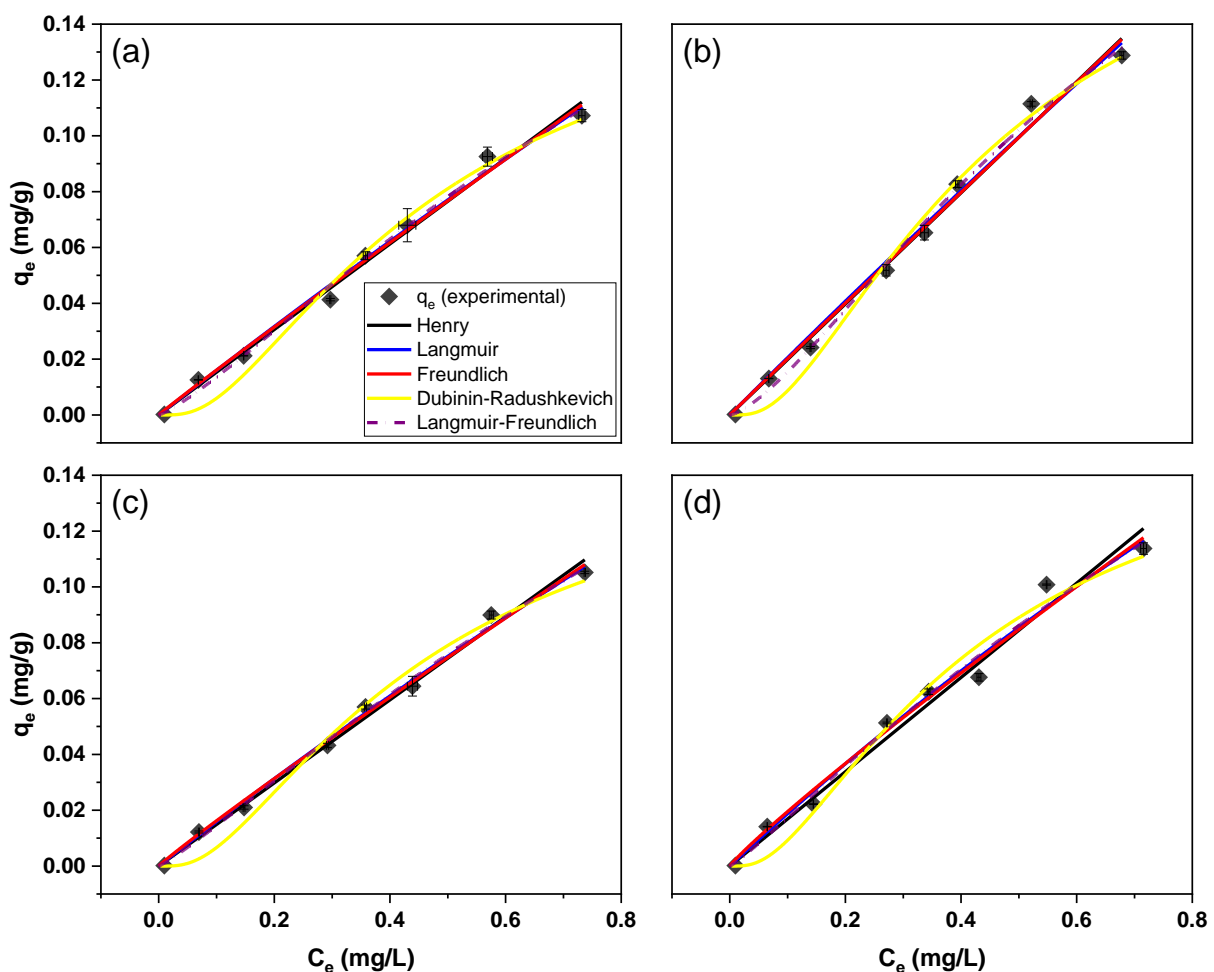
Figure 34. Sorption isotherm of DCF on humic acid coated (a) PE, (b) PP, (c) PS and (d) PVC

The fitted parameters of Henry, Langmuir, Freundlich, Langmuir-Freundlich, and Dubinin–Radushkevich adsorption models describing the adsorption of DCF on HA-coated microplastics are presented in Table 21. The data indicate varying adsorption behaviours among different types of microplastics, with significant insights into their sorption capacities and affinities. The Henry model shows high R^2 values ranging from 0.994 to 0.998 and best modelled the adsorption behaviour of all HA-coated microplastics with the analyte. This suggests a linear adsorption isotherm, implying consistent partitioning and unchanged sorption energy even as the adsorbate concentration increases. The oxygen-containing functional groups present on the surfaces of the HA-coated MPs may have facilitated the partitioning interactions with the hydrophobic DCF.

Table 21. Parameters of Henry, Langmuir, Freundlich and Dubinin–Radushkevich equations for adsorption of DCF on HA-coated MPs

Model	Parameter	PE	PP	PS	PVC
Henry	K (L/mg)	0.15 ± 0.003	0.20 ± 0.004	0.15 ± 0.003	0.17 ± 0.018
	R^2	0.997	0.997	0.998	0.994
Langmuir	q_m (mg/g)	1.65 ± 2.19	2.66 ± 0.06	1.11 ± 0.75	0.76 ± 0.55
	K_L (L/mg)	0.10 ± 0.14	0.08 ± 0.15	0.15 ± 0.11	0.21 ± 0.21
	R^2	0.992	0.991	0.996	0.986
Freundlich	K_F (mg/g)	0.15 ± 0.006	0.20 ± 0.010	0.14 ± 0.005	0.16 ± 0.009
	n	1.0 ± 0.06	1.0 ± 0.06	1.1 ± 0.05	1.1 ± 0.09
	R^2	0.992	0.991	0.995	0.985
Langmuir-Freundlich	Q_m (mg/g)	0.33 ± 0.24	0.28 ± 0.10	0.40 ± 0.32	0.38 ± 0.46
	K_a	0.77 ± 0.75	1.35 ± 0.63	0.55 ± 0.58	0.67 ± 1.14
	n	1.23 ± 0.25	1.42 ± 0.23	1.34 ± 0.18	1.13 ± 0.34
	R^2	0.993	0.995	0.996	0.987
Dubinin–Radushkevich	q_s (mg/g)	0.16 ± 0.01	0.20 ± 0.01	0.15 ± 0.01	0.16 ± 0.01
	E (kJ/mol)	2.3 ± 0.5	2.3 ± 0.2	2.3 ± 0.5	2.5 ± 0.5
	R^2	0.98	0.99	0.98	0.97

K_d is the linear sorption coefficient; q_m is the maximum adsorption capacity of the adsorbent; K_L is the Langmuir constant related to the affinity of the binding sites; K_F is the Freundlich constant that indicates the overall adsorption capacity; n is the index heterogeneity; Q_m is the maximum adsorption capacity, K_a is the affinity constant for adsorption; q_s represents the theoretical isotherm saturation capacity; E is the mean free energy of adsorption.

The Langmuir model's maximum adsorption capacity (q_m) reveals that HA-coated PP has the highest adsorption capacity (2.66 mg/g), followed by HA-coated PE (1.65 mg/g), PS (1.11 mg/g), and PVC (0.76 mg/g). The affinity constant (K_L) shows variability with PVC having the highest affinity (0.21 L/mg). R² values (0.986 to 0.996) suggest a good fit but are slightly less accurate compared to the Henry model. The Freundlich model shows K_F values similar to the Henry model's K values, with PP having the highest value (0.20 mg/g) and PE the lowest (0.14 mg/g). The n values close to 1 indicate relatively homogenous adsorption sites. R² values (0.985 to 0.995) suggest a reasonable fit, which complements the findings of the Langmuir model regarding the adsorption capacity and affinity. The Langmuir-Freundlich model combines aspects of both Langmuir and Freundlich models. The Q_m values show PP with the highest capacity (0.40 mg/g), consistent with previous models. The n values above 1 indicate favourable adsorption conditions, and R² values (0.987 to 0.996) suggest a good fit. The Dubinin–Radushkevich model

parameters show q_s values with PP again having the highest adsorption capacity (0.20 mg/g). The E values around 2.3 to 2.5 kJ/mol suggest physisorption as they are less than 8 kJ/mol. The R^2 values (0.97 to 0.99) indicate a decent fit but slightly lower than other models.

Generally, there was an increase in adsorption capacity and affinity for DCF after HA coating, probably due to the introduced oxo groups that provided more sites for adsorption (Fan et al., 2018). However, the adsorption potential of HA-coated microplastics is lower than that of UV-aged microplastics. Considering the experimental pH which was higher than the pH of the point of zero charge (Figure 20) of all the MPs, electrostatic interactions are unlikely. As mentioned previously, the humic acid coating reduces the hydrophobic nature of the microplastics due to the induced oxo groups, which in turn promote dipole-dipole interactions because of the differences in electronegativity between oxygen and carbon/hydrogen atoms. Thus, hydrophobic interactions are likely diminished, leading to enhanced hydrogen bonding and van der Waals interactions.

4.4.7 Sorption behaviour comparison between treatments

The study investigated the adsorption capacity and mechanisms of SMX and DCF on various fresh and aged microplastics (PE, PP, PS, and PVC), fitting the experimental data to five isotherm models (Henry, Langmuir, Freundlich, Langmuir-Freundlich, and Dubinin–Radushkevich). Fresh microplastics exhibited type-C behaviour, with Henry and Langmuir models fitting the data best, indicating a simple partitioning and monolayer adsorption on homogeneous surfaces. PS showed the highest adsorption capacity and affinity for SMX, primarily driven by π–π interactions and van der Waals forces, while PE and PP exhibited adsorption dominated by partitioning mechanisms due to their low glass transition temperatures. PVC, despite its hydrophilicity, demonstrated significant adsorption likely due to van der Waals interactions. Similarly, for DCF, the adsorption on fresh microplastics involved primarily van der Waals interactions and hydrophobic effects, with PS again showing the highest affinity due to its aromatic structure facilitating π–π interactions with the aromatic rings of DCF. PE and PP adsorbed DCF mainly through partitioning, while PVC showed a notable adsorption capacity likely influenced by specific interactions between the DCF molecules and the polar groups of PVC.

Upon UV-aging, microplastics showed enhanced adsorption capacities, with the Freundlich model fitting the data best, suggesting multilayer adsorption on heterogeneous surfaces.

The increase in oxygen-containing functional groups and surface area due to ageing facilitated improved adsorption. Aged PVC and PP showed higher sorption capacities and affinities for SMX, driven by hydrogen bonding interactions facilitated by introduced functional groups. Similarly, DCF adsorption on UV-aged microplastics indicated increased capacity and affinity, with the Freundlich model fitting the data well, highlighting the role of new functional groups in enhancing adsorption through hydrogen bonding.

Humic acid-coated microplastics exhibited improved adsorption performance for both SMX and DCF, with all empirical data following type-C behaviour. The coating process introduced oxygen-bearing moieties on the surface, facilitating adsorption through hydrogen bonding. The Henry model best described the adsorption of DCF on HA-coated microplastics, indicating consistent partitioning and sorption energy. Langmuir and Freundlich models also provided insights into the adsorption capacities and affinities, with PP consistently showing the highest values, demonstrating the significant impact of surface modifications on adsorption behaviour.

Compared with other areas, studies on the adsorption behaviour and interactions of MPs with organic contaminants are limited, and most of them are presented in Table 22. The most commonly studied MPs are poly(ethylene terephthalate), PE, PP, PS, and PVC, likely due to their widespread presence in the environment. The primary interactions between organic contaminants and fresh (sometimes referred to as pristine) MPs are hydrophobic (especially with hydrophobic pollutants) and van der Waals forces. Similar to this study, the main factors influencing adsorption behaviour are reported to be the physicochemical properties of both the pollutants and the MPs. For instance, Siri et al. (2021) suggested surface sorption and pore filling for progesterone on fresh PE, PP, and PS, while Munoz et al. (2021) attributed the adsorption of DCF on fresh PS, poly(ethylene terephthalate), PP, and high-density PE to their hydrophobic characteristics. Ageing of the MPs is reported to affect their adsorption behaviour with organic pollutants.

Table 22. Comparison of the sorption interactions in this study with those reported in other studies

MP	Modification	Contaminant	Fitted model	Proposed interactions	Reference
PA, PE, PET, PS, PVC and PP	-	SMX	External mass transfer resistance, internal mass transfer resistance, adsorption on active sites, linear, Langmuir and Freundlich	Electrostatic and hydrogen bonding	(Guo et al., 2019)
PE and PP	-	Carbofuran and barbendazim	Pseudo-first-order, pseudo-first-order, intra-particle diffusion, Langmuir and Freundlich	van der Waals and electrostatic interaction	(Mo et al., 2021)
PP	HNO$_3$	Sulfathiazole, sulfamerazine, sulfamethazine, SMX, ciprofloxacin, enrofloxacin, ofloxacin, norfloxacin, tetracycline, chloramphenicol,	Pseudo-first-order, pseudo-first-order, Weber-Morris intra-particle diffusion, Boyd, Langmuir and Freundlich	Electrostatic, hydrogen and hydrophobic	(Yao et al., 2022)
PE, PP and PS	-	Progesterone	Pseudo-first-order, pseudo-first-order, Langmuir and Freundlich	van der Waals	(Siri et al., 2021)
PP	K$_2$S$_2$O$_8$	Triclosan	Pseudo-first-order, pseudo-first-order and Freundlich	Electrostatic	(Wu et al., 2020)
PLA, PET and PP	K$_2$S$_2$O$_8$	SMX	Pseudo-first-order, pseudo-first-order, linear, Langmuir and Freundlich	-	(Kong et al., 2021)
PS, PE, PVC and PET	UV and vacuum UV	Benzene and ciprofloxacin	Langmuir and Freundlich	Hydrophobic and π–π interaction	(Lin et al., 2020)
PS and PBAT	-	DCF	Pseudo-first-order, pseudo-first-order, Freundlich and Dubinin-Radushkevich	Electrostatics and hydrogen bonding	(Liang et al., 2023)
PS, PET, PP and PE	Fenton	DCF and metronidazole	-	Hydrophobic and π–π interaction	(Munoz et al., 2021)
PU	UV and biofilm	Bisphenol A	Pseudo-first-order, pseudo-first-order, intra-particle diffusion, Langmuir and Freundlich	Hydrogen bonding and π–π interaction	(Chen & Sweetman, 2024)

PA = polyamide, PET = poly(ethylene terephthalate), PLA = polylactic acid, PBAT - poly(butylene adipate-co-terephthalate), PU = polyurethane

The two common ageing methods cited in the literature are chemical degradation and photodegradation. Cracking, wrinkling, and an increase in oxygen-containing functional groups

are reported as characteristic evidence of MP ageing (Lin et al., 2020). The extent of ageing depends on the method used and the duration. In this study, UV-C irradiation modified the MPs within 20 minutes, whereas Chen and Sweetman (2024) only achieved similar results after seven days of accelerated ageing of polyurethane under UV light. Ageing enhances the adsorption capacity of MPs for organic pollutants (Wu et al., 2020). Munoz et al. (2021) observed that the performance of aged MPs is influenced by their hydrophobicity. Changes in adsorption interactions following ageing have also been reported in the literature, as observed in the present study (Chen & Sweetman, 2024; Yao et al., 2022). Hydrogen bonding interactions, which are stronger than van der Waals forces, are common between organic pollutants and aged MPs. Consequently, the environmental prevalence of aged MPs could significantly impact the adsorption and transport of organic pollutants, thereby influencing contaminant dynamics within ecosystems.

4.5 Desorption of contaminants from microplastics

Adsorption and desorption processes are critical in understanding the interactions between pollutants and various adsorbents. Desorption, the detachment of adsorbed substances from the surface of the adsorbent mostly due to weak interactions, can be facilitated by changes in solvent composition, interaction time, solvent volume, and agitation. This phenomenon is widely studied across various adsorbents, such as activated carbon and microplastics, and substances including heavy metals and organic pollutants (Akpomie et al., 2015; Tiotsop Kuete et al., 2022), and increased attention has been given to microplastics due to their ability to transport pollutants within the environment and into the fluids and organs of organisms that ingest them (Lu et al., 2021; Siri et al., 2021; Wu et al., 2022). Research predominantly addresses endocrine-disrupting chemicals, hormones and other pollutants, except for SMX and DCF.

A desorption study was undertaken to examine the rate and quantity of emerging contaminants released into organisms by microplastics, focusing on two distinct regions of the gastrointestinal tract. To achieve this, two distinct biological fluids were simulated: artificial gastric fluid (AGF, pH 2.12) to simulate stomach conditions and artificial intestinal fluid (AIF, pH 7.04) to replicate intestinal conditions. These fluids were prepared with specific compositions of gastrointestinal tract juices to evaluate their respective impacts on the desorption of hydrophobic

and hydrophilic pollutants into organisms. Desorption experiments were conducted at intervals of 0, 0.3, 1, 2, 4, 6, 12, and 24 h, using simulated freshwater (SFW, pH 6.54) and the two biological fluids for desorption studies. Initially, 10 mL of 10,000 µg/L SMX and DCF solutions were separately adsorbed on 1 g of each microplastic, and the equilibrium and adsorbed concentrations are presented in Table 23. This approach allowed the examination of the rate and quantity of emerging contaminants released into organisms by microplastics.

Table 23. Adsorbed SMX and DCF on fresh microplastics before adsorption (C_i = 10000 µg/L)

MP	SMX		DCF	
	C_e (µg/L)	q_e (mg/g)	C_e (µg/L)	q_e (mg/g)
PE	1133.06	11.33	1847.97	18.48
PP	3166.38	31.66	2005.41	20.05
PS	3272.53	32.73	1604.45	16.04
PVC	2384.55	23.85	2396.55	23.97

4.5.1 Desorption of SMX from fresh microplastics

Figure 35 presents the results of the desorption of SMX in SFW which were relatively low across all types of microplastics. For PE, the desorption increased from an initial value of 11.72% to 17.68% at 24 hours. PP showed an increase from 2.69% to 7.83%, PS from 2.50% to 3.124%, and PVC from 3.92% to 4.42% at 24 hours. The near-neutral pH of SFW maintains minimal electrostatic repulsion between SMX and the microplastic surfaces, resulting in relatively stable interactions and lower desorption efficiencies. This indicates that under freshwater conditions, SMX remains more tightly bound to the microplastics. These results contradict Razanajatovo et al. (2018), which suggested that the adsorption of SMX onto microplastics is irreversible, thereby rendering desorption impossible. Meanwhile, Wang et al. (2023) reported more than 50% desorption of SMX from polyamide 6.

Figure 35. Percentage of SMX desorbed from fresh (a), PE, (b) PP, (c) PS and (d) PVC. Error bars indicate ± SD (n = 2)

Besides understanding the impact of gastric juice on the desorption of hydrophilic pollutants from microplastics, this study aims to provide insight into the desorption rate of the pollutants into the stomach, thereby elucidating the potential health risks associated with the ingestion of microplastic-contaminated food. The desorption of SMX in AGF exhibited mixed results compared to SFW (Figure 35), with some microplastics showing lower desorption. For PE, the desorption was consistent at about 20% for the 24 h desorption process, while PP showed an increase from 8.57 to 10.82% with a higher initial desorption rate compared to SFW. The fresh PS and PVC exhibited a lower desorption in AGF, from 4.12 to 4.41% and from 6.01 to 6.23%, respectively, compared to SFW. Considering microplastics, the semi-crystalline nature and less brittleness of fresh PE and PP might have inhibited a stronger adhesion of SMX to their surfaces while the PS and PVC must have held SMX stronger due to the glassy and amorphous nature. The

119

acidic pH and presence of pepsin in AGF can facilitate the release of SMX from some microplastics, although to a lower extent in this study. The desorption of SMX from PS and PVC, was less efficient than in SFW, likely due to specific interactions between SMX and the microplastic surface under acidic conditions. Food typically undergoes gastric digestion, mixing with gastric juices to form chyme, for approximately 2 to 6 hours in the stomach, depending on factors such as the type of food, organism, and health status. The desorption of SMX from microplastics into AGF was initially rapid, exceeding 75% within 6 hours, suggesting that fouled microplastics are likely to release hydrophilic pollutants into the stomach during the relatively short chyme production phase.

The gastrointestinal transit of ingested particles from the stomach to the small intestine necessitates an investigation into the desorption kinetics of SMX in this study to gain insight into the effects of intestinal juice on the sorption process. The desorption of SMX in AIF was the highest among all simulated conditions except for fresh PP. About 23.57% to 29.97% of SMX desorbed from fresh PE, 6.78% to 9.91% from PP, 6.41% to 7.16% from PS, and 9.01% to 9.89% from PVC. The neutral pH and presence of special components in AIF might have enhanced the solubilization of SMX, resulting in higher desorption rates. Siri et al. (2021) studied the desorption of progesterone from PE, PP, and PS and found desorption to be high in synthesized intestinal fluid, just as obtained in this study. The neutral pH must have reduced the electrostatic interactions between SMX and the microplastics, allowing for more efficient desorption compared to the acidic AGF and near-neutral SFW conditions.

Polyethylene consistently exhibited the highest desorption rates across all conditions, indicating that the interaction between SMX and the fresh PE surface was readily disrupted by the biological fluids. The desorption of SMX from fresh PE followed the order: AIF > AGF > SFW. While PP, PS, and PVC showed lower desorption values compared to PE. The desorption of SMX from fresh PP followed the order: AGF > AIF > SWF, while the desorption order from PS and PVC was consistent with the order for PE. The pH of the desorbing media plays a crucial role, with neutral conditions in AIF promoting higher desorption compared to the acidic pH of AGF and near-neutral pH of SFW. Consistent with this finding, Wang et al. (2023) reported similar results in their study on the desorption of SMX from polyamide 6, further supporting the validity of our results. The higher performance of AIF may be attributed to the presence of bile, which

forms micelles, in its composition. Siri et al. (2021) submitted that the micelles might have the ability to solubilize the pollutants by scavenging hydrophobic organic contaminants in the hydrophobic region of the micelles. The same might be true for hydrophilic organic contaminants, such as SMX, being sequestered by the hydrophilic regions of the micelles.

4.5.2 Desorption of DCF from fresh microplastics

Figure 36 presents the results of the desorption of DCF in SFW across different types of microplastics. The analysis shows distinct desorption patterns for each type of microplastic under various conditions, including SFW, AGF, and AIF.
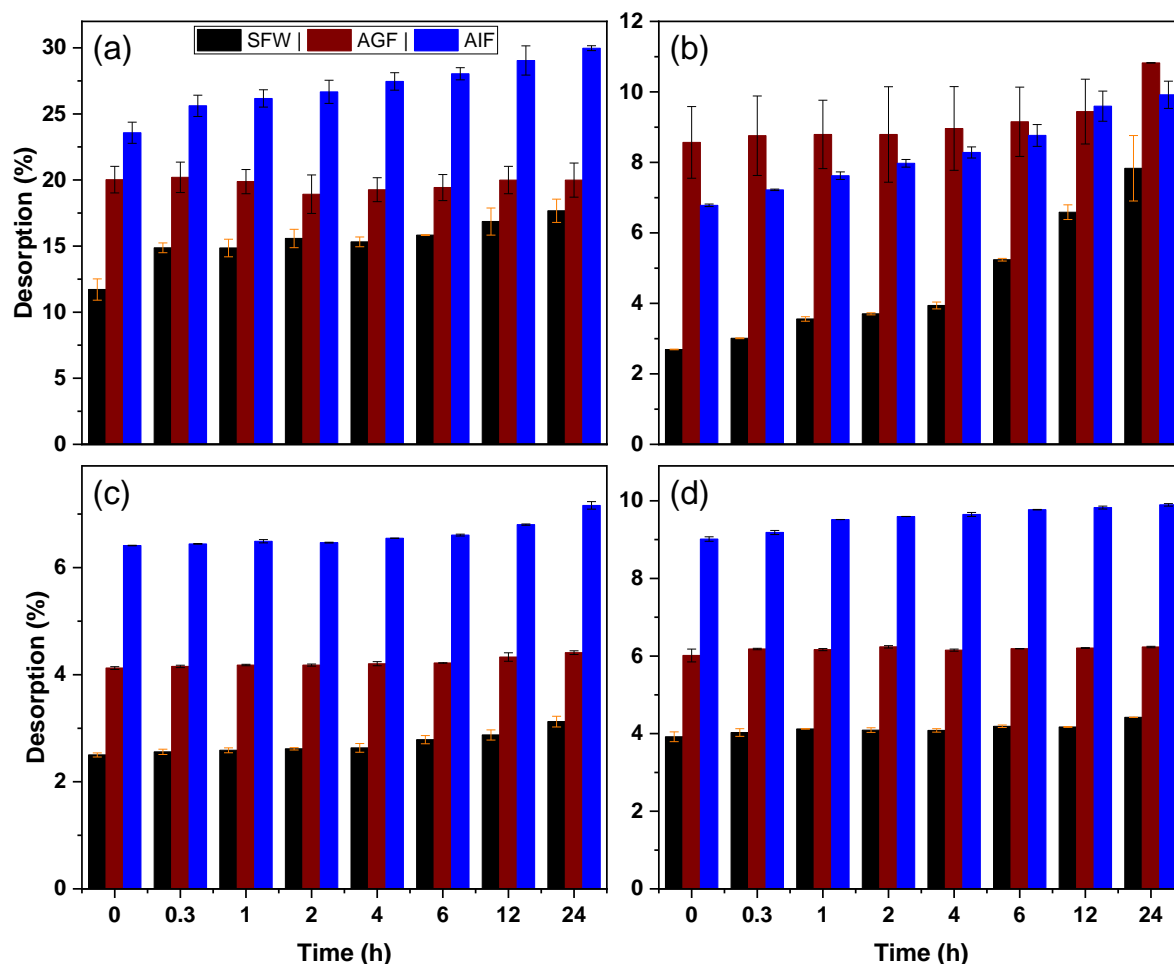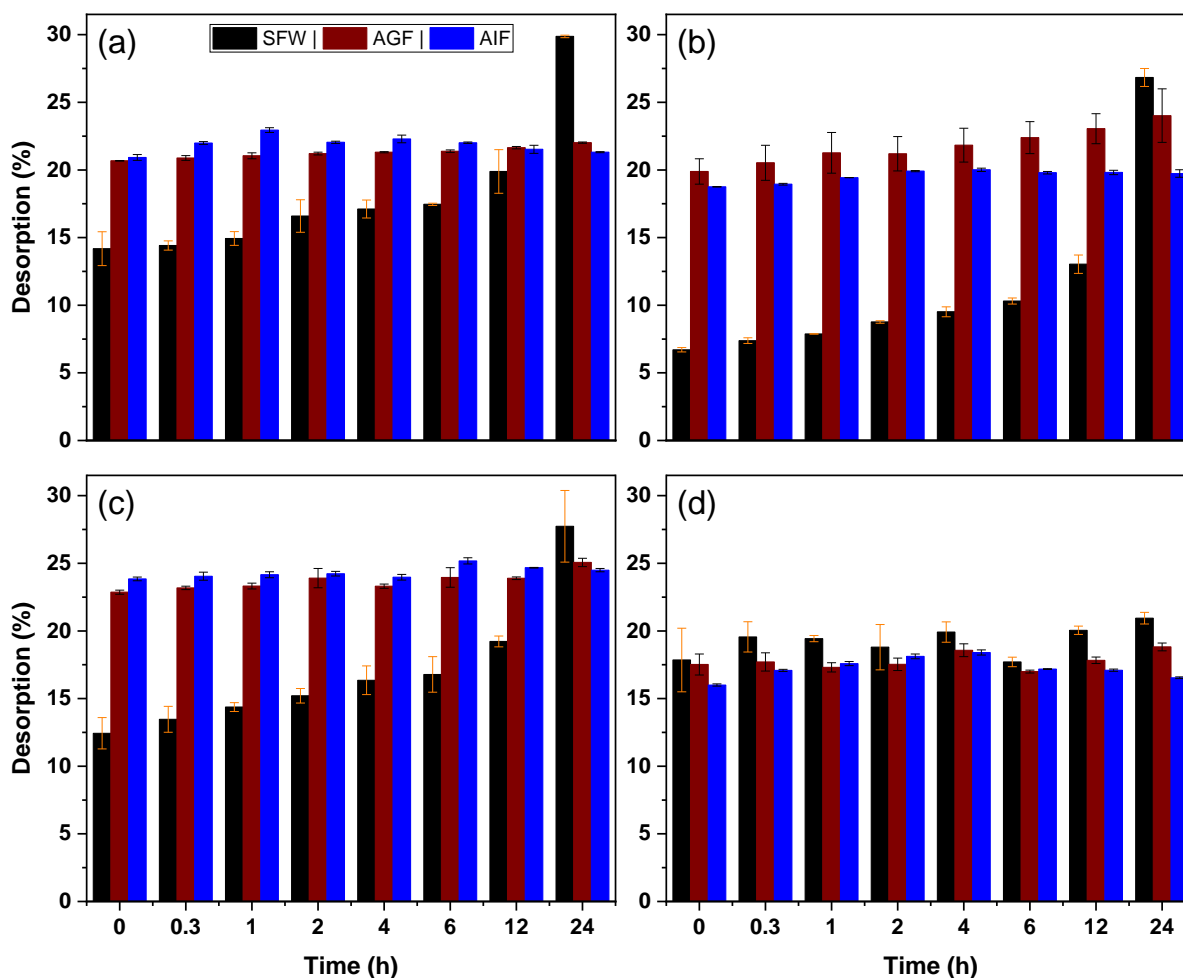

Figure 36. Percentage of DCF desorbed from fresh (a), PE, (b) PP, (c) PS and (d) PVC. Error bars indicate ± SD (n = 2)

In SFW, the desorption of DCF was relatively low across all types of microplastics. For PE, the desorption increased from an initial value of 14.19 to 29.87% at 24 hours. PP showed an increase from 6.71 to 26.84%, PS from 12.44 to 27.73%, and PVC from 17.85 to 20.94%. In AGF, the desorption behaviour was distinct, with higher values compared to SFW. The desorption of DCF from PE ranged from 20.68 to 22.02%, 19.89 to 24.02% for PP, 22.87 to 25.07% for PS, and 17.52 to 18.82% for PVC. The increased desorption in AGF may be attributed to the acidic environment and the hydrophobic nature of DCF. In AIF, the desorption of DCF showed varying patterns. For PE, desorption initially increased from 20.92 to 22.29% within 4 h but then decreased to 21.32% until 24 h of the process. This fluctuation suggests a possible re-adsorption of the pollutant, indicating a dynamic interaction between DCF and PE in the intestinal environment. For PP, desorption increased consistently from 18.76 to 19.74% within the 24 h. PS showed an increase from 23.85 to 25.18%, and PVC exhibited an initial increase from 16.00 to 18.12% within 2 h, followed by a decrease to 16.54% at 24 h.

The desorption of DCF from PE, PP, PS, and PVC varies significantly across the three media. Generally, SFW exhibited the highest desorption ability for all polymers, indicating a greater tendency for DCF to desorb in freshwater environments, followed by AGF and AIF. This order suggests that the desorption of hydrophobic pollutants is independent of the solution's pH, corroborating similar findings reported for progesterone by Siri et al. (2021).

The initial high DCF released from the microplastics compared to SMX can be attributed to the hydrophobic interactions between the pollutants and the microplastics. Furthermore, the higher desorption rates of DCF in biological fluids may be due to the enzymatic activity of pepsin in AGF, which can alter the surface properties of microplastics, and the presence of bile in AIF, which forms micelles that are capable of solubilising hydrophobic pollutants. The desorption behaviour observed for DCF aligns with the findings of Wang et al. (2023) and Siri et al. (2021).

4.5.3 Comparison of the desorption rates between treatments

The adsorption and desorption dynamics of pollutants on various adsorbents are fundamental for comprehending their environmental fate and potential health impacts. Desorption processes, influenced by factors like solvent composition and interaction time, are crucial in evaluating the release of organic pollutants from microplastics. The desorption of SMX and DCF

was investigated under different conditions, revealing distinct patterns. In SFW, SMX desorption was relatively low across all microplastics, while in AGF and AIF, the desorption rates varied significantly. PE exhibited the highest desorption rates, suggesting that SMX's interaction with PE surfaces is readily disrupted by biological fluids. Desorption in AGF and AIF demonstrated that factors like pH and the presence of enzymes or bile significantly influence the desorption efficiency. For DCF, desorption patterns also varied across media, with the highest rates observed in SFW. The behaviour in AGF and AIF highlighted the influence of the solution's pH and the presence of biological components like pepsin and bile, also. These findings underscore the complex interplay between pollutant properties, microplastic characteristics, and environmental conditions, providing valuable insights into the potential health risks posed by microplastic-associated pollutants.

4.6 Strength and limitations

Interactions between microplastics and pollutants have been previously studied, and this research aimed to further investigate these interactions using both hydrophobic and hydrophilic pharmaceuticals as contaminant models and explore different approaches. Firstly, the concentrations of the contaminants studied are environmentally relevant, providing insight into their real-world interactions with microplastics. In this sense, all adsorption studies were carried out using simulated freshwaters as a more controlled media.

Microplastics were successfully photoaged within 20 min using UV-C irradiation in a more controlled environment, providing the necessary surface modifications that are commonly found in environmental MPs. This was confirmed by the variations between fresh and modified microplastics reported by the physicochemical analysis and the improved adsorption capability of the UV-aged microplastics. Although UV-C is not an environmentally achievable condition on Earth for ageing real environmental microplastics, its use has advanced our understanding that plastics can age rapidly. It enabled us to quickly produce UV-aged microplastics, which we then interacted with organic pollutants.

Unlike what has been reported in the literature, we coated the microplastics directly before exposing them to the analytes in the adsorption phase. We observed that the coating improved the adsorption capacity of the microplastics for organic pollutants. Most studies on the influence of

humic acid on the interactions of organic pollutants with microplastics involve humic acid being simultaneously included in the contaminant solution. To date, there is no clear explanation of the dynamics of the sorption process, whether it initially involves analytes and humic acid or analytes and the adsorbent. Also, the literature has not indicated the extent to which humic acids compete for active sites on microplastics against the monitored contaminants. In this study, microplastics were first coated and instead of impeding adsorption, as seen in most other studies, it enhanced the sorption performance of the microplastics.

The desorption studies were conducted in biological fluids that truly mimic gastrointestinal juices. Some studies have used pH ranges within the gastrointestinal tract, while others have used limited reagents. We carefully prepared both gastric and intestinal fluids using the correct proportions of salts and enzymes to understand their implications on the desorption rates of organic pollutants from microplastics into organisms' tracts. However, we could investigate desorption from UV-aged and humic acid-coated microplastics due to time constraints.

This study intended to investigate triclosan as the hydrophobic analyte (see Appendix A), but due to its loss during the filtration process, it was substituted with diclofenac. The loss might have been due to the low concentration adopted and to possible interactions with the polymeric structure of the filters. Additionally, we were unable to explore other options for a wider range of filter materials due to time constraints, and increasing the concentration would have changed the focus of the study.

5 CONCLUSION

This research has provided comprehensive insights into the adsorption-desorption processes of hydrophilic and hydrophobic organic pollutants on PE, PP, PS, and PVC microplastics under diverse environmental conditions. UV irradiation and humic acid coating were found to significantly alter the properties of the microplastics; enhancing surface roughness, wrinkles, and cracks; introducing oxygen-containing functional groups; and impacting crystallinity and stability in water. As expected, these modifications led to varied sorption rates and capacities for pharmaceutical contaminants such as SMX and DCF. Notably, UV-aged and HA-coated microplastics exhibited enhanced sorption performance probably due to increased surface area and chemical reactivity.

In fresh microplastics, sorption interactions such as van der Waals forces, π-π and hydrophobic interactions were likely predominant. Upon modification, hydrogen bonding became more significant due to the presence of oxygen-containing functional groups on the surface of the microplastics. This shift in sorption mechanisms underscores the impact of surface modifications on the behaviour of microplastics in environmental contexts. These findings are critical for understanding how microplastics interact with various pollutants and the implications for environmental health.

Desorption studies revealed that both analytes were desorbed from fresh microplastics in all the simulated media: freshwater, gastric juice, and intestinal fluid. The desorption of analytes in simulated freshwater was low initially and gradually increased over time, whereas desorption into gastrointestinal fluids occurred at a relatively constant rate throughout the process. The desorption was generally impacted by the hydrophobicity of the analytes, and the desorption behaviour in simulated biological fluids highlighted the role of pH and enzymatic activity in contaminant release, with PE demonstrating the highest desorption rates among the tested microplastics. This suggests that microplastics can act as carriers, releasing pollutants under certain environmental conditions, thereby posing potential risks to aquatic life and human health.

These findings underscore the complex interactions between microplastics and pollutants, emphasising the critical environmental and health risks associated with microplastics as carriers of contaminants in aquatic ecosystems. The study highlights the need for further research to

understand the long-term impacts of microplastic pollution and to develop strategies to mitigate these risks. An enhanced understanding of the adsorption-desorption mechanisms can inform the design of more effective water treatment processes and environmental policies aimed at reducing microplastic pollution.

Finally, this research provides valuable data on the behaviour of microplastics in various environmental and biological contexts, contributing to the broader understanding of their role in pollutant dynamics and their potential threat to environmental and human health. The insights gained from this study are crucial for developing strategies to manage and mitigate the impact of microplastics on the environment, ensuring the protection of ecosystems and public health.

Challenges and recommendations for further studies

Arriving in Brasília in 2019, I took some Portuguese classes and sorted research objectives focusing on the adsorption of emerging contaminants using activated carbon with my supervisor. In the second semester, I started developing an analytical method for determining analytes of interest, utilising liquid chromatography coupled with mass spectrometry (LC-MS/MS). The instrument, a hybrid quadrupole-linear ion trap (3200 QTrap, AB Sciex), was located in the Department of Civil Engineering at the university of Brasília. Unfortunately, the need for maintenance and the high demand from students using the equipment severely hampered my progress.

As I was hoping for the best opportunities to advance my method development, my initial enthusiasm and high expectations were soon challenged by the unforeseen COVID-19 pandemic, which drastically altered my plans. The pandemic led to a suspension of research activities at the University in March 2020, resulting in restricted laboratory access and necessitating adjustments to my research topic. Consequently, Graduate Program in Chemistry of the University extended the duration of affected doctoral programs by 25 months, extending my study period until May 2025.

During the pandemic, Prof. Dr. Fernando Fabriz Sodré initiated a research project with the Ministry of Justice and Public Security, which facilitated the acquisition of a new LC-MS/MS instrument in April 2021. However, import quota reductions delayed the delivery until January

2022, with installation following in March 2022. Shortly after installation, the autosampler wash module required replacement, which was completed on 29th July 2022. Subsequently, a malfunction in the autosampler caused micro leaks, leading to a complete loss of the analytical signal. A defect in a leak sensor further halted the LC-MS/MS. Parts needed to be imported, delaying repairs until 30th September 2022. Consequently, between 25 March 2022 and 30 September 2022, the equipment functioned properly for only three months, severely affecting my experimental schedule.

Scholarship presented another significant challenge. I held a TWAS-CNPq scholarship that ended in March 2023. Despite attempts to secure additional scholarships, I only managed to obtain a two-month extension. This period was incredibly frustrating. However, thanks to Prof. Fernando's efforts, I secured another scholarship, a gesture of immense support that I will cherish forever. Unfortunately, this scholarship does not cover the extended study period until May 2025, preventing me from fulfilling part of my research objectives. These objectives include investigating the influence of biofilm coating on the sorption interactions of microplastics and studying the desorption of organic pollutants from all modified microplastics, including UV-aged, HA-coated, and biofilm-coated microplastics.

Recommendations for further studies

Given these challenges, I recommend that future studies focus on the following areas to provide deeper insights into how MPs generally interact with pollutants in the natural environment:

1. Expanding sorption studies involving MPs coated with biofilm is essential for a more comprehensive understanding of their environmental behaviour. Biofilms, which are layers of microorganisms that colonise MPs, can significantly alter the sorption properties of these particles. By incorporating biofilm-coated MPs, we can examine how biological processes impact the adsorption of contaminants like DCF and SMX among others. This is crucial, as biofilms may either enhance or hinder sorption, depending on the surface chemistry and environmental conditions, providing more accurate insights into MPs' roles as pollutant carriers.

2. It is recommended to expand desorption studies to include UV-aged, humic acid-coated, and biofilm-coated MPs. These modifications are crucial, as UV exposure alters the surface

properties of MPs, potentially influencing the release of adsorbed contaminants like DCF. Similarly, coatings formed by humic acids and biofilms can impact desorption behaviour, affecting the interaction between MPs and pollutants. By studying these transformations, we can gain deeper insight into the environmental fate of MPs and their role as vectors for contaminant transport, thereby improving risk assessments.

3. Extend ageing studies to more environmentally relevant conditions to better simulate the natural ageing processes of MPs. This would involve using solar UV-A and UV-B irradiation over extended periods to more accurately represent environmental exposure.

4. Conduct simultaneous adsorption studies involving multiple contaminants to elucidate the dynamics of sorption processes. This approach will allow a more comprehensive understanding of how these substances interact with MPs in environmental contexts.

5. It is recommended to conduct adsorption studies using MP samples gathered from freshwater environments. Environmentally aged MPs may behave differently with pollutants and give more robust information probably due to the many environmental factors that would impact their ageing.

REFERENCES

Abbas, Q., Yousaf, B., Amina, Ali, M. U., Munir, M. A. M., El-Naggar, A., . . . Naushad, M. (2020). Transformation pathways and fate of engineered nanoparticles (ENPs) in distinct interactive environmental compartments: A review. *Environment international*, *138*, 105646. https://doi.org/https://doi.org/10.1016/j.envint.2020.105646

ABIPLAST. (2022). *The Plastic Transformation and Recycling Industries in Brazil* (ABIPLAST Perfil, Issue. http://www.abiplast.org.br/wp-content/uploads/2022/09/PERFIL_2021_EN_FINAL.pdf

Abuwatfa, W. H., Al-Muqbel, D., Al-Othman, A., Halalsheh, N., & Tawalbeh, M. (2021). Insights into the removal of microplastics from water using biochar in the era of COVID-19: A mini review. *Case Studies in Chemical and Environmental Engineering*, *4*, 100151.

Agboola, O. D., & Benson, N. U. (2021). Physisorption and chemisorption mechanisms influencing micro (nano) plastics-organic chemical contaminants interactions: a review. *Frontiers in Environmental Science*, *9*, 678574.

Ahmed, S. F., Mofijur, M., Nuzhat, S., Chowdhury, A. T., Rafa, N., Uddin, M. A., . . . Show, P. L. (2021). Recent developments in physical, biological, chemical, and hybrid treatment techniques for removing emerging contaminants from wastewater. *Journal of Hazardous Materials*, *416*, 125912. https://doi.org/https://doi.org/10.1016/j.jhazmat.2021.125912

Akpomie, K. G., Dawodu, F. A., & Adebowale, K. O. (2015). Mechanism on the sorption of heavy metals from binary-solution by a low cost montmorillonite and its desorption potential. *Alexandria Engineering Journal*, *54*(3), 757-767.

Ali, I., Tan, X., Peng, C., Naz, I., Zhang, Y., Hernández, A., . . . Ruan, Y. (2024). Eco-and bio-corona-based microplastics and nanoplastics complexes in the environment: Modulations in the toxicological behavior of plastic particles and factors affecting. *Process Safety and Environmental Protection*.

Ali, S. S., Elsamahy, T., Koutra, E., Kornaros, M., El-Sheekh, M., Abdelkarim, E. A., . . . Sun, J. (2021). Degradation of conventional plastic wastes in the environment: A review on current status of knowledge and future perspectives of disposal. *Science of The Total Environment*, *771*, 144719. https://doi.org/https://doi.org/10.1016/j.scitotenv.2020.144719

Alsharef, J. M., Taha, M. R., & Khan, T. A. (2017). Physical dispersion of nanocarbons in composites—A review. *Jurnal Teknologi*, *79*(5), 69-81.

Amobonye, A. E., Bhagwat, P., Singh, S., & Pillai, S. (2023). Biodegradability of Polyvinyl chloride. In *Biodegradability of Conventional Plastics* (pp. 201-220). Elsevier.

Anah, L., & Astrini, N. (2018). Isotherm adsorption studies of Ni (II) ion removal from aqueous solutions by modified carboxymethyl cellulose hydrogel. IOP Conference Series: Earth and Environmental Science,

Arowojolu, I. M., de Oliveira Alves, I., Benson, N. U., & Sodré, F. F. (2023). Microplastics in aquatic environments: a growing, unresolved concern. *Chemistry of the Total Environment*, *3*(1), 8-22.

Arthur, C., Baker, J. E., & Bamford, H. A. (2009). Proceedings of the International Research Workshop on the Occurrence, Effects, and Fate of Microplastic Marine Debris, September 9-11, 2008, University of Washington Tacoma, Tacoma, WA, USA.

Ashrafy, A., Liza, A. A., Islam, M. N., Billah, M. M., Arafat, S. T., Rahman, M. M., & Rahman, S. M. (2023). Microplastics Pollution: A Brief Review of Its Source and Abundance in

Different Aquatic Ecosystems. *Journal of Hazardous Materials Advances*, *9*, 100215. https://doi.org/https://doi.org/10.1016/j.hazadv.2022.100215

Athulya, P. A., & Chandrasekaran, N. (2023). Interactions of natural colloids with microplastics in aquatic environment and its impact on FTIR characterization of polyethylene and polystyrene microplastics. *Journal of Molecular Liquids*, *369*, 120950. https://doi.org/https://doi.org/10.1016/j.molliq.2022.120950

Barbosa, C. C., Gomes, L. N. L., & Minoti, R. T. (2021). A modelling approach to simulate Chlorophyta and Cyanobacteria biomasses based on historical data of a Brazilian urban reservoir. *Revista Ambiente & Água*, *16*.

Barnes, D. K., Galgani, F., Thompson, R. C., & Barlaz, M. (2009). Accumulation and fragmentation of plastic debris in global environments. *Philosophical Transactions of the Royal Society B: Biological Sciences*, *364*(1526), 1985-1998.

Bazrafshan, E., Biglari, H., & Mahvi, A. H. (2012). Humic acid removal from aqueous environments by electrocoagulation process using iron electrodes. *E-Journal of Chemistry*, *9*(4), 2453-2461.

Bellasi, A., Binda, G., Pozzi, A., Galafassi, S., Volta, P., & Bettinetti, R. (2020). Microplastic contamination in freshwater environments: A review, focusing on interactions with sediments and benthic organisms. *Environments*, *7*(4), 30.

Bhagat, K., Barrios, A. C., Rajwade, K., Kumar, A., Oswald, J., Apul, O., & Perreault, F. (2022). Aging of microplastics increases their adsorption affinity towards organic contaminants. *Chemosphere*, *298*, 134238.

Bittelli, M., Campbell, G. S., & Flury, M. (1999). Characterization of particle-size distribution in soils with a fragmentation model. *Soil Science Society of America Journal*, *63*(4), 782-788.

Borghi, F., Podestà, A., Di Vece, M., Piazzoni, C., & Milani, P. (2018). Cluster-Assembled Materials: From Fabrication to Function. In K. Wandelt (Ed.), *Encyclopedia of Interfacial Chemistry* (pp. 417-427). Elsevier. https://doi.org/https://doi.org/10.1016/B978-0-12-409547-2.12935-X

Bowen, W. R., & Jenner, F. (1995). Theoretical descriptions of membrane filtration of colloids and fine particles: an assessment and review. *Advances in Colloid and Interface Science*, *56*, 141-200.

Bredács, M., Kanatschnig, E., Frank, A., Oreski, G., Pinter, G., & Gergely, S. (2023). Identifying active and degraded phenolic antioxidants in aged PE with IR-microscopy. *Polymer Degradation and Stability*, *212*, 110345. https://doi.org/https://doi.org/10.1016/j.polymdegradstab.2023.110345

Brooks, A. L., Wang, S., & Jambeck, J. R. (2018). The Chinese import ban and its impact on global plastic waste trade. *Science advances*, *4*(6), eaat0131.

Cai, Y., Li, C., & Zhao, Y. (2021). A review of the migration and transformation of microplastics in inland water systems. *International Journal of Environmental Research and Public Health*, *19*(1), 148.

Changmai, M., Banerjee, P., Nahar, K., & Purkait, M. K. (2018). A novel adsorbent from carrot, tomato and polyethylene terephthalate waste as a potential adsorbent for Co (II) from aqueous solution: Kinetic and equilibrium studies. *Journal of Environmental Chemical Engineering*, *6*(1), 246-257.

Chen, H., Gao, B., Li, H., & Ma, L. Q. (2011). Effects of pH and ionic strength on sulfamethoxazole and ciprofloxacin transport in saturated porous media. *Journal of contaminant hydrology*, *126*(1-2), 29-36.

Chen, X., Hossain, M. F., Duan, C., Lu, J., Tsang, Y. F., Islam, M. S., & Zhou, Y. (2022). Isotherm models for adsorption of heavy metals from water - A review. *Chemosphere*, *307*, 135545. https://doi.org/https://doi.org/10.1016/j.chemosphere.2022.135545

Chen, X., & Sweetman, A. J. (2024). An investigation into the effect of UV irradiation and biofilm colonization on adsorption and desorption behavior of polyurethane (PU) microplastics for bisphenol A (BPA). *Environmental Technology & Innovation*, *35*, 103662. https://doi.org/https://doi.org/10.1016/j.eti.2024.103662

Clogston, J. D., & Patri, A. K. (2011a). Zeta potential measurement. *Methods Mol Biol*, *697*, 63-70. https://doi.org/10.1007/978-1-60327-198-1_6

Clogston, J. D., & Patri, A. K. (2011b). Zeta potential measurement. *Characterization of nanoparticles intended for drug delivery*, 63-70.

Costa, N. Y. M. d. (2014). Estudo geoquímico e de contaminantes emergentes na bacia do lago Paranoá.

Cruz, P. P. R., da Silva, L. C., Fiuza-Jr, R. A., & Polli, H. (2021). Thermal dehydrochlorination of pure PVC polymer: Part I—thermal degradation kinetics by thermogravimetric analysis. *Journal of Applied Polymer Science*, *138*(25), 50598.

da Costa, J. P., Avellan, A., Tubić, A., Duarte, A. C., & Rocha-Santos, T. (2024). Understanding Interface Exchanges for Assessing Environmental Sorption of Additives from Microplastics: Current Knowledge and Perspectives. *Molecules*, *29*(2), 333.

de la Orden, M. U., Montes, J. M., Martínez Urreaga, J., Bento, A., Ribeiro, M. R., Pérez, E., & Cerrada, M. L. (2015). Thermo and photo-oxidation of functionalized metallocene high density polyethylene: Effect of hydrophilic groups. *Polymer Degradation and Stability*, *111*, 78-88. https://doi.org/https://doi.org/10.1016/j.polymdegradstab.2014.10.023

Desforges, J.-P. W., Galbraith, M., Dangerfield, N., & Ross, P. S. (2014). Widespread distribution of microplastics in subsurface seawater in the NE Pacific Ocean. *Marine pollution bulletin*, *79*(1), 94-99. https://doi.org/https://doi.org/10.1016/j.marpolbul.2013.12.035

Dimitris, S., & Achilias, L. (2014). Recent advances in the chemical recycling of polymers (PP, PS, LDPE, HDPE, PVC, PC, Nylon, PMMA). *Mater. Recycl. Trends Perspect*, *3*, 64.

Doğan, M. (2021). Ultraviolet light accelerates the degradation of polyethylene plastics. *Microscopy Research and Technique*, *84*(11), 2774-2783.

Dong, Y., Gao, M., Qiu, W., & Song, Z. (2020). Adsorption of arsenite to polystyrene microplastics in the presence of humus. *Environmental Science: Processes & Impacts*, *22*(12), 2388-2397.

Donohue, M. J. (2005). Eastern Pacific Ocean source of Northwestern Hawaiian Islands marine debris supported by errant fish aggregating device. *Marine pollution bulletin*, *50*(8), 886-888.

Du, H., Zhang, Y., Jiang, H., & Wang, H. (2022). Adsorption of rhodamine B on polyvinyl chloride, polystyrene, and polyethylene terephthalate microplastics in aqueous environments. *Environmental Technology & Innovation*, *27*, 102495. https://doi.org/https://doi.org/10.1016/j.eti.2022.102495

Duan, J., Bolan, N., Li, Y., Ding, S., Atugoda, T., Vithanage, M., . . . Kirkham, M. (2021). Weathering of microplastics and interaction with other coexisting constituents in terrestrial and aquatic environments. *Water Research*, *196*, 117011.

Duis, K., & Coors, A. (2016). Microplastics in the aquatic and terrestrial environment: sources (with a specific focus on personal care products), fate and effects. *Environmental Sciences Europe*, *28*(1), 2.

Dümichen, E., Barthel, A.-K., Braun, U., Bannick, C. G., Brand, K., Jekel, M., & Senz, R. (2015). Analysis of polyethylene microplastics in environmental samples, using a thermal decomposition method. *Water Research*, *85*, 451-457. https://doi.org/https://doi.org/10.1016/j.watres.2015.09.002

Elizalde-Velazquez, A., Subbiah, S., Anderson, T. A., Green, M. J., Zhao, X., & Cañas-Carrell, J. E. (2020). Sorption of three common nonsteroidal anti-inflammatory drugs (NSAIDs) to microplastics. *Science of The Total Environment*, *715*, 136974.

Elizalde-Velázquez, A., Subbiah, S., Anderson, T. A., Green, M. J., Zhao, X., & Cañas-Carrell, J. E. (2020). Sorption of three common nonsteroidal anti-inflammatory drugs (NSAIDs) to microplastics. *Science of The Total Environment*, *715*, 136974. https://doi.org/https://doi.org/10.1016/j.scitotenv.2020.136974

Evode, N., Qamar, S. A., Bilal, M., Barceló, D., & Iqbal, H. M. (2021). Plastic waste and its management strategies for environmental sustainability. *Case Studies in Chemical and Environmental Engineering*, *4*, 100142.

Fan, Q., Sun, J., Chu, L., Cui, L., Quan, G., Yan, J., . . . Iqbal, M. (2018). Effects of chemical oxidation on surface oxygen-containing functional groups and adsorption behavior of biochar. *Chemosphere*, *207*, 33-40.

Foo, K. Y., & Hameed, B. H. (2010). Insights into the modeling of adsorption isotherm systems. *Chemical engineering journal*, *156*(1), 2-10.

Gao, L., Fu, D., Zhao, J., Wu, W., Wang, Z., Su, Y., & Peng, L. (2021). Microplastics aged in various environmental media exhibited strong sorption to heavy metals in seawater. *Marine pollution bulletin*, *169*, 112480. https://doi.org/https://doi.org/10.1016/j.marpolbul.2021.112480

Gewert, B., Plassmann, M. M., & MacLeod, M. (2015). Pathways for degradation of plastic polymers floating in the marine environment. *Environmental Science: Processes & Impacts*, *17*(9), 1513-1521.

Ghabbour, E. A., & Davies, G. (1998). *Humic substances: structures, properties and uses*. The Royal Society of Chemistry, UK.

Giles, C. H., Macewan, T. H., Nakhwa, S. N., & Smit, D. (1960). Studies in adsorption. Part XI. A system of classification of solution adsorption isotherms, and its use in diagnosis of adsorption mechanisms and in measurements of specific surface areas of solids. *J. Chem. Soc.*, *786*, 3973-3993.

Grassi, M. T., Shi, B., & Allen, H. E. (2000). Partition of copper between dissolved and particulate phases using aluminum oxide as an aquatic model phase: effects of pH, solids and organic matter. *Journal of the Brazilian Chemical Society*, *11*, 516-524.

Gregory, M. R. (2009). Environmental implications of plastic debris in marine settings—entanglement, ingestion, smothering, hangers-on, hitch-hiking and alien invasions. *Philosophical Transactions of the Royal Society B: Biological Sciences*, *364*(1526), 2013-2025.

Grigg, M. N. (2006). *Thermo-oxidative degradation of polyamide 6* Queensland University of Technology].

Guazzotti, V., Gruner, A., Juric, M., Hendrich, V., Störmer, A., & Welle, F. (2022). Migration testing of GPPS and HIPS polymers: Swelling effect caused by food simulants compared to real foods. *Molecules*, *27*(3), 823.

Gulmine, J. V., & Akcelrud, L. (2006). FTIR characterization of aged XLPE. *Polymer Testing*, *25*(7), 932-942. https://doi.org/https://doi.org/10.1016/j.polymertesting.2006.05.014

Guo, C., Wang, L., Lang, D., Qian, Q., Wang, W., Wu, R., & Wang, J. (2023). UV and chemical aging alter the adsorption behavior of microplastics for tetracycline. *Environmental Pollution*, *318*, 120859.

Guo, X., Chen, C., & Wang, J. (2019). Sorption of sulfamethoxazole onto six types of microplastics. *Chemosphere*, *228*, 300-308.

Guo, X., Pang, J., Chen, S., & Jia, H. (2018). Sorption properties of tylosin on four different microplastics. *Chemosphere*, *209*, 240-245.

Guo, X., & Wang, J. (2019). Sorption of antibiotics onto aged microplastics in freshwater and seawater. *Marine pollution bulletin*, *149*, 110511. https://doi.org/https://doi.org/10.1016/j.marpolbul.2019.110511

Guo, X., Wang, X., Zhou, X., Kong, X., Tao, S., & Xing, B. (2012). Sorption of four hydrophobic organic compounds by three chemically distinct polymers: role of chemical and physical composition. *Environmental science & technology*, *46*(13), 7252-7259.

Harshvardhan, K., & Jha, B. (2013). Biodegradation of low-density polyethylene by marine bacteria from pelagic waters, Arabian Sea, India. *Marine pollution bulletin*, *77*(1), 100-106. https://doi.org/https://doi.org/10.1016/j.marpolbul.2013.10.025

Hawkins, W. L. (1984). Polymer degradation. In *Polymer degradation and stabilization* (pp. 3-34). Springer.

Henry, W. (1803). III. Experiments on the quantity of gases absorbed by water, at different temperatures, and under different pressures. *Philosophical Transactions of the Royal Society of London*(93), 29-274.

Ho, Y. S., & McKay, G. (1999). Pseudo-second order model for sorption processes. *Process Biochemistry*, *34*(5), 451-465. https://doi.org/https://doi.org/10.1016/S0032-9592(98)00112-5

Hossain, M. R., Jiang, M., Wei, Q., & Leff, L. G. (2019). Microplastic surface properties affect bacterial colonization in freshwater. *Journal of Basic Microbiology*, *59*(1), 54-61. https://doi.org/https://doi.org/10.1002/jobm.201800174

Huang, W., Jiang, G., Xie, L., Chen, X., Zhang, R., & Fan, X. (2024). Effect of oxygen-containing functional groups on the micromechanical behavior of biodegradable plastics and their formation of microplastics during aging. *Journal of Hazardous Materials*, *463*, 132911.

Hubbe, M. A., Azizian, S., & Douven, S. (2019). Implications of apparent pseudo-second-order adsorption kinetics onto cellulosic materials: A review. *BioResources*, *14*(3).

Hüffer, T., & Hofmann, T. (2016). Sorption of non-polar organic compounds by micro-sized plastic particles in aqueous solution. *Environmental Pollution*, *214*, 194-201.

Inoue, M. (1963). Studies on crystallization of high polymers by differential thermal analysis. *Journal of Polymer Science Part A: General Papers*, *1*(8), 2697-2709.

Iyer, S., Rissanen, M. P., & Kurtén, T. (2019). Reaction between Peroxy and Alkoxy Radicals Can Form Stable Adducts. *The Journal of Physical Chemistry Letters*, *10*(9), 2051-2057. https://doi.org/10.1021/acs.jpclett.9b00405

Jambeck, J., Moss, E., Dubey, B., Arifin, Z., Godfrey, L., Hardesty, B. D., . . . Matlock, M. (2023). Leveraging multi-target strategies to address plastic pollution in the context of an already stressed ocean. In *The Blue Compendium: From Knowledge to Action for a Sustainable Ocean Economy* (pp. 141-184). Springer.

Jambeck, J. R., Geyer, R., Wilcox, C., Siegler, T. R., Perryman, M., Andrady, A., . . . Law, K. L. (2015). Plastic waste inputs from land into the ocean. *Science*, *347*(6223), 768-771.

Jeppu, G. P., & Clement, T. P. (2012). A modified Langmuir-Freundlich isotherm model for simulating pH-dependent adsorption effects. *Journal of contaminant hydrology*, *129*, 46-53.

Junaid, M., & Wang, J. (2021). Interaction of nanoplastics with extracellular polymeric substances (EPS) in the aquatic environment: A special reference to eco-corona formation and associated impacts. *Water Research*, *201*, 117319.

Kang, K.-H., Nam, K.-B., Jeong, B.-S., Kim, J.-S., & Yoo, J.-C. (2023). The use of plastic litter as nesting material by the azure-winged magpie Cyanopica cyanus in an agricultural environment of South Korea. *Environmental Science and Pollution Research*, *30*(35), 84814-84821.

Khan, F. R., Shashoua, Y., Crawford, A., Drury, A., Sheppard, K., Stewart, K., & Sculthorp, T. (2020). 'The plastic nile': First evidence of microplastic contamination in fish from the nile river (Cairo, Egypt). *Toxics*, *8*(2), 22.

Khan, S., Naushad, M., Govarthanan, M., Iqbal, J., & Alfadul, S. M. (2022). Emerging contaminants of high concern for the environment: Current trends and future research. *Environmental Research*, *207*, 112609. https://doi.org/https://doi.org/10.1016/j.envres.2021.112609

Klein, S., Dimzon, I. K., Eubeler, J., & Knepper, T. P. (2018). Analysis, occurrence, and degradation of microplastics in the aqueous environment. In *Freshwater microplastics* (pp. 51-67). Springer, Cham.

Kołbuk, D., Ciechomska, M., Jeznach, O., & Sajkiewicz, P. (2022). Effect of crystallinity and related surface properties on gene expression of primary fibroblasts. *RSC advances*, *12*(7), 4016-4028.

Kong, F., Xu, X., Xue, Y., Gao, Y., Zhang, L., Wang, L., . . . Zhang, Q. (2021). Investigation of the adsorption of sulfamethoxazole by degradable microplastics artificially aged by chemical oxidation. *Archives of Environmental Contamination and Toxicology*, *81*(1), 155-165.

Kowalski, N., Reichardt, A. M., & Waniek, J. J. (2016). Sinking rates of microplastics and potential implications of their alteration by physical, biological, and chemical factors. *Marine pollution bulletin*, *109*(1), 310-319.

Kuang, B., Chen, X., Zhan, J., Zhou, L., Zhong, D., & Wang, T. (2023). Interaction behaviors of sulfamethoxazole and microplastics in marine condition: Focusing on the synergistic effects of salinity and temperature. *Ecotoxicology and Environmental Safety*, *259*, 115009. https://doi.org/https://doi.org/10.1016/j.ecoenv.2023.115009

Kühn, S., Van Oyen, A., Booth, A. M., Meijboom, A., & Van Franeker, J. A. (2018). Marine microplastic: Preparation of relevant test materials for laboratory assessment of ecosystem impacts. *Chemosphere*, *213*, 103-113.

Lagergren, S. (1898). Zur theorie der sogenannten adsorption geloster stoffe.

Langmuir, I. (1918). The adsorption of gases on plane surfaces of glass, mica and platinum. *Journal of the American Chemical society*, *40*(9), 1361-1403.

Lee, H., Lee, H.-J., & Kwon, J.-H. (2019). Estimating microplastic-bound intake of hydrophobic organic chemicals by fish using measured desorption rates to artificial gut fluid. *Science of The Total Environment*, *651*, 162-170.

Lee, H., Shim, W. J., & Kwon, J.-H. (2014). Sorption capacity of plastic debris for hydrophobic organic chemicals. *Science of The Total Environment*, *470-471*, 1545-1552. https://doi.org/https://doi.org/10.1016/j.scitotenv.2013.08.023

Leiser, R., Wu, G.-M., Neu, T. R., & Wendt-Potthoff, K. (2020). Biofouling, metal sorption and aggregation are related to sinking of microplastics in a stratified reservoir. *Water Research*, *176*, 115748.

Li, Y., Zeng, Q., Sun, Y., Liu, Q., Yang, Q., Hao, Y., . . . Gong, Z. (2024). Revealing the complex oxidation behavior of extracellular polymeric substances interacted with pristine and aged polypropylene microplastics. *Journal of Water Process Engineering*, *63*, 105492. https://doi.org/https://doi.org/10.1016/j.jwpe.2024.105492

Li, Y., Zhang, Y., Su, F., Wang, Y., Peng, L., & Liu, D. (2022). Adsorption behaviour of microplastics on the heavy metal Cr(VI) before and after ageing. *Chemosphere*, *302*, 134865. https://doi.org/https://doi.org/10.1016/j.chemosphere.2022.134865

Liang, S., Wang, K., Wang, K., Wang, T., Guo, C., Wang, W., & Wang, J. (2023). Adsorption behavior of diclofenac on polystyrene and poly (butylene adipate-co-terephthalate) microplastics: influencing factors and adsorption mechanism. *Langmuir*, *39*(34), 12216-12225.

Lin, J., Yan, D., Fu, J., Chen, Y., & Ou, H. (2020). Ultraviolet-C and vacuum ultraviolet inducing surface degradation of microplastics. *Water Research*, *186*, 116360.

Liu, G., Zhu, Z., Yang, Y., Sun, Y., Yu, F., & Ma, J. (2019). Sorption behavior and mechanism of hydrophilic organic chemicals to virgin and aged microplastics in freshwater and seawater. *Environmental Pollution*, *246*, 26-33. https://doi.org/https://doi.org/10.1016/j.envpol.2018.11.100

Liu, P., Zhan, X., Wu, X., Li, J., Wang, H., & Gao, S. (2020). Effect of weathering on environmental behavior of microplastics: Properties, sorption and potential risks. *Chemosphere*, *242*, 125193.

Liu, Q., Wu, H., Chen, J., Guo, B., Zhao, X., Lin, H., . . . Huang, C. (2022). Adsorption mechanism of trace heavy metals on microplastics and simulating their effect on microalgae in river. *Environmental Research*, *214*, 113777. https://doi.org/https://doi.org/10.1016/j.envres.2022.113777

Liu, R., Wu, X., Zhang, W., Chen, Y., Fu, J., & Ou, H. (2023). Volatile organic compounds generation pathways and mechanisms from microplastics in water: Ultraviolet, chlorine and ultraviolet/chlorine disinfection. *Journal of Hazardous Materials*, *441*, 129813. https://doi.org/https://doi.org/10.1016/j.jhazmat.2022.129813

Lu, J., Wu, J., Wu, J., Zhang, C., & Luo, Y. (2021). Adsorption and desorption of steroid hormones by microplastics in seawater. *Bulletin of Environmental Contamination and Toxicology*, *107*, 730-735.

Luo, H., Liu, C., He, D., Sun, J., Zhang, A., Li, J., & Pan, X. (2022). Interactions between polypropylene microplastics (PP-MPs) and humic acid influenced by aging of MPs. *Water Research*, *222*, 118921.

Mane, V. S., Mall, I. D., & Srivastava, V. C. (2007). Use of bagasse fly ash as an adsorbent for the removal of brilliant green dye from aqueous solution. *Dyes and Pigments*, *73*(3), 269-278. https://doi.org/https://doi.org/10.1016/j.dyepig.2005.12.006

McColley, C. J. (2023). Eco-corona formation and impact on environmentally relevant micro-and nanoplastics.

Mei, W., Chen, G., Bao, J., Song, M., Li, Y., & Luo, C. (2020). Interactions between microplastics and organic compounds in aquatic environments: a mini review. *Science of The Total Environment*, *736*, 139472.

Mena, R. L., Cacuro, T. A., de Freitas, A. S., Rangel, E. C., & Waldman, W. R. (2020). Polymer photodegradation followed by infrared: A tutorial. *Revista Virtual de Química*, 959-968.

Meng, Q., Dong, Y., Yang, Y., Wang, J., Li, J., & Zhu, J. (2024). Synthesis and evaluation of dioctyl 2,5-thiophenedicarboxylate as a potentially bio-based plasticizer for poly(vinyl chloride). *Journal of Applied Polymer Science*, *141*(9), e55033. https://doi.org/https://doi.org/10.1002/app.55033

Miloloža, M., Kučić Grgić, D., Bolanča, T., Ukić, Š., Cvetnić, M., Ocelić Bulatović, V., . . . Kušić, H. (2020). Ecotoxicological assessment of microplastics in freshwater sources—A review. *Water*, *13*(1), 56.

Min, K., Cuiffi, J. D., & Mathers, R. T. (2020). Ranking environmental degradation trends of plastic marine debris based on physical properties and molecular structure. *Nature communications*, *11*(1), 727.

Mo, Q., Yang, X., Wang, J., Xu, H., Li, W., Fan, Q., . . . Liao, D. (2021). Adsorption mechanism of two pesticides on polyethylene and polypropylene microplastics: DFT calculations and particle size effects. *Environmental Pollution*, *291*, 118120.

Moussout, H., Ahlafi, H., Aazza, M., & Maghat, H. (2018). Critical of linear and nonlinear equations of pseudo-first order and pseudo-second order kinetic models. *Karbala International Journal of Modern Science*, *4*(2), 244-254. https://doi.org/https://doi.org/10.1016/j.kijoms.2018.04.001

Munoz, M., Ortiz, D., Nieto-Sandoval, J., de Pedro, Z. M., & Casas, J. A. (2021). Adsorption of micropollutants onto realistic microplastics: Role of microplastic nature, size, age, and NOM fouling. *Chemosphere*, *283*, 131085. https://doi.org/https://doi.org/10.1016/j.chemosphere.2021.131085

Nicholson, J. W. (1991). *The chemistry of polymers*. Royal Society of Chemistry.

NOAA, N. O. a. A. A. (2014). *Entanglement of marine species in marine debris with an emphasis on species in the United States*. https://marinedebris.noaa.gov/sites/default/files/mdp_entanglement.pdf

O'Driscoll, K. F. (1964). *The Nature and Chemistry of High Polymers*. Reinhold Publishing Corporation.

Peng, J., Wang, J., & Cai, L. (2017). Current understanding of microplastics in the environment: occurrence, fate, risks, and what we should do. *Integrated environmental assessment and management*, *13*(3), 476-482.

Peters, E. N. (2002). *Plastics: thermoplastics, thermosets, and elastomers*. Wiley-Interscience, New York.

Piccin, J., Dotto, G., & Pinto, L. (2011). Adsorption isotherms and thermochemical data of FD&C Red n 40 binding by chitosan. *Brazilian Journal of Chemical Engineering*, *28*, 295-304.

Piccin, J. S., Cadaval, T. R. S. A., De Pinto, L. A. A., & Dotto, G. L. (2017). Adsorption isotherms in liquid phase: experimental, modeling, and interpretations. *Adsorption processes for water treatment and purification*, 19-51.

Pittarello, M., Busato, J. G., Carletti, P., Sodré, F. F., & Dobbss, L. B. (2019). Dissolved humic substances supplied as potential enhancers of Cu, Cd, and Pb adsorption by two different mangrove sediments. *Journal of Soils and Sediments*, *19*, 1554-1565.

Popelka, A., Zavahir, S., & Habib, S. (2020). Chapter 2 - Morphology analysis. In M. A. A. AlMaadeed, D. Ponnamma, & M. A. Carignano (Eds.), *Polymer Science and Innovative Applications* (pp. 21-68). Elsevier. https://doi.org/https://doi.org/10.1016/B978-0-12-816808-0.00002-0

Provencher, J. F., Vermaire, J. C., Avery-Gomm, S., Braune, B. M., & Mallory, M. L. (2018). Garbage in guano? Microplastic debris found in faecal precursors of seabirds known to ingest plastics. *Science of The Total Environment*, *644*, 1477-1484. https://doi.org/https://doi.org/10.1016/j.scitotenv.2018.07.101

Rangel-Buitrago, N., Neal, W., & Williams, A. (2022). The Plasticene: Time and rocks. *Marine pollution bulletin*, *185*, 114358. https://doi.org/https://doi.org/10.1016/j.marpolbul.2022.114358

Razanajatovo, R. M., Ding, J., Zhang, S., Jiang, H., & Zou, H. (2018). Sorption and desorption of selected pharmaceuticals by polyethylene microplastics. *Marine pollution bulletin*, *136*, 516-523. https://doi.org/https://doi.org/10.1016/j.marpolbul.2018.09.048

Rosenfeld, P. E., & Feng, L. G. H. (2011). 16 - Emerging Contaminants. In P. E. Rosenfeld & L. G. H. Feng (Eds.), *Risks of Hazardous Wastes* (pp. 215-222). William Andrew Publishing. https://doi.org/https://doi.org/10.1016/B978-1-4377-7842-7.00016-7

Ryberg, M. W., Hauschild, M. Z., Wang, F., Averous-Monnery, S., & Laurent, A. (2019). Global environmental losses of plastics across their value chains. *Resources, Conservation and Recycling*, *151*, 104459.

Saeedi, M. (2023). How microplastics interact with food chain: a short overview of fate and impacts. *Journal of Food Science and Technology*, 1-11.

Saleh, T. A. (2022). Chapter 4 - Isotherm models of adsorption processes on adsorbents and nanoadsorbents. In T. A. Saleh (Ed.), *Interface Science and Technology* (Vol. 34, pp. 99-126). Elsevier. https://doi.org/https://doi.org/10.1016/B978-0-12-849876-7.00009-9

Sarkar, A. K., Rubin, A. E., & Zucker, I. (2021). Engineered Polystyrene-Based Microplastics of High Environmental Relevance. *Environmental science & technology*, *55*(15), 10491-10501. https://doi.org/10.1021/acs.est.1c02196

Sarkar, S., & Aparna, K. (2020). Food packaging and storage. *Research Trends in Home Science and Extension AkiNik Pub*, *3*, 27-51.

Schlautman, M. A., & Morgan, J. J. (1994). Adsorption of aquatic humic substances on colloidal-size aluminum oxide particles: Influence of solution chemistry. *Geochimica et Cosmochimica Acta*, *58*(20), 4293-4303. https://doi.org/https://doi.org/10.1016/0016-7037(94)90334-4

Sena, M. M., Alcântara, G. B., Busato, J. G., da Costa, A. C. S., & Sodré, F. F. (2018). Multiple Approaches to Assess Copper Behavior in Soils from a Tropical Savanna Toposequence. *International Journal of Environmental Research*, *12*, 189-201.

Sharma, A., & Anthal, R. (2016). Humic substances in aquatic ecosystems: A review. *International Journal of Innovative Research in Science, Engineering and Technology*, 18462-18470.

Shi, X., Chen, Z., Wei, W., Chen, J., & Ni, B.-J. (2023). Toxicity of micro/nanoplastics in the environment: Roles of plastisphere and eco-corona. *Soil & Environmental Health*, *1*(1), 100002.

Singh, B., & Sharma, N. (2008). Mechanistic implications of plastic degradation. *Polymer Degradation and Stability*, *93*(3), 561-584. https://doi.org/https://doi.org/10.1016/j.polymdegradstab.2007.11.008

Singla, P. (2020). Plant Synthetic Biology: A Paradigm Shift Targeting Stress Mitigation, Reduction of Ecological Footprints and Sustainable Transformation in Agriculture. *Plant Stress Biology: Strategies and Trends*, 435-489.

Sips, R. (1948). On the structure of a catalyst surface. *The journal of chemical physics*, *16*(5), 490-495.

Siri, C., Liu, Y., Masset, T., Dudefoi, W., Oldham, D., Minghetti, M., . . . Breider, F. (2021). Adsorption of progesterone onto microplastics and its desorption in simulated gastric and intestinal fluids. *Environmental Science: Processes & Impacts*, *23*(10), 1566-1577.

Smith, B. (2021). The infrared spectra of polymers II: polyethylene. *Spectroscopy*, *36*(9), 24–29-24–29.

Smith, E. J., Davison, W., & Hamilton-Taylor, J. (2002). Methods for preparing synthetic freshwaters. *Water Res*, *36*(5), 1286-1296. https://doi.org/10.1016/s0043-1354(01)00341-4

Sodré, F. F., Arowojolu, I. M., Canela, M. C., Ferreira, R. S., Fernandes, A. N., Montagner, C. C., . . . Waldman, W. R. (2023). How natural and anthropogenic factors should drive microplastic behavior and fate: The scenario of Brazilian urban freshwater. *Chemosphere*, *340*, 139813. https://doi.org/https://doi.org/10.1016/j.chemosphere.2023.139813

Sodré, F. F., Peralta-Zamora, P. G., & Grassi, M. T. (2004). Microwave-assisted photochemical digestion of natural waters: application in partition and speciation studies of copper. *Química Nova*, *27*, 695-700.

Sodré, F. F., & Sampaio, T. R. (2020). Development and application of a SPE-LC-QTOF method for the quantification of micropollutants of emerging concern in drinking waters from the Brazilian capital. *Emerging Contaminants*, *6*, 72-81.

Song, Y., Zhao, J., Zheng, L., Zhu, W., Xue, X., Yu, Y., . . . Wang, H. (2022). Adsorption behaviors and mechanisms of humic acid on virgin and aging microplastics. *Journal of Molecular Liquids*, *363*, 119819. https://doi.org/https://doi.org/10.1016/j.molliq.2022.119819

Strungaru, S.-A., Jijie, R., Nicoara, M., Plavan, G., & Faggio, C. (2019). Micro- (nano) plastics in freshwater ecosystems: Abundance, toxicological impact and quantification methodology. *TrAC Trends in Analytical Chemistry*, *110*, 116-128. https://doi.org/https://doi.org/10.1016/j.trac.2018.10.025

Sun, Y., Yuan, J., Zhou, T., Zhao, Y., Yu, F., & Ma, J. (2020). Laboratory simulation of microplastics weathering and its adsorption behaviors in an aqueous environment: a systematic review. *Environmental Pollution*, *265*, 114864.

Taheri, S., Shoshtari-Yeganeh, B., Pourzamani, H., & Ebrahimpour, K. (2023). Investigating the pollution of bottled water by the microplastics (MPs): the effects of mechanical stress, sunlight exposure, and freezing on MPs release. *Environmental Monitoring and Assessment*, *195*(1), 62.

Tiotsop Kuete, I.-H., Tchuifon Tchuifon, R. D., Bopda, A., Sadeu Ngakou, C., Nche, G. N.-A., & Gabche Anagho, S. (2022). Adsorption of indigo carmine onto chemically activated carbons derived from the Cameroonian agricultural waste garcinia cola nut shells and desorption studies. *Journal of Chemistry*, *2022*(1), 1236621.

Tseng, L. Y., You, C., Vu, C., Chistolini, M. K., Wang, C. Y., Mast, K., . . . Eusebi, A. L. (2022). Adsorption of contaminants of emerging concern (CECs) with varying hydrophobicity on macro-and microplastic polyvinyl chloride, polyethylene, and polystyrene: kinetics and potential mechanisms. *Water*, *14*(16), 2581.

Vadera, S., & Khan, S. (2021). A critical analysis of the rising global demand of plastics and its adverse impact on environmental sustainability. *J. Environ. Pollut. Manag*, *3*, 105.

van Zomeren, A. (2008). *On the nature of organic matter from natural and contaminated materials: isolation methods, characterisation and application to geochemical modelling*. Wageningen University and Research.

Vasile, C. (2000). Degradation and decomposition. *PLASTICS ENGINEERING-NEW YORK-*, *59*, 413-476.

Vieira, Y., Lima, E. C., Foletto, E. L., & Dotto, G. L. (2021). Microplastics physicochemical properties, specific adsorption modeling and their interaction with pharmaceuticals and other emerging contaminants. *Science of The Total Environment*, *753*, 141981.

Wang, F., Shih, K. M., & Li, X. Y. (2015). The partition behavior of perfluorooctanesulfonate (PFOS) and perfluorooctanesulfonamide (FOSA) on microplastics. *Chemosphere*, *119*, 841-847.

Wang, F., Zhang, M., Sha, W., Wang, Y., Hao, H., Dou, Y., & Li, Y. (2020). Sorption behavior and mechanisms of organic contaminants to nano and microplastics. *Molecules*, *25*(8), 1827.

Wang, K., Wang, K., Chen, Y., Liang, S., Zhang, Y., Guo, C., . . . Wang, J. (2023). Desorption of sulfamethoxazole from polyamide 6 microplastics: Environmental factors, simulated gastrointestinal fluids, and desorption mechanisms. *Ecotoxicology and Environmental Safety*, *264*, 115400.

Wang, T., Ma, Y., & Ji, R. (2021a). Aging processes of polyethylene mulch films and preparation of microplastics with environmental characteristics. *Bulletin of Environmental Contamination and Toxicology*, *107*, 736-740.

Wang, T., Ma, Y., & Ji, R. (2021b). Aging processes of polyethylene mulch films and preparation of microplastics with environmental characteristics. *Bulletin of Environmental Contamination and Toxicology*, *107*(4), 736-740.

Wang, Y., Zhao, J., Fu, Z., Guan, D., Zhang, D., Zhang, H., . . . Wang, D. (2024). Innovative overview of the occurrence, aging characteristics, and ecological toxicity of microplastics in environmental media. *Environmental Pollution*, 123623.

Wang, Z., Ding, J., Razanajatovo, R. M., Huang, J., Zheng, L., Zou, H., . . . Liu, J. (2022). Sorption of selected pharmaceutical compounds on polyethylene microplastics: Roles of pH, aging, and competitive sorption. *Chemosphere*, *307*, 135561.

Williams, A., & Rangel-Buitrago, N. (2019). Marine litter: Solutions for a major environmental problem. *Journal of coastal research*, *35*(3), 648-663.

Windsor, F. M., Durance, I., Horton, A. A., Thompson, R. C., Tyler, C. R., & Ormerod, S. J. (2019). A catchment-scale perspective of plastic pollution. *Global change biology*, *25*(4), 1207-1221.

Witzmann, T., Ramsperger, A. F., Wieland, S., Laforsch, C., Kress, H., Fery, A., & Auernhammer, G. n. K. (2022). Repulsive interactions of eco-corona-covered microplastic particles quantitatively follow modeling of polymer brushes. *Langmuir*, *38*(29), 8748-8756.

Wong, J. K. H., Lee, K. K., Tang, K. H. D., & Yap, P.-S. (2020). Microplastics in the freshwater and terrestrial environments: Prevalence, fates, impacts and sustainable solutions. *Science of The Total Environment*, *719*, 137512.

Wu, J., Lu, J., & Wu, J. (2022). Effect of gastric fluid on adsorption and desorption of endocrine disrupting chemicals on microplastics. *Frontiers of Environmental Science & Engineering*, *16*, 1-13.

Wu, X., Liu, P., Gong, Z., Wang, H., Huang, H., Shi, Y., . . . Gao, S. (2021). Humic acid and fulvic acid hinder long-term weathering of microplastics in lake water. *Environmental science & technology*, *55*(23), 15810-15820.

Wu, X., Liu, P., Huang, H., & Gao, S. (2020). Adsorption of triclosan onto different aged polypropylene microplastics: critical effect of cations. *Science of The Total Environment*, *717*, 137033.

Wunderlich, B. (2013). *Macromolecular Physics: Crystal Melting*. Academic Press.

Xiang, Y., Jiang, L., Zhou, Y., Luo, Z., Zhi, D., Yang, J., & Lam, S. S. (2022). Microplastics and environmental pollutants: Key interaction and toxicology in aquatic and soil environments. *Journal of Hazardous Materials*, *422*, 126843.

Xu, B., Liu, F., Brookes, P. C., & Xu, J. (2018a). Microplastics play a minor role in tetracycline sorption in the presence of dissolved organic matter. *Environmental Pollution*, *240*, 87-94.

Xu, B., Liu, F., Brookes, P. C., & Xu, J. (2018b). The sorption kinetics and isotherms of sulfamethoxazole with polyethylene microplastics. *Marine pollution bulletin*, *131*, 191-196.

Yao, J., Wen, J., Li, H., & Yang, Y. (2022). Surface functional groups determine adsorption of pharmaceuticals and personal care products on polypropylene microplastics. *Journal of Hazardous Materials*, *423*, 127131.

Yassin, A. A., & Sabaa, M. W. (1990). Degradation and stabilization of poly (vinyl chloride). *Journal of Macromolecular Science—Reviews in Macromolecular Chemistry and Physics*, *30*(3-4), 491-558.

Yu, H., Yang, B., Waigi, M. G., Peng, F., Li, Z., & Hu, X. (2020). The effects of functional groups on the sorption of naphthalene on microplastics. *Chemosphere*, *261*, 127592.

Yu, J., Sun, L., Ma, C., Qiao, Y., & Yao, H. (2016). Thermal degradation of PVC: A review. *Waste management*, *48*, 300-314.

Zeng, F., He, Y., Lian, Z., & Xu, J. (2014). The impact of solution chemistry of electrolyte on the sorption of pentachlorophenol and phenanthrene by natural hematite nanoparticles. *Science of The Total Environment*, *466*, 577-585.

Zhang, C., Wang, C., Cao, G., Wang, D., & Ho, S.-H. (2020). A sustainable solution to plastics pollution: An eco-friendly bioplastic film production from high-salt contained Spirulina sp. residues. *Journal of Hazardous Materials*, *388*, 121773. https://doi.org/https://doi.org/10.1016/j.jhazmat.2019.121773

Zhang, H. (2017). Transport of microplastics in coastal seas. *Estuarine, Coastal and Shelf Science*, *199*, 74-86.

Zhang, P., Huang, P., Sun, H., Ma, J., & Li, B. (2020). The structure of agricultural microplastics (PT, PU and UF) and their sorption capacities for PAHs and PHE derivates under various salinity and oxidation treatments. *Environmental Pollution*, *257*, 113525.

Zhao, L., Rong, L., Xu, J., Lian, J., Wang, L., & Sun, H. (2020). Sorption of five organic compounds by polar and nonpolar microplastics. *Chemosphere*, *257*, 127206. https://doi.org/https://doi.org/10.1016/j.chemosphere.2020.127206

Zhao, X., Wang, J., Yee Leung, K. M., & Wu, F. (2022). Color: an important but overlooked factor for plastic photoaging and microplastic formation. *Environmental science & technology*, *56*(13), 9161-9163.

Zhao, Y., Liu, F., & Qin, X. (2017). Adsorption of diclofenac onto goethite: Adsorption kinetics and effects of pH. *Chemosphere*, *180*, 373-378.

Zhu, J., Pigna, M., Cozzolino, V., Caporale, A. G., & Violante, A. (2010). Competitive sorption of copper(II), chromium(III) and lead(II) on ferrihydrite and two organomineral complexes. *Geoderma*, *159*(3), 409-416. https://doi.org/https://doi.org/10.1016/j.geoderma.2010.09.006

APPENDIX A

      The stability of triclosan in the hydrophilic PVDF filtered materials was tested. A-500 µg/L solution of triclosan was filtered through a 0.22 µm syringe filter. 0.95 mL of the filtrates were transferred into 1.5 mL vials containing 0.05 mL triclosan-D_3 internal standard and analyzed using LC-MS/MS. The percentage losses were then calculated. The working condition of the LC-MS/MS are presented in section 3.4.3. Meanwhile, the precursor ion of triclosan in the quadrupole analyzer was deprotonated $[M-H]^-$ at 288.8 amu in negative mode. From the two daughter ions, the one producing the highest intensity was used for quantification and it is 35.3 amu while *m/z* d 37.2 was used to identify the analyte. The percentage lost of trclosan to the process is presented in Table A-1. Other filter materials, including hydrophobic PVDF, cellulose acetate and mixed cellulose esters and the results were similar to that of hydrophilic PVDF.

Table A-1. Results of triclosan stability test in filter material

Control	Concentration (µg/L)	Loss (%)
S_{FIL}	23.43 ± 6.73	95.3

S_{FIL} = stability tests of the triclosan in the filtration process

DECLARAÇÃO DE ORIGINALIDADE DE TESE DE DOUTORADO

Declaro que a presente tese é original, elaborada especialmente para este fim, não tendo sido apresentada para obtenção de qualquer ítulo e que identifico e cito devidamente todas as autoras e todos os autores que contribuíram para o trabalho, bem como as contribuições oriundas de outras publicações de minha autoria. Declaro estar ciente de que a cópia ou o plágio podem gerar responsabilidade civil, criminal e disciplinar, consistindo em grave violação à ética acadêmica.

Brasília, 12 de setembro de 2024.

Assinatura da discente:

Programa: Programa de Pós-Graduação em Química – Universidade de Brasília.

Nome completo: Imisi Michael Arowojolu

Título do Trabalho: Sorption interactions of sulfamethoxazole and diclofenac with fresh, UV-aged, and humic acid-coated microplastics

Nível: ( ) Mestrado (X) Doutorado

Orientador: Prof. Dr. Fernando Fabriz Sodré